

8-2017

## Optogenetic interrogation of primary visual cortex and its impact on neural coding and behavior

Ariana R. Andrei

Follow this and additional works at: [https://digitalcommons.library.tmc.edu/utgsbs\\_dissertations](https://digitalcommons.library.tmc.edu/utgsbs_dissertations)



Part of the [Behavioral Neurobiology Commons](#), and the [Systems Neuroscience Commons](#)

### Recommended Citation

Andrei, Ariana R., "Optogenetic interrogation of primary visual cortex and its impact on neural coding and behavior" (2017). *The University of Texas MD Anderson Cancer Center UTHealth Graduate School of Biomedical Sciences Dissertations and Theses (Open Access)*. 747.  
[https://digitalcommons.library.tmc.edu/utgsbs\\_dissertations/747](https://digitalcommons.library.tmc.edu/utgsbs_dissertations/747)

This Dissertation (PhD) is brought to you for free and open access by the The University of Texas MD Anderson Cancer Center UTHealth Graduate School of Biomedical Sciences at DigitalCommons@TMC. It has been accepted for inclusion in The University of Texas MD Anderson Cancer Center UTHealth Graduate School of Biomedical Sciences Dissertations and Theses (Open Access) by an authorized administrator of DigitalCommons@TMC. For more information, please contact [digitalcommons@library.tmc.edu](mailto:digitalcommons@library.tmc.edu).

**OPTOGENETIC INTERROGATION OF PRIMARY VISUAL CORTEX AND ITS  
IMPACT ON NEURAL CODING AND BEHAVIOR**

By

*Ariana R. Andrei, MSc*

APPROVED:

---

Roger Janz, Ph.D.  
Advisory Professor

---

John H. Byrne, Ph.D.

---

Daniel J. Felleman, Ph.D.

---

Dora Angelaki, Ph.D.

---

John Spudich, Ph.D.

APPROVED:

---

Dean, The University of Texas  
MD Anderson Cancer Center UTHealth Graduate School of Biomedical Sciences

**OPTOGENETIC INTERROGATION OF PRIMARY VISUAL CORTEX AND ITS  
IMPACT ON NEURAL CODING AND BEHAVIOR**

A

DISSERTATION

Presented to the Faculty of

The University of Texas

MD Anderson Cancer Center UTHealth

Graduate School of Biomedical Sciences

in Partial Fulfillment

of the Requirements

for the Degree of

DOCTOR OF PHILOSOPHY

By

*Ariana R. Andrei, MSc*  
Houston, Texas

Date of Graduation (*August, 2017*)

*For Gus MacCauly who introduced me to the dance of the universe*

## **ACKNOWLEDGEMENTS**

**Sorin Pojoga, PhD** began the collaborative effort between the Janz and Dragoi labs to implement extremely novel at the time optogenetic techniques in non-human primates. He designed the technical aspects of the laser stimulation, and the original computer codes used for the behavioral tasks. We worked together for several years collecting data, designing and redesigning experimental details, and analyzing the data most of which is presented in Chapter III. **Sam Debes, BSc** was closely involved in the GtACR-2 experiments presented in Chapter IV, starting from the initial virus injections, to data collection, spike sorting and data analyses. **Elsa Rodarte Rascon, MD & Xiaoqin Lin, PhD** were responsible for the fixing, mounting and immunohistochemistry of the biopsied tissue presented in Chapter IV. Elsa performed the biopsy. **Valentin Dragoi, PhD** generously supplied his monkeys, laboratory space, key personnel and expertise for these studies. **Roger Janz, PhD** handled matters relating to virus construction and preparation in addition to his formal role of wisdom purveyor.

*I would also like to thank (in no particular order) the many people who provided critical input and stimulating conversations regarding this project over the years: Daniel Felleman, Jack Byne, John Spudich, Dora Angelaki, Michael Beierlein, Neda Shahidi, Ming Hu, Marcello Mulas, Russell Milton, and Mircea Chelaru.*

## ***ABSTRACT***

# **OPTOGENETIC INTERROGATION OF PRIMARY VISUAL CORTEX AND ITS IMPACT ON NEURAL CODING AND BEHAVIOR**

By Ariana Ruxandra Andrei, Msc

Advisory Professor: Roger Janz, Ph.D.

Understanding the mechanism by which the brain transforms simple sensory inputs into rich perceptual experiences is one of the great mysteries of systems neuroscience. Undoubtedly this involves the activity of large populations of interconnected neurons, but while the responses of individual neurons to a variety of sensory stimuli have been well-characterized, how *populations* of such neurons organize their activity to create our sensory perceptions is almost entirely unknown. To investigate this complex circuitry requires the ability to causally manipulate the activity of neural populations and monitor the resultant effects. Here we focus on primary visual cortex (V1), which has been shown to be crucial for visual perception, and utilize optogenetic tools to render the activity of genetically- defined neural populations sensitive to light. By simultaneously recording and modulating (either driving or silencing) the activity of excitatory (glutamatergic) neurons, we are able to causally examine their role in visual perception. Here we report 3 major findings. First, we show that activating subpopulations of excitatory neurons can improve visual perception under certain conditions and that information in V1 used for perceptual decisions is integrated across spatially-limited populations of neurons. Further, we show that a key signature of this information integration is a reduction in correlated variability

between neurons. Correlated variability has been implicated as a major source of behavioral choice related activity in the cortex, and theorized to be a major factor limiting information in cortical populations. However, until now, there has not been a way to manipulate correlations without altering firing rates or other task related variables. Here we demonstrate a novel method using optogenetic stimulation to causally manipulate correlated variability between cortical neurons without altering their firing rates. Lastly, with the goal of expanding the currently limited repertoire of optogenetic tools for non-human primates, we establish the viability of a novel optogenetic construct capable of dramatically silencing neural populations using a recently discovered anion conducting channelrhodopsin.

## TABLE OF CONTENTS

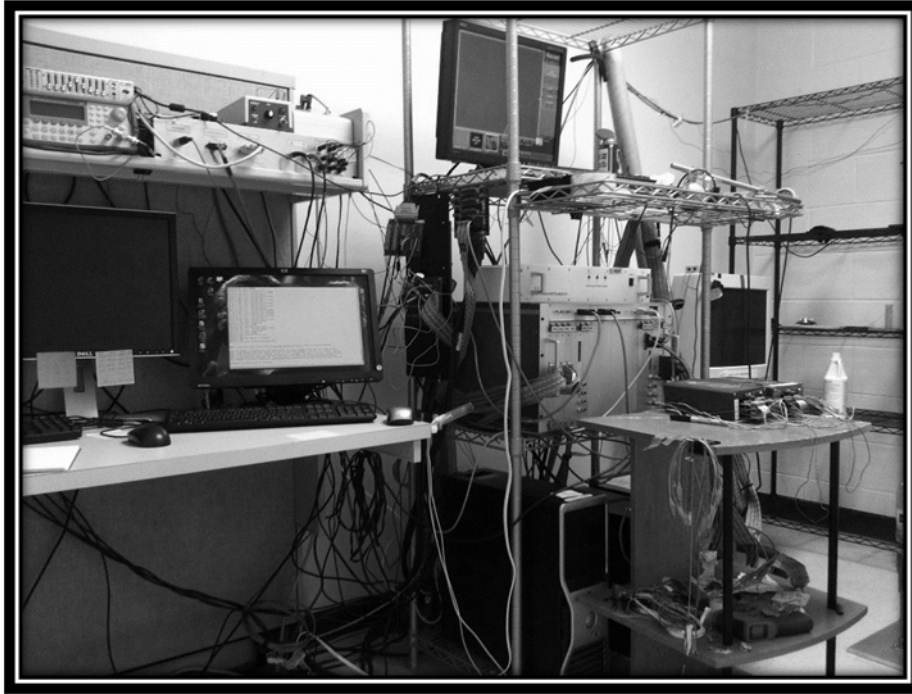
<b>APPROVAL PAGE</b> .....	i
<b>TITLE PAGE</b> .....	ii
<b>DEDICATION</b> .....	iii
<b>ACKNOWLEDGEMENTS</b> .....	iv
<b>ABSTRACT</b> .....	v
<b>TABLE OF CONTENTS</b> .....	vii
<b>LIST OF FIGURES</b> .....	ix
<b>Preface</b> .....	x
<b>CHAPTER I: INTRODUCTION &amp; BACKGROUND</b> .....	1
<b>1.0 Introduction</b> .....	1
<b>1.1 Functional organization of early visual circuits</b> .....	2
<b>1.2 Gain control &amp; surround modulation</b> .....	7
<b>1.3 Coding visual stimuli with neural population activity</b> .....	10
<b>1.4 Stimulating cortical networks overview</b> .....	12
<b>1.5 Hypotheses and Research Aims</b> .....	16
<b>CHAPTER II: METHODS</b> .....	19
<b>2.1 Animal subjects</b> .....	19
<b>2.2 Viral vector injections</b> .....	19
2.2.1 Channelrhodopsin-2 (ChR2) construct .....	19
2.2.2 Gt-ACR2 construct .....	20
2.2.3 Cortical biopsy & immunohistochemistry .....	21
<b>2.3 Electrophysiological recordings</b> .....	22
<b>2.4 Delivering light to neurons</b> .....	23
<b>2.5 Behavioral tasks</b> .....	24
2.5.1 ChR2 detection task .....	24
2.5.2 Gt-ACR2 detection task .....	26
2.5.3 Experimental order .....	27
<b>2.6 Data analysis</b> .....	28
2.6.1 Spike sorting .....	28
2.6.2 Cell identification .....	28
2.6.3 Orientation selectivity .....	29



2.6.4 Noise correlations .....	30
2.6.5 Population Signal to Noise Ratio .....	31
<b>CHAPTER III: SPATIALLY-LIMITED NEURAL POOLING FOR VISUAL PERCEPTION .....</b>	<b>32</b>
3.0 Introduction .....	32
3.1 Targeting excitatory neural populations in monkey primary visual cortex .....	34
3.2 The effects of optogenetic stimulation on behavioral performance .....	36
3.3 Behavioral changes are unlikely to be caused by phosphene induction .....	45
3.4 Optogenetic stimulation increases V1 responses uniformly across conditions .....	48
3.5 Optogenetic stimulation influences population coding .....	51
3.6 Spatially-limited signal pooling captures changes in behavioral performance .....	56
3.7 Discussion .....	66
4.0 Introduction .....	73
4.1 Delayed decrease of noise correlations following optogenetic stimulation .....	75
4.2 Correlated variability changes are not due to firing rate changes .....	79
4.3 Delayed correlation change is an intrinsic network feature, not plasticity .....	80
4.4 Discussion .....	84
<b>CHAPTER V: SUPPRESSING VISUAL CORTICAL NETWORKS .....</b>	<b>87</b>
5.0 Introduction .....	87
5.1 Gt-ACR2 suppresses neural activity in monkey cortex .....	88
5.2 Novel circuit dynamics revealed by optogenetic inhibition .....	90
5.3 Discussion .....	97
<b>CHAPTER VI: CONCLUSIONS AND FUTURE DIRECTIONS .....</b>	<b>102</b>
<b>REFERENCES .....</b>	<b>108</b>
<b>VITA .....</b>	<b>129</b>

## ***LIST OF FIGURES***

Figure 1   Targeting neural subpopulations.....	37
Figure S1   Propagation of optically-induced neuronal activity across the network. ....	39
Figure 2   Detection performance is enhanced with optical stimulation according to functional distance.....	42
Figure S2   Differences in optical stimulation parameters did not cause systematic differences in firing rates and perceptual detection performance.....	45
Figure 3   Optogenetic stimulation is unlikely to induce phosphenes.....	47
Figure S3   Optical stimulation of untransfected cortex.....	49
Figure 4   Light-induced changes in neuronal responses. ....	51
Figure S4   Non-linear laser-induced changes in neuronal responses. ....	54
Figure 5   Effect of optical stimulation on noise correlations and network performance. ....	57
Figure 6   Spatially-weighted signal pooling models observed behavioral changes. ....	60
Figure S5   Estimating the total SNR to predict behavioral performance.....	62
Figure 7   Abrupt reduction in noise correlations after optical stimulation of glutamatergic neurons. ....	77
Figure 8   Noise correlation changes are not due changes in firing rates.....	81
Figure 9   Late reduction in correlations due to network property, not plasticity. ....	83
Figure 10   Suppression of monkey visual cortex with novel anion channelrhodopsin. ....	93
Figure 11   Neighborhood suppression non-linearly affects firing rates.....	95
Figure 12   Local network modulates inhibition to neighboring cell responses as a function of visual stimulus strength.....	96
Figure 13   Most neurons are suppressed at lower contrasts following suppression of neighboring activity. ....	98



***Preface***  
***small answers to BIG questions***

Ah, the brain. A tangled web of biological wires far more daunting in complexity than any jungle of cables snaking across the back wall of a typical electrophysiology lab (above). Despite what the philosophically-inclined would have you believe, the brain is not actually self-aware. I wish it were. If the brain were truly self-aware then we would not need complicated experiments using monkeys and lasers and viruses, or millions of genetically engineered mice with glow in the dark brains to solve what future scientists will undoubtedly view as the most basic questions about neural computations. With a self-aware brain we could simply ask our most burning questions to the brain and it could respond, either through intuition or with words (we could even make this a fun interactive task and pose questions to someone else's brain). We could ask things like, *How do I see? What is smell? Why do I profoundly*

*forget dreams upon waking, but then vividly recall them hours later when my head returns to the pillow? What is the neurological nature of this strange experience of cuteness?* And following a little bit of introspection, and perhaps exposure to a cat or a baby, we would have our answers and we could dust off our hands, satisfied with a day's work. But alas, there is no innate perception of the mechanisms that underlie how the brain functions. At best, we, and I suspect most animals (fish included) are aware of the final tip of the sensory processing iceberg. Millions of years of evolution (and convolution) have produced a neural architecture that requires painstaking work to decipher –like picking through a knotty ball of hair with a fine tooth comb. You start at the ends and slowly work your way towards the middle of the knot, freeing up a few strands of hair at a time. For the curious amongst us, the path to answers for such big questions is long, and requires the accumulation of answers to much smaller questions along the way. Here I present the few strands of knowledge that have been untangled over the course of this degree. They relate to the big umbrella question of *How do we see?* Though as you will soon appreciate, this big question must be broken down in much smaller question detailing the intricate stimulus-neural response interplay at work. This work builds upon almost 80 years of electrophysiological interrogation of visual cortical circuits, and which I will attempt to summarize for you shortly. But as the accordion of details opens up and attempts to swallow you into its bellows, I want to assure you, my dear reader, that I will return to the basic question posed here and provide you with the simplest, most distilled answered I have at this moment in time.

# ***CHAPTER I: INTRODUCTION & BACKGROUND***

## ***1.0 Introduction***

Visual detection is the most basic, yet the most important task the visual system performs. Whether it's monitoring for the movement of a predator in the environment, or scanning the produce section for the bananas, the visual system has evolved as a master of change detection. Here I will provide a brief overview of the current state of knowledge of how the brain accomplishes this feat, focusing on cortical circuits. The goal of this introduction is to provide the reader with a broader context regarding the function of primary visual cortex (V1) within which to interpret the experimental findings, and to provide a greater level of detail (though hardly exhaustive) regarding the known circuitry and properties of V1 neurons.

Sensory information is represented in cerebral cortex in a distributed, hierarchical manner, with increasingly complex stimulus features being encoded at each subsequent stage of processing. This is true for vision, somatic sensation and audition. As the major conduits of sensory information to the rest of the cortex, neuronal responses in primary sensory cortex are absolutely essential for normal sensory perception, with lesions to primary visual cortex (V1), for example, resulting in perceptual blindness to affected visual field (1, 2). However, while response properties of individual neurons in V1 have been extensively studied, little is known about how information is structured across populations of neurons, and how this contributes to final sensory percepts. This understanding is crucial for our basic understanding of visual processing, and sensory processing in

general. The neural correlates of sensory perception along this hierarchy have been well established by studying the degree of correlation between neuronal responses and perceptual reports (3–17). The overwhelming pattern is that areas processing more complex stimulus features contain a greater proportion of neurons whose activity reliably covaries with perceptual reports (4, 10, 17, 18). In contrast, the trial-by-trial activity of neurons in primary sensory cortex is predominantly independent of the animal's behavioral decisions (3, 17). That is, the stimulus-evoked responses of neurons in primary sensory areas are generally invariant to whether or not the animal subsequently reports having perceived the stimulus or not. How then is the information from primary sensory areas used to generate these more complex responses? Is all information in primary sensory areas available to higher cortical areas for use in perceptual decision-making, or is it quantized or filtered in some way?

### ***1.1 Functional organization of early visual circuits***

V1 receives input from the lateral geniculate nucleus (LGN) of the thalamus, which acts as a relay, shuttling information from the retina to the cortex. The receptive field properties of neurons in V1 are derived from the response properties of neurons in LGN (19). Interestingly, the vast majority of input to V1 actually comes from feedback originating in higher cortical areas (20–22), which act to modulate responses in V1. For example, V2 sends approximately 10 times more axons to V1 than does the lateral geniculate nucleus (23). V1 then sends direct projections to V2 (24), and some sparse projections to V4 have also been reported (25). Following V2, visual information branches into the famed dorsal and ventral streams of visual processing. Responses of neurons in the dorsal

stream (including the middle temporal area MT, and lateral intraparietal area, LIP) are consistent with its role in the detection of movement and organization of spatial relationships between the subject and objects. The ventral stream (including V4, and inferotemporal cortex, IT) shows responses consistent with its role in object recognition. For example, neurons in IT show the fascinating property of object constancy, that is, they respond to presentations of the same object regardless of size, three-dimensional rotation, color of the object (26).

One of the most striking aspects of V1 is the presence of an orderly mosaic of visual feature sensitivities laid out like psychedelic blanket over the cortical surface, representing retinotopic spatial locations, ocular dominance, visual stimulus orientation and luminance/color information. This clustering of similarly-tuned activity is present at several spatial scales. First and largest is the retinotopic map, by which spatially adjacent representations in the retina are translated into spatially adjacent receptive field locations in V1. Receptive fields are the location in visual space (relative to the position of the fovea) where the presence of visual stimulus will lead to changes in the spontaneous firing of a neuron. In V1 receptive fields are about 0.5- 1 degree in diameter near the fovea and increase in size in the periphery, and also change in size as a function of visual stimulus contrast (27). Additionally, the retina is not evenly represented across V1. There is an over-representation of foveal versus parafoveal areas. In other words, a greater number of V1 neurons process information originating from the foveal retina compared to the peripheral retina. This is known as cortical magnification, and decreases linearly as a function of eccentricity from the center of the visual field (28).

Next are ocular dominance columns, in which signals from the two eyes are interlaced across the cortical surface, alternating every 400-500  $\mu\text{m}$  (29, 30). When stained by the reduced silver method of Liesegang, these parallel paths show up as regularly spaced stripes across the cortical surface (31), and bear an uncanny resemblance to zebra stripes. Within the boundaries of the ocular dominance bands are at least two other distinct feature representations.

First, there are patches, called color domains or “blobs” (30), which contain cells with increased levels of cytochrome oxidase (a mitochondrial enzyme critical for energy production via the electron transport chain). Functionally, these blobs are more sensitive to luminance and color and are mostly located within 50  $\mu\text{m}$  of the center of the ocular dominance band they occupy (30, 32), though color sensitive regions have also been reported to span across ocular dominance columns (33). Color-responsive neurons have also been found to extend beyond the boundaries of blobs(33). Blob neurons have higher baseline firing rates compared with non-blob cells (49% greater), and this has been proposed as an explanation for the abundance of cytochrome oxidase that defines these patches (34).

Between the blobs are regions called “interblobs”, containing neurons that respond strongly to visual stimuli of particular orientations. In cats, monkeys, humans, but not rodents, orientation selectivity is highly organized across the cortical surface, with orientation preferences gradually varying linearly (35). These portions are known as “iso-



orientation domains". The second conspicuous feature within ocular dominance bands are "pin-wheel centers" - focal regions in which orientation tuning rapidly changes, spiraling out from a singularity. Tuning of neurons at pinwheel centers is broader than in iso-orientation domains when high contrast, optimally-sized stimuli are presented. At low contrast stimuli, the tuning of both groups are equal (36). Pinwheels and blobs are distinct features (32, 37), but it is important to note that neurons within blobs are also sensitive to orientations, but their tuning is slightly broader (mean orientation bandwidth is about 3.5 degrees larger than in iso-orientation domains)(34). Of particular importance to the current study, is the fact that the presence of blob does not seem to impact the smoothness of the orientation tuning gradient across the cortical surface (32). Lastly, spatial frequency of visual stimuli also appears to be mapped, and varies orthogonally to the orientation map (38). If one wonders whether this architecture is of any functional value, it is worth noting that projections from V1 to V2, the next stage of cortical processing, emanate from 4 distinct regions V1 related to this blob/interblob architecture and maintaining their independence in V2's unique topographical feature map (37).

So far we have only discussed properties that vary across the cortical surface. Diving into the depth dimension, cell properties across cortical layers have also been extensively described. In cat and monkey sensory cortex, cells arranged vertically (perpendicular to the cortical surface) have been found to share very similar tuning preferences (39, 40) and have thus been dubbed "cortical columns". Within a cortical column, neurons have similar orientation preferences, but horizontally across the cortex, orientation preferences spiral out from pinwheel centers and progress linearly between pinwheels in iso-

orientation domains (35). Hubel and Wiesel in their seminal work (40) described a putative larger functional scale of organization, called the hypercolumn, consisting of a set of cortical columns representing a particular feature space. Nowadays, a hypercolumn in V1 refers most often to a group of columns with overlapping receptive field locations, whose orientation preferences cumulatively represent the entire 180 degrees of possible orientations, though it was originally also defined to include a complete of information from each eye across two ocular dominance columns. In the portions of V1 that represent visual space up to about 15° eccentricity from the fovea, the size of such functionally-defined hypercolumns is remarkably consistent, spanning 0.5-1 mm across the cortical surface. This hold true for the individual stimulus features of ocular dominance, orientation and color, which so a strikingly consistent periodicity between nearest neighbor hypercolumns of about 0.8 mm, as measured using intrinsic imaging in macaques (41). Thus, moving laterally across the cortical surface, every 2-3 millimeters corresponds to a new region of visual space and is represented by a completely novel set of hypercolumns (42). The hypercolumn was proposed to describe the minimum amount of cortical real estate required to house all of the necessary machinery to analyze a patch of visual space. But is this actually the case? Are cortical computations about a portion of visual space completely described by the activity of a population of cells with 1 square millimeter? Is there support for this functional module from local connectivity patterns observed in anatomical studies?

Cortical columns are defined by the prevalence of vertical connectivity and relatively sparse horizontal connections (43, 44). Only within superficial layers (2/3) do pyramidal

(excitatory) neurons make extensive connections with other pyramidal neurons within the same layer (45). Tracer injection studies into V1 have shown a patchy labeling pattern across columns, with patches measuring about 200-500  $\mu\text{m}$  in diameter, indicating the area in which cells make reciprocal connections with one another(45). Long-range horizontal connections, also emerge from superficial layers (2/3, but also 5) and span distance up to 6-8 mm monosynaptically connecting similarly tuned populations (46–48) in multiple species. Long range horizontal connections arise from pyramidal neurons and project onto both excitatory and inhibitory distant cell targets (48, 49). Thus short range connections between nearby columns are slightly smaller than the size of hypercolumn, while the long range connections are clearly too long (not to mention sparse) to denote a tight functional coupling. A critical aspect for understanding how information is organized across a large neural population is to understand under which conditions local networks may communicate and modulate one another.

## ***1.2 Gain control & surround modulation***

Contrast gain modulation and surround suppression are two of the most studied examples of how network-interactions modulate single cell responses to incoming stimuli. When a sensory cortical area is presented with a stimulus of increasing intensity, the responses of neurons sensitive to the stimulus do not scale linearly with the stimulus strength. Rather, as stimulus strength increases, responses of neurons tend to be sigmoidal, with responses to strong stimuli saturating as intensity increases. This phenomenon, known as gain control, has been extensively explored in primary visual cortex (50–55), but has also been characterized in the auditory system, olfaction and somatic sensation (27). It

has been modelled by Heeger et al (1991) as the response of an individual neuron divided by the sum of responses of the local population of neurons, called divisive normalization. Gain control modulates neural responses as a function of stimulus intensity rather than stimulus size, is believed to function very locally, affecting populations of neurons whose receptive fields are within about 1 degree of one another. Evidence suggests that gain control is mediated by local inhibitory cells which modulate local excitatory cell responses(51, 55), but has also been suggested to be due to a decrease in excitatory synaptic strength(56). Normalization has been proposed to be canonical computation performed ubiquitously by neural circuits(52). The simplest example of such a circuit mechanism consists of a strong stimulus that drives an excitatory neuron, which then activates an inhibitory neuron that feeds back onto the excitatory cell and over the course of a few milliseconds (the time required for synaptic transmission) acts to suppress the activity of the excitatory cell. As the stimulus strength is increased, so is the overall amount of inhibition, such that the total inhibition scales as a function of the excitatory drive to the network.

Surround suppression is second example of how local networks shape the activity of individual neurons. When stimulus extends in size beyond the boundaries of the classical receptive field of a neuron, it is said to be in its 'surround', or in the extraclassical receptive field. The presence of a stimulus in the surround will modulate the firing of neurons to stimuli in the center. For example, as a visual stimulus increases in size, the firing rate of the neuron will initially increase with increasing stimulus size, but then when the stimulus exceeds about 1 degree, the response will begin to decline dramatically. The area over

which a neuron's responses increase with larger and larger stimuli is called its "summation field". As the stimulus continues to increase in diameter, the neuron's response begins to decline, due to the activation of surround inhibition. Surround effects have been subdivided into "near" (when stimuli are 0.5- of a degree of the peak response size) or "far" (when stimuli expand to 5-13 degrees from center)(57, 58). This is the most common type of surround modulation, known as surround suppression. Lateral, horizontal connections between cortical columns are sufficient to explain the mechanism by which gain control (described above) and near surround operates. But there exists also a 'far' surround that acts at distances ranging from 2 degrees to greater than 13 degrees for some cells(59–61). Far surround suppression can only be mechanistically possible by feedback connections from higher cortical areas(27, 44, 59, 62), and is highly dependent on the orientation of the stimuli in the surround, with maximum suppression produced by annular gratings with orientations matching the preferred orientation of neurons (58, 63). The reason extrastriate circuits must be invoked to explain far surround modulation is that there are simply no known horizontal, or geniculocortical connections between populations of cells within a cortical area that traverse the extent of visual space at which these effects are routinely observed (62, 64). Previous studies of surround suppression have shown that far surround suppressions is most likely mediated by feedback from extrastriate cortical areas, including V2, and not via the local cortical circuit within V1. By optogenetically inactivating V2 in anesthetized monkeys, Angelucci et al, showed that the V1 responses to stimuli of increasing size showed reduced surround suppression (49).

### **1.3 Coding visual stimuli with neural population activity**

Thanks to recent technological advancements, recording from many neurons simultaneously is now *de rigueur* for many electrophysiologists. While a great deal has been learned about how individual neurons respond to a multitude of stimuli, how they meaningfully interact was not a tractable problem prior to the development of multi-contact electrode arrays. Examining population activity is of vital importance – although the responses of single cells are clearly essential, sensory information is actually encoded in a distributed manner across populations of neurons (65). Otherwise why have so many neurons in the first place? Behavioral performance in visual, auditory, or motor tasks (66–68) is known to be much more accurate than would be predicted from the responses of single neurons (69, 70), with some neurons outperforming the animal (71). Furthermore, theoretical studies have demonstrated that coding strategies based on the responses of a population of neurons encode more information than coding strategies based on single-cell responses (72, 73). However, the rules by which signals across a distributed neural population are combined for perceptual decisions are unknown, and is a critical question addressed in the current work. To test how distant signals are combined for perception, separate populations of neurons in V1 must be simultaneously activated. While there exists a trove of psychophysical literature(74–76) examining how the presentation concurrent stimulus features (spatial frequency, orientation etc) interact to affect perception, electrophysiological studies on the topic are quite rare. Those that exist have primarily tested neural pooling rules in two ways: 1) by using a combination of orientation within a single stimulus, resulting in what are known as plaids(77), or 2) by electrically stimulating at two spatially disparate sites(78). While the first strategy lacks

causal manipulations of the local circuitry, and the second suffers from the non-specificity of electrical microstimulation (addressed in detail below), the common conclusions reached both types of studies is that for perceptual decisions, local populations of neurons form individual groups based on both function and spatial distance. At nearby locations (either in orientation space, or physical spacing of the stimulating electrodes at less than 1 mm) the activity of the separate populations is facilitative for behavior measures (77, 78).

Analyses of population activity that extends beyond the activity of individual cell responses to stimuli is still quite new, as recording from large populations is still gaining popularity. A commonly employed measures of population activity involves examining the variability of responses of pairs of cells across trials. This would be a good time to mention that cortical responses are notoriously variable across trials. Despite presentations of identical stimuli across trials, a neuron will respond with a slightly different number of spikes each time. This variability appears to be modulated by internal network states (79–81). Noise correlations, also called correlated variability, estimates the degree to which two cells (82) activity varies together. Noise correlations have been shown to vary across layers in a cortical column (82, 83), to decrease with attention (84, 85) and increase with anesthesia (81), and to change its structure depending on behavioral context (86). The horizontal distance between the pair of cells inversely affects the correlated variability between them, with the largest correlation values observed between cells spaced less 1 mm apart with similar orientation tuning(87). Vertically, across cortical layers, correlated variability is highest for superficial and infragranular layers, and lowest for layer 4C, which

is the recipient layer of LGN projections(82, 83). One commonly cited source of correlated variability is common input – two cells receive input from a common source, which then results in shared trial by trial variability. The common input may be bottom-up or top-down, as in the case of attention or task design. To date, no methods have been reported by which noise correlations can be causally manipulated without altering firing rates or other large scale confounding variables, such as arousal state (81, 87, 88).

#### ***1.4 Stimulating cortical networks overview***

In order to investigate the causal relationship between primary sensory cortex and perceptual decisions, external perturbations of neuronal populations are required. Prior to recent technological advances, the primary way to manipulate neuronal activity was by electrical microstimulation. This technique was made famous by the experiments of Penfield and Rasmussen (89), who electrically stimulated the brains of patients undergoing surgery. It has been used extensively to test the impact of cortical and subcortical areas in various behavioral tasks. In areas downstream to primary sensory cortex, manipulation of neuronal activity, has been consistently shown to influence perceptual decisions (5, 6, 8, 90–92). While this method provided many causal links between the activity of higher visual cortical areas and their role in perception(5, 6, 8, 90–92), the tool is imperfect for the study of V1. Experiments attempting to causally link neuronal responses in primary sensory cortex to behavioral decisions have rarely been performed (11, 93, 94) and in those rare instances when primary sensory areas were externally stimulated neuronal responses were measured using a single electrode. Microstimulation of V1 activates a large population of neurons with various properties,



and it does so synchronously. This results in phosphenes, which appear as uniform patches of luminance in the visual field, and bear little resemblance to the properties of individual V1 neurons (most of which are known to prefer oriented gratings(19)). When a phosphene is generated, it suggests that the perceptual circuitry is being engaged too strongly, thus making it impossible to disentangle the role of V1 from those of later stages of processing. As the cortex is a veritable salad of cell types with varying properties and connection motifs (45), stimulating all of them simultaneously is of limited use when studying the circuitry mediating behaviors (95). Although the psychophysical detection thresholds for electrical stimulation of V1 have been shown to vary as a function of cortical layer (96–98), I find no evidence of cell-type specific differences in activation thresholds. The recent development of optogenetics techniques has greatly helped in circumventing many of the limitations of electrical microstimulation.

It's not an overstatement to say that optogenetics has revolutionized electrophysiology in the last decade, by opening up the possibility of isolating genetically-defined cell types within a heterogeneous network. Optogenetics, in a nutshell, is the introduction of single genes encoding light-gated, ion-conducting proteins ("opsins") into genetically targeted cell types, enabling their activity to be driven or suppressed with the use of light. When these proteins are expressed in neurons, light can be used to open these channels, thus modulating the intra/extracellular ionic balance and thereby elicit or suppress action potential generation. These opsins have generally been isolated from various microbial sources such as archaebacteria and algae, and recently modified variants are also being developed (99–101). One of the first and still commonly used opsins is

Channelrhodopsin-2 (ChR2) which opens when excited by light. This channel conducts cations, primarily sodium and calcium, and has fairly fast off kinetics (~10 ms)(102, 103). As mentioned, electrical microstimulation affects all cells in the vicinity of the stimulating electrode and has long lasting effects after the stimulation period ends(104). Optogenetic stimulation, in stark contrast, using cell-type specific promoter sequences, confers the ability to specifically target individual cell types for stimulation *in vivo*, and the time course of stimulation can be controlled to with millisecond precision(105), depending on the kinetics of the light gated channel employed. The mouse model in particular has seen an explosion of research taking advantage of the availability of well-defined transgenic mouse lines to specifically express optogenetic constructs in subtypes of cells, and dissect individual roles for each one within a single network. In particular, identifying and subsequently stimulating or inhibiting 3 distinct subtypes of inhibitory neurons in mice has revealed their differential roles in modulating the responses of local excitatory, pyramidal cells, with some cell types performing multiplicative/divisive-type actions and other playing more additive/subtractive roles(55, 106, 107). For example, when driving visual cortex with oriented gratings to produce tuning curves, the activity of somatostatin-positive interneurons has a subtractive effect on the activity of connected pyramidal neurons, reducing the amount of activity uniformly across all stimulus orientations, while the action of parvalbumin-positive interneurons is best described as divisive, showing a greater effect for optimally-tuned stimuli(55). Further, this strategy has illuminated the role these cells play in modulating gain control mechanisms(108, 109) discussed above. Using a combination of optogenetic stimulation and intracellular recordings in mouse visual cortex, Sato et al (108) were able to demonstrate that normalization functions not by an

increase in synaptic inhibition as previously thought, but by a decrease in synaptic excitation.

In recent years, there have been an increasing number of studies using optogenetic modulation in non-human primates with varying levels of success (11, 60, 94, 101, 105, 110–113). Studies in non-human primates are particularly important for understanding a complex visual system, and complex decision-making in general, more than can be expected from rodent models. Moreover, successful implementation of such tools in non-human primates greatly improves the prospects of therapeutic uses of optogenetics in humans. Unfortunately, optogenetic tools for use in non-human primates continue to be limited and have been developing at a much slower pace than those for mice, with very few of these current studies take advantage of the ability to target genetically-defined cell-types. Recently, Stauffer et al (114) used a two-virus system to target dopaminergic neurons in the midbrain, and while a couple (94, 115) studies used a glutamatergic cell targeting promoter sequence (CaMKII $\alpha$ ), they did so in conjunction with an adeno-associated viral vector (AAV), which has been shown to be less specific for targeting excitatory cells (116), compared to lentiviral vectors (105).

Our work uses recently developed optogenetic techniques, which have the advantages over electrical microstimulation in that 1) genetically specified cell types can be targeted and stimulated independently of their local circuit and 2) stimulation is highly precise in the temporal and spatial domains(117). Additionally, it has been shown that optogenetic

techniques function more so on the sub-action potential threshold level, altering resting membrane voltage rather than always generating a volley of action potentials(113). The subtlety of this this type of stimulation makes it more difficult to produce phosphenes, and thus, makes it an ideal choice for stimulating V1 and characterizing its role in visual perception. The work presented here addresses two important issues – 1) determining how information across populations of V1 excitatory neurons is integrated for perceptual decisions, and identifying population metrics which are indicative of this integration and 2) developing a novel optogenetic tool for non-human primates based on the recent discovery of an anion-conducting channelrhodopsin capable of silencing neurons(99). We addressed these issues using by recording from neural populations in V1 of awake rhesus macaques performing cognitive tasks.

### ***1.5 Hypotheses and Research Aims***

The central hypothesis that my work aims to address is that information encoded by subpopulations of glutamatergic neurons in primary visual cortex (V1) contributes directly to the formation of visual perceptions, and the modulating the activity of these neurons can directly alter the perception of visual stimuli.

#### **AIM 1: Demonstrate the viability of optogenetic techniques in non-human primates.**

Since optogenetic tools for non-human primates are very recent, implementing them is a non-trivial task. Our first aim was to 1) design an injection protocol to deliver the viral vectors containing opsin-encoding genes, 2) demonstrate expression of light-sensitive ion channels, by recording light-modulated neural activity and 3) ensure that our stimulation

and recording protocols did not evoke artifacts. Specifically, we targeted glutamatergic neurons by using a lentivirus vector, carrying the channelrhodopsin (ChR2) gene, under the control of an  $\alpha$ -CaMKII promoter.

**AIM 2: Measure the effect on visual perception following activation of glutamatergic neuron populations in V1.** Animals were trained on a contrast detection task, and half of the trials are paired with optogenetic stimulation. In addition, 50% of the trials contain no visual stimulus ('catch trials') which allows us to ensure that the animals was correctly performing the task and provides a measure of whether our stimulation protocol is evoking phosphenes. If our hypothesis is correct, the small changes in firing rate associated with the optogenetic stimulation could alter the animal's ability to see near-psychophysical threshold stimuli (stimuli that are barely visible), as the addition of a few spikes could make the difference between a hit and a miss.

**AIM 3: Characterize how the optogenetic stimulation affects the activity of individual neurons and populations of neurons and how these changes in activity correlate with behavioral changes.** To address this, we examined 1) the firing rate changes following optical stimulation of various neuron populations (neurons that responded to the optical stimulation, neurons that responded to the visual stimulation, neurons that responded to both), 2) the effect of optical stimulation on noise correlations (trial-by-trial firing rate correlations between pairs of neurons) and the subsequent effect on the population signal to noise ratio, and 3) how the changes in behavior might reveal

the underlying dynamics by which signals in V1 are pooled for use in perceptual decision-making.

**AIM 4: Develop a novel optogenetic tool for non-human primates using GtACR-2 and examine how *suppressing* glutamatergic neural populations impacts stimulus encoding, detection behavior and measures of population coding.** The recent discovery of a new light gated channelrhodopsin(99) capable of strongly suppressing the activity of neurons presented an irresistible opportunity to modulate the neural circuit in the opposite direction as in the previous aims and to look at the effects on perception and neural coding. This study presents the first implementation of this novel channel in the non-human primate. First we demonstrated that this novel channel is capable of strongly suppressing neural activity in macaque primary visual cortex. Next, we explored how inactivating neighboring cortical columns affected stimulus responses in V1. The strength of a visual stimulus drives responses in V1 in a non-linear fashion that is due to alterations in the balance of excitation and inhibition (118). Specifically, we asked whether we could find direct evidence of this change in excitatory/inhibitory balance present in the network, by suppressing a portion of the local neighborhood and recording the responses of neurons to visual stimuli of differing contrast. We also asked whether suppressing neural activity would affect the detection of the visual stimuli by the animal.

## **CHAPTER II: METHODS**

### **2.1 Animal subjects**

Two male rhesus monkeys (*Macaca mulatta*; M1, 15 kg; M2, 13 kg) were used in the experiments. Monkeys were previously trained in visual discrimination and detection tasks and were surgically implanted with a titanium headpost device and two 19 mm recording chambers (Crist Instruments) over areas V1 and V4.

### **2.2 Viral vector injections**

#### **2.2.1 Channelrhodopsin-2 (ChR2) construct**

ChR2 was expressed specifically in V1 excitatory cells using VSVg-pseudotyped lentivirus carrying the ChR2-GFP gene with behind the CaMKII $\alpha$  promoter - the same lentiviral vector as used previously in monkeys by Han et al(105). High titer ( $> 10^9$  IU/ml) purified lentivirus was obtained from the University of North Carolina Gene Therapy Center Vector Core. With the animal, awake and head-fixed, virus suspension was injected through a 29 gauge needle connected via mineral oil filled tubing to a Hamilton syringe mounted on a syringe pump (KD Scientific), mounted over the stainless steel recording chamber. The needle was advanced by a precision, computer controlled micro-manipulator (NAN instruments) to a pre-established depth (corresponding to the lowest depth at which unit activity was found in preliminary experiments). After a 15 minute of waiting (to allow for stabilization), 1  $\mu$ l of virus suspension was delivered over a 10 minute period. Following a wait period of 5 minutes (to allow the suspension to diffuse into the tissue) the needle was then retracted slowly upwards (0.1 mm/min) in 200-300  $\mu$ m steps

and an additional 1  $\mu$ l of virus suspension was delivered at 3-4 additional depths. Five minute wait periods were interleaved before and after each virus delivery and retraction steps. A specially designed grid with either 0.6 or 1 mm spacing was used to position the injections and subsequently precisely target the injection sites for stimulation. Multiple injections across columnar sites (8 columns for M1, 11 for M2) were performed in each V1 chamber, closely grouped together and forming a rectangular pattern. A total of 60-70  $\mu$ l of the viral construct was delivered in each V1 area, separated into 2 or more continuous clusters. 1  $\mu$ l of virus has been shown to diffuse across 1 mm of cortex. To ensure a target area where expression was dense and easily detectable, we purposefully spaced injection sites between 200-300 microns vertically, and 600-1000 microns laterally. The external boundary of each injection site cluster was about 3 by 2 mm.

### **2.2.2 Gt-ACR2 construct**

Injections of the lentiviral vector containing the gene for Gt-ACR2 under the control of the  $\alpha$ -CaMKII promoter was performed in similar fashion to the ChR2 injections, with a few notable differences. The plasmid for this construct was obtained from Dr. John Spudich's group that had isolated the channel(99), and was packaged in a lentivirus carrier by the University of North Carolina Gene Therapy Center Vector Core. Using the same two monkeys as before, we injected a total of 20  $\mu$ l of virus in each V1 chamber. The injection sites were chosen to be as distal from the ChR2 injection sites as possible, at least 6 mm away (the distance long range horizontal connections traverse). The total virus volume was divided amongst 4 distinct vertical sites, spaced maximally 1 mm apart. Within each vertical site we delivered 1  $\mu$ l of virus suspension at 5 different depths, spaced vertically



about every 0.75 mm, starting with the lowest depth. Unlike the ChR2 injections, rather than use the perfusion pump, the loaded syringe with the needle was mounted right onto the grid and could be positioned in the z direction in to the cortex with the computer-controlled micro-manipulator. To deliver the virus suspension, a custom adaptor, mounted a separate channel of the micro-manipulator unit, was made to push down the syringe plunger. To obtain a rate of 0.1  $\mu\text{l}/\text{min}$ , the speed of the microdrive was adjusted to 0.004 mm/sec (using a 29 gauge, 10  $\mu\text{l}$  Hamilton syringe).

### **2.2.3 Cortical biopsy & immunohistochemistry**

To assess the expression patterns of Gt-ACR2 in monkey cortical tissue, we developed a novel biopsy procedure that allowed for continued neural recordings in this highly-trained animal, albeit not at the site of the biopsy. To do this, we enlarged the opening of one hole on a grid, similar to those used for recordings and injections, to accommodate the diameter of an 18 gauge needle. The grid was mounted on the recording chamber, and the enlarged hole was positioned over a site at which we had previously recorded robust suppression in response to optical stimulation. The grid was also positioned at the lowest point possible in the chamber, to be nearly flush with the tissue. An 18G needle, mounted on 1 ml syringe, filled with saline, was slowly inserted through the dura to a pre-determined depth such that the start of the needle bevel would reach 2 mm below the dura, slightly overestimating the thickness of the cortex. The syringe was allowed to rest in place for approximately 10 minutes. Next the syringe was then rotated slowly, to cut through the tissue laterally. While pulling up on the syringe plunger, to create a small amount of negative pressure sufficient to keep the tissue sample inside the needle, the

syringe was slowly withdrawn from the brain. The tissue sample was then immediately put into an iced paraformaldehyde solution (4%) and allowed to soak for 5 hours. The monkey was awake during the procedure and did not indicate signs of discomfort (the needle was only moderate larger than the electrodes used on a near daily basis). Following the biopsy we noticed some bleeding, but concluded that it was from the layer of granulation tissue on the surface of the chamber rather than from within the brain itself. The monkey shows no adverse effects 2 months following the procedure. Immunohistochemistry and microscopy was performed by Dr. Elsa Rodarte Rascon. Briefly, the sample was stained with three antibodies against: 1) Gt-ACR2 (custom from the Janz lab), 2) NeuN, a pan neuronal marker, and 3)  $\alpha$ -CaMKII, an excitatory neuron marker.

### ***2.3 Electrophysiological recordings***

The laminar electrodes (U-probe, Plexon Inc) consisted of a linear array of 16 or 24 equally spaced contacts (100  $\mu$ m inter-contact spacing). Each electrode contact was 25  $\mu$ m in diameter and platinum iridium coated. The impedance at each contact was 0.3–1.0 M $\Omega$ . Real-time extracellular neuronal signals (simultaneous 40 kHz A/D conversion on each channel) were analyzed using the Multichannel Acquisition Processor system (MAP system, 64 channel, Plexon Inc). Single-unit recordings were amplified, filtered (0.7-300 Hz for local field potentials; 100-8000 Hz for spikes), and heard through a speaker. Waveforms and continuous signals were recorded and viewed online (Sort Client, Plexon Inc.) Light-induced artifacts were sometimes present in the local field potentials (noticeable as large, downward voltage deflections coincident with laser onset and offset

across multiple channels), but not in the high-pass filtered spike data. This was confirmed with periodic recordings in saline. Electrodes and optical fibers were positioned in the grid using stainless steel guidetubes and advanced in the z direction with a chamber-mounted Microdrive system (NAN instruments) at speeds ranging from 1-200 microns per second.

## ***2.4 Delivering light to neurons***

Optical stimulation was achieved using a 100 mW, TTL controlled, DPSS blue (473 nm) laser (RGLase) coupled to a 200  $\mu\text{m}$  optical fiber. The end of the fiber was inserted into a 356  $\mu\text{m}$  cannula and mounted on the NAN Microdrive. The power at the tip of the fiber optic was measured every few months *ex vivo* using a light power meter (Coherent Lasermate power meter). The light intensity at the tip of the cannula was kept to  $\leq 50\text{mW/mm}^2$ . The cannula was then slowly lowered into the brain at one of the injection sites. One laminar electrode (U-probe, Plexon Inc) was also mounted on the microdrive and advanced transdurally through the grid at 0.6 mm (center-to-center) distance from the fiber. In some of the recording sessions a second laminar electrode was used, located 1 mm from the optic fiber. The largest possible distance between the surface of the optic fiber and the recording contacts on the electrode was approximately 200  $\mu\text{m}$  for the nearest electrode and 640  $\mu\text{m}$  for the furthest electrode. However, in the region where the fiber optic approaches with the recording contacts of electrodes, we often observed a much closer spacing due to a very slight angle inside the guide tube towards the optic fiber, with the fiber optic nearly touching the surface of one of the electrodes. Efforts were made to point the fiber optic, which was beveled on one side toward, the nearest electrode's contacts, in order to maximize the chances of recording light driven neural

activity. The optic fiber and electrodes were mounted separately and could be manipulated independently. In some of the sessions, recordings were made from area V4 from neurons with matching receptive fields to injected V1 area, using a third laminar electrode mounted on a separate microdrive over the V4 chamber. After advancing the optic fiber and recording electrode into the cortex and reaching the injection depth, optical stimulation of the neurons was achieved by delivering 10-15 bursts of 5-15 ms light pulses at 15-50 Hz. The laser output was regulated via TTL pulses driven by a waveform generator (Model 3220A, Agilent Technologies), controlled by the experiment control module (FHC Inc). Data across sessions was combined since there was no significant difference across stimulation frequencies. The control sessions were completed utilizing the same procedures described above, except that the optic fiber was positioned 1-3 mm from the nearest injection site. Only sessions in which we recorded statistically significant light responses (see section 2.6.2) were included in subsequent analysis, as this was the only way to confirm that the light was hitting a transfected cell population.

## ***2.5 Behavioral tasks***

### **2.5.1 ChR2 detection task**

Monkeys performed a detection task using gray-scale sinusoidal gratings of various luminance-varying contrasts. Stimuli were generated using Matlab with Psychophysics Toolbox (119) and presented binocularly on a computer screen on a dark background at a viewing distance of 90 cm. Monkeys were required to fixate on a central point ( $0.4^\circ$  in size) within a  $1^\circ$  fixation window while stimuli with a diameter of 2-3 deg were displayed at 2-4 deg eccentricity. The location and size of the stimuli covered the multiple receptive

fields of the cells recorded. Receptive fields were mapped at the beginning of each recording session using a sequence of 6 oriented gratings flashed for 1 frame each (presented at 60Hz on a Sony CRT) with a size of 0.5 degrees (square). This stimulus sequence was repeated and placed randomly at 324 positions on the screen, comprising an area of 9 by 9 degrees. Receptive field maps were generated by calculating the firing rates of individual neurons to optimally oriented stimuli across this 9 by 9 grid. Monkeys were required to maintain fixation throughout each trial. If fixation was broken, trials would abort. Eye position was continuously monitored using an infrared, mirror-based eye tracking system operating at 1 KHz (EyeLink II, SR Research Ltd.). Monkeys were also required to grasp a metal lever at the onset of each trial and maintain contact until the behavioral response was cued by the disappearance of the fixation point. Custom Matlab scripts monitored behavioral parameters and delivered juice rewards.

Stimuli consisted of gray-scale sinusoidal gratings with fixed spatial frequency (2.2 cycles per degree), displayed for 800-1300 ms, starting 450-1000 ms after fixation onset. While spatial frequency was held constant for all sessions, the orientation of the grating could vary within and across sessions. The low luminance contrast values were chosen such that stimuli elicited small, unsaturated neural responses, around the psychophysical detection threshold determined for each monkey in preliminary experiments. Stimulus duration was titrated to obtain a range of behavioral performances in both monkeys. We aimed to define a stimulus set that would yield a typical psychometric response curve, with behavioral detections of 25%, 50%, 75% and 100%. Luminance contrast was defined as the change in luminance (peak to trough), divided by the mean luminance for

each sinusoidal grating. Peak luminance values for each stimulus were 0.107, 0.120, 0.133, 0.280  $\text{cd/m}^2$  and 0.08  $\text{cd/m}^2$  in the no stimulus condition (Tektronix, J17). Stimuli could have one of 4 different luminance contrasts and were present on 50% of the trials. At the end of stimulus presentation, monkeys were required to signal the presence of the stimulus by releasing the lever or maintaining contact if no stimulus was displayed. Correct behavioral responses were rewarded with 5 drops of juice. Optical stimulation was triggered simultaneously with the onset of the visual stimuli (or at the time when a stimulus was expected, on no-stimulus trials). Optical stimulation was present on 50% of trials, evenly distributed for each stimulus condition, including the blank (no stimulus) condition. Each session consisted of 160-720 total trials. Sessions in which more than one stimulus orientation was presented, trials were split according to orientation, and analyzed independently. In 11 sessions we were unable to derive clear tuning curves for the population and grouped these sessions into near and far categories based on the presence or absence of a neural response to the oriented grating (these sessions had receptive fields). These sessions were excluded from any analyses that required measurements of orientation difference, such as Figure 2H. Behavioral and neural results are robust to the exclusion of these 11 sessions.

### **2.5.2 Gt-ACR2 detection task**

Monkeys performed a similar visual stimulus detection task as with the ChR2 experiments, with a few notable detail differences. Oriented sinusoidal gratings of 2-3 degrees in diameter of varying contrasts (0, 2.5, 3.5, 10, 20, 50 or 100%) were presented

for 300 ms on a medium gray background ( $20.5 \text{ cd/mm}^2$ ) (Figure 11B). Optical stimulation occurred on 50% of all trials, and again was synchronized with the start of the visual stimulus, consisting of 300 ms of continuous illumination. Again, all trials were randomly interleaved. Continuous light was used for these experiments for two reasons: 1) previous pilot experimenting using a different inhibitory opsin, ArchT, showed that continuous light was better able to show indirect suppressive responses. 2) A recent study showed that by using continuous light with Gt-ACR2 would minimize excitatory responses if the light shone at the synaptic terminal, which has a chloride concentration gradient of opposing drive than at the cell body (120). This latter point is discussed in further detail in Chapter V.

### **2.5.3 Experimental order**

For each recorded population of neurons, several tasks had to be run in order to characterize essential responses of the population, amounting to >1000 trials for the animals. First, once a stable neuronal population was isolated on the electrode contacts, their responsiveness to the laser was tested. Briefly, animals would fixate on a computer screen during trials that involved a balanced combination of laser/no laser and stimulus/no stimulus events (stimuli when present consisted of cardinally oriented, 100% contrast gratings on a gray background). If cells proved to be laser responsive (assessed by preliminary analyses on unsorted data, comparing laser versus control trials with T-tests), then further tests were performed to assess the location of the receptive fields and the preferred orientation of the population. If neurons proved not be laser responsive, the electrode would be moved until a new population of cells was present and the laser-

responsiveness testing would recommence. Once these three parameters (laser responsiveness, RF location, and orientation preference) were established, the position and orientation of the stimulus to be used in the detection task could be programmed. Monkeys were limited to work for a maximum 6 hours per day. The total number of trials we were able to run on the detection task depended on how long it took to establish these cell properties.

## **2.6 Data analysis**

### **2.6.1 Spike sorting**

Spike sorting was performed offline using waveform-based principal component analysis software (Offline sorter, Plexon Inc). Briefly, following noise and electrical artifact removal, single units were identified based principle component cluster separation, waveform amplitude ( $>2\times$  background amplitude) and interspike intervals ( $<0.5\%$  of spikes occurring within less than 1 ms). Any channel that did not meet these criteria was considered a potential multiunit. Subsequent analysis to definitively identify signals was performed using custom scripts (Matlab, Mathworks Inc) described in the next section.

### **2.6.2 Cell identification**

Optically modulated cells were identified by comparing the firing rates during the laser-on period with both the equivalent period in the control trials, and the 400 ms period before the onset of the first laser pulse (Wilcoxon rank sum test). Cells that were augmented and that were suppressed by the laser were both considered “laser responsive” and grouped together unless otherwise stated. Stimulus responsive cells were identified by comparing



the firing rates during a fixed period of 300 ms, beginning 35 ms after the onset of the visual stimulus and the corresponding period during the no-stimulus trials. This was done for each luminance contrast separately and a neuron was labeled stimulus responsive if the test was significant (Wilcoxon rank sum test) for either of the 2 of the high luminance contrast conditions, or for both of the 2 low luminance contrast conditions. Visual responsiveness was also assessed based on cell responses to full contrast oriented grating stimuli using the same statistical criteria. Only control trials (without laser stimulation) were considered for stimulus responsiveness.

### **2.6.3 Orientation selectivity**

Orientation preference for each cell was measured before the behavioral task. Monkeys were required to fixate on the central fixation spot while a reverse correlation stimulus consisting of a sequence of 48 circular full (100%) contrast sinusoidal gratings (8 equidistant orientations randomly flashed at 30 Hz) was presented for a total duration of 1.6 s. The size and location of the stimuli were kept identical to the ones used in the detection task. Preferred orientation and orientation selectivity index (OSI) for each neuron were computed from Fourier components extracted from the orientation tuning curves as described previously (121, 122). To obtain the mean orientation preference for each penetration, we averaged over all responsive neurons within the vertical column spanned by each laminar electrode. Fifteen sessions included recordings from 2 laminar electrodes, placed near the optical fiber. In 5/15 sessions, laser responses were found along both electrodes and we estimated the tuning of the entire population by averaging orientation preferences across both electrodes (the differences in preferred orientation

across the electrodes was between 5-25 deg). For most of these sessions laser responses were found only along one laminar electrode (10/15), in which case the data from the unresponsive electrode was not included in the analysis.

#### **2.6.4 Noise correlations**

Noise correlations are calculated as specific definition of the more general Pearson correlation,  $R(x,y)$ , of two signals,  $x(n)$  and  $y(n)$ . The MATLAB function *corrcoef* was used to calculate correlations. In this case,  $x$  and  $y$  are spike counts from pairs of simultaneously recorded neurons in each session, obtained from the first 335 ms of each trial ( $n$ ). Noise correlations were calculated separately for laser and control trials. Aberrant trials in which either of the cell pair's firing rate was greater than 4 standard deviations from the mean were excluded, as were neurons whose mean firing rate across trials was less than 1Hz. To compare across visual stimulus conditions given the similarity in firing rate and behavioral changes, the two lowest and the two highest stimuli were grouped together to increase the total number of trials for each pair, and thus increase the reliability of the noise correlation coefficient estimate. This was done by first z-scoring the firing rates in each condition, then combining trials across stimuli prior to calculating the noise correlation coefficient. Statistical significance of these results was assessed by bootstrapping (with replacement) 1,000 times. Figure 5B shows the un-bootstrapped average noise correlation values in each condition. The distributions shown in Figures 5C&D were bootstrapped across all pairs in each condition. For the blank/no stimulus condition, pairs across both near and far conditions (see Chapter III for descriptions of near and far criteria) were sampled, since the stimulus conditions were equivalent.

### 2.6.5 Population Signal to Noise Ratio

The population SNR ( $SNR_p$ ) was calculated using methods identical to Zohary et al (1994) (equation 1), which, estimates the contribution of  $M$  identically distributed neurons to a sensory decision pool as a function of correlation strength between neurons.

$$(1) \quad SNR_p = \frac{M\langle X \rangle}{\sqrt{M\sigma^2 + M(M-1)r\sigma^2}}$$

Where  $M$  is the number of neurons,  $\langle X \rangle$  is the mean spike count for  $M$  neurons,  $\sigma^2$  the standard deviation of this spike count, and  $r$  mean noise correlation. Calculations were performed with spike counts from laser-responsive neurons, separately for laser and control trials using the first 335 ms following stimulus onset. For Figure 6 panels F&G, to calculate the changes in total SNR, we arranged the neural data according to the average difference in orientation of the simultaneously recorded cell population and that of the stimulus orientation in any one session, ranging from smallest to largest. We then calculated the total SNR based on average responses (firing rates and noise correlations) from bootstrapped samples from cells distributed across 10 sessions. This process was repeated sliding in increments of 5 sessions until all sessions were included. For each group of 10 sessions, we also calculated the average difference in orientation (plotted on the abscissa) and the average change in behavioral performance following optogenetic stimulation (Fig.6G).

# **CHAPTER III: SPATIALLY-LIMITED NEURAL POOLING FOR VISUAL PERCEPTION**

## **3.0 Introduction**

Detection is the crucial first step for any perception-based decision-making. From an information processing perspective, visual detection can be described with an explicit encoding stage, and a decoding stage. The encoding stage generates a noisy representation of the stimulus that is then used by the decoder to maximize task performance, with the decoder comparing the result of the encoding stage with a decision criteria (Fig. 1A). Further, it has become evident that visual stimuli are encoded in a distributed manner across populations of neurons (10, 124, 125), rather than within individual, independent cells, as previously proposed (126, 127). Thus perceptual decisions critically depend on the pooling of neural signals, but the rules governing this process have rarely been explored electrophysiologically. The simplest strategy is to interrogate only the responses of neurons tuned to incoming stimuli. However, sensory neurons typically have bell-shaped tuning curves, and neurons are often activated by stimuli that differ widely from their preferred features. Thus, an alternative strategy is that behavioral performance relies on the responses of diverse populations of neurons that include the cells that do not prefer the stimulus. While both of these strategies have been proposed to mediate the encoding of neural activity relevant for perception, exactly how the pooling of signals originating from diverse neural subpopulations is accomplished remains mysterious. How could we identify the rules by which perceptually relevant signals are integrated by neuronal populations in sensory cortical areas?

Here we examined how diverse neural signals are pooled during perceptual decision-making by focusing on macaque primary visual cortex (V1), which is the first cortical site of visual processing and provides the majority of afferent inputs to higher visual areas (1). To examine how the information across distinct neural populations in V1 is pooled during visual perception, we simultaneously activated two sub-groups of neurons using a combination of visual and optogenetic stimulation while animals performed a contrast detection task. Area V1 exhibits a striking feature map of orientation selectivity, a common motif across many species of mammals, including, but not limited to, cats, monkeys, tree shrews and humans. Such feature space maps have been hypothesized to contribute to visual perception (128). We considered two, simple potential pooling rules for information integration as viable possibilities- 1) uniform or 2) non-uniform. In principle, for a basic yes/no detection task, a uniform pooling rule by which all available cortical signals are integrated irrespective of their tuning properties would be the better strategy for stimulus detection. However, V1, like many sensory cortical areas, has a conspicuous functional organization, whose role in neural coding is yet unknown. Hence, we considered the second possibility, that information from functionally similar populations might be preferentially integrated for perceptual decisions. In V1, functional similarity between two populations is inversely proportional the distance between them (with pinwheel centers being a special case). As the physical distance between pairs of cells increases, the probability that they will share a common orientation preference decreases systematically (129). Because of this property, we will use the terms “functionally” and “spatially” interchangeably from here on. We found that despite optogenetic stimulation elevating the firing rates of V1 cells across stimulus conditions (orientation and contrast),

behaviorally, improvements in stimulus detection were observed only when light targeted the neuronal population was functionally (and likely spatially) proximal to the visually-driven population. The optically-induced changes in behavioral performance could be well described by estimating the population signal to noise ratio using a spatially-weighted pooling rule. Our results indicate that, at a very local scale, information from neuronal subgroups is combined in a perceptually-relevant manner only when the subgroups consist of functionally similar, and likely spatially proximal, cell populations, in accordance with the functional organization of orientation in V1.

### ***3.1 Targeting excitatory neural populations in monkey primary visual cortex***

Populations of V1 excitatory neurons were rendered sensitive to light by expressing Channelrhodopsin-2 (ChR2), a broadly used light-sensitive cation channel. We recorded from a total of 1031 units (both single unit and multiunit activity were included) that were significantly responsive to visual stimuli or to optical stimulation. Of these, 597 (57.9%) showed a significant light modulation, with 92% showing an increase in firing rate, and 8% showing a decrease. The ChR2 gene was delivered via columnar injections of a VSV-pseudotyped lentivirus carrying the ChR2-GFP gene under the control of an  $\alpha$ -CaMKII promoter (Fig. 1B). This viral construct has previously been shown to express exclusively in glutamatergic neurons in primate cortical slices (105). Recordings were performed using 16-channel laminar probes closely aligned with a fiber optic for light delivery. Light was provided by a 473 nm, 100 mW laser, spaced about 290  $\mu$ m from the electrode contacts (see Methods). Of the cells whose responses were augmented by the laser,

72.5% also showed a significant response to strong visual stimuli presented over their receptive fields (76% of the cells suppressed by laser were visually responsive). Examples of single unit responses to optical stimulation are shown in Fig. 1C-E. Although stimulation of excitatory neurons may indirectly activate local inhibitory interneurons, we reasoned that this type of stimulation would be more similar to responses induced by natural stimuli (130) compared with other electrical and optical stimulation protocols that strongly activate all neuron types simultaneously.

Prior to any experiments, we confirmed that our stimulation and recording parameters did not evoke optical recording artifacts by comparing the spike waveforms and patterns of responses to continuous versus pulsed light stimulation *in vivo*, and the results were validated by additional controls in saline. Figs. 1D-E (inset) show the interspike interval (ISI) distributions for the units in Fig. 1D-E during the pulse laser stimulation which demonstrate the lack of light-induced artifacts (the artifacts would have been time-locked to the laser onset and offset). The direct effects of optical stimulation were observed across multiple channels of the laminar array and decayed exponentially as a function of distance from the electrode site nearest to the light source (Fig. 1F). Across sessions, the average direct laser-induced activity was found within 190  $\mu\text{m}$  (full width at half maximum, aligned to channel with strongest laser response, Fig. 1G), and the light-induced spiking activity was diminished drastically at longer distances. Weaker, indirect, network-based activation profiles were evident at latencies longer than 3 ms (Fig. S1). These results confirm that optical stimulation affects the activity of a small, spatially restricted subpopulation of neurons. To estimate the lateral spread of optical activation, we

reasoned that since light disperses through cortex in an approximately spherical manner from the tip of the fiber optic (117), and given that direct laser activation was maximally observed over a vertical range of about 190  $\mu\text{m}$  (Fig. 1G), we inferred that the horizontal light spread would be approximately equivalent, spanning about a quarter of the width of a hypercolumn in V1 one hypercolumn spans about 1mm (Hubel and Wiesel, 1968; Hubel and Wiesel, 1977).

### ***3.2 The effects of optogenetic stimulation on behavioral performance***

To understand how cortical signals are combined during perception, we simultaneously activated nearby or distant populations of neurons using visual and optogenetic stimulation (Fig.2A) while animals performed a visual detection task (Fig. 2B). To do this, we estimated the average preferred orientation of the laser responsive population online, and adjusted the orientation of the grating used in the detection task, to be either ‘near’ (within 45 degrees) or far (greater than 45 degrees) from the population preferred. (The final population average preferred orientation was then calculated offline, following spike sorting.) Given the prevalence of iso-orientation domains in V1, where orientation preferences smoothly transition across the cortical surface, the functional distance between the visually-driven and the optogenetically-driven populations could be varied by changing the orientation of the visual stimulus. The larger the orientation difference between the preferred orientation of the recorded cells and that of the visual stimulus, the greater the probability that the two populations would be physically separated across the cortical surface(129). Since the absolute relationship between physical distance and orientation preference is not a fixed one, depending on the proximity to the nearest



## Figure 1 | Targeting neural subpopulations.

(A) Even within a cortical area, natural sensory stimuli evoke a diversity of neural responses. How signals across subpopulations are integrated for sensory perception is unclear. In this study we used optogenetic activation of subpopulations to address this question.

(B) Virus injections and subsequent recordings were performed using a custom recording grid. We injected 1.0  $\mu\text{l}$  of virus in V1 at five cortical depths in a columnar fashion, at 8 locations in monkey 1, and 11 locations in monkey 2. Electrophysiological recordings were performed using 16-channel laminar electrodes. The laser power was titrated such that we used the maximum power that did not elicit any low frequency optical artifacts, caused by light shining directly onto the electrode contacts (105, 117), either in saline or *in vivo*.

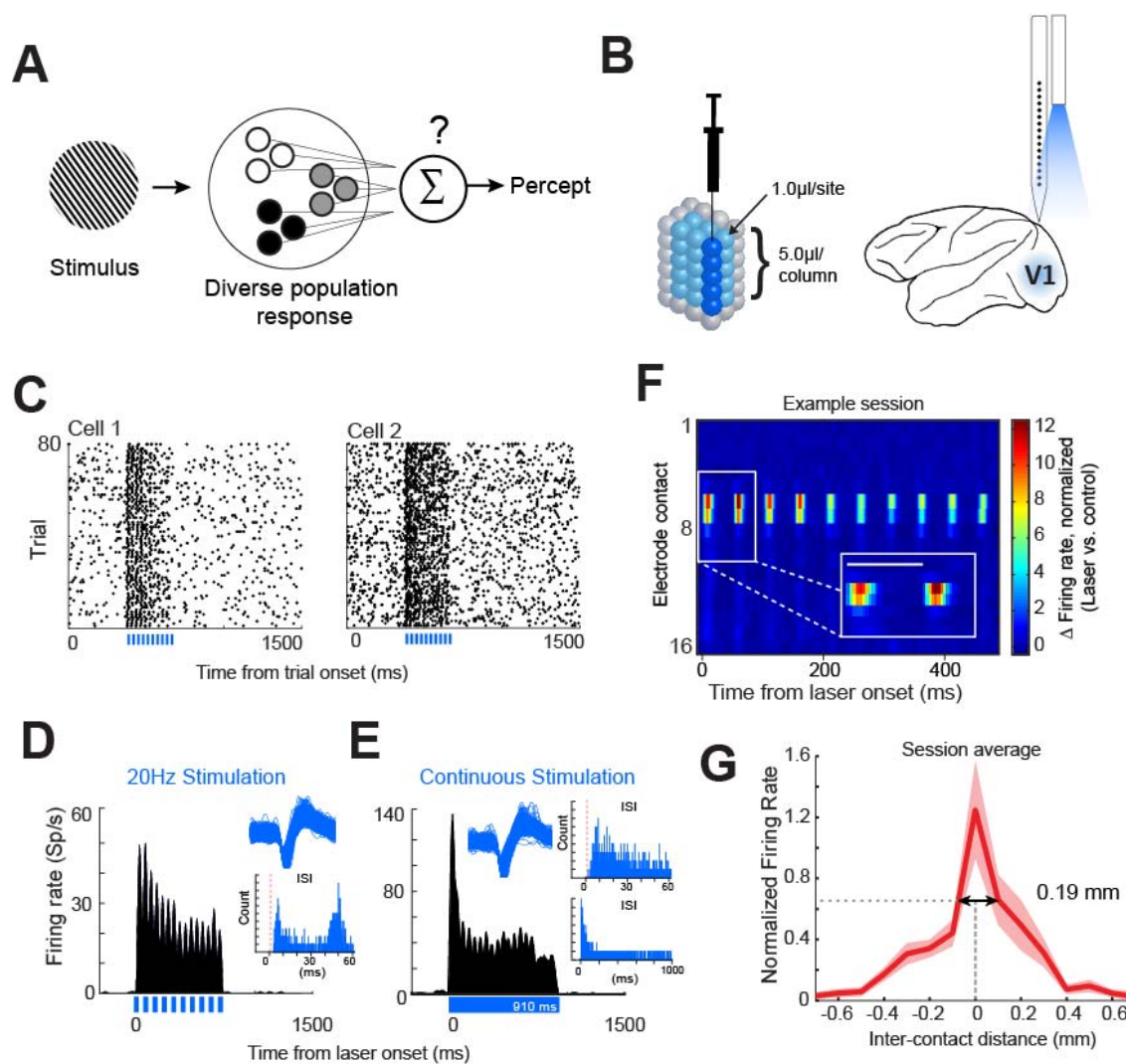
(C) Raster plots from 4 example V1 neurons showing increased activity in response to pulsed optical stimulation (laser timing shown in blue at the bottom of each plot), while the monkey fixated on a central point on a computer screen.

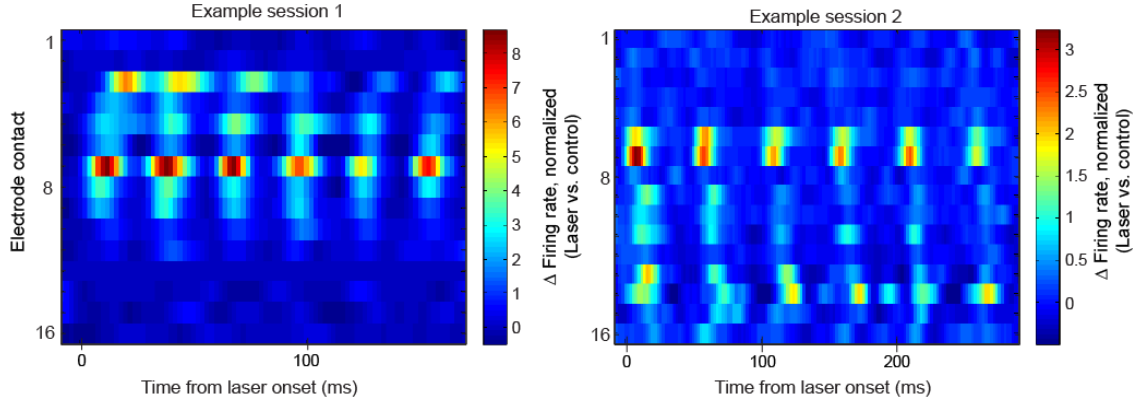
(D-E) To confirm the absence of optical artifacts, we compared the waveforms and firing rates of a sample of neurons (one example neuron shown in D, E) during pulsed (D) and continuous (E) laser stimulation. Left insets show the distinct action potential waveforms recorded in each respective experiment. Right insets show the interspike intervals (ISIs) in each stimulation condition. Vertical red dashed line denotes the 1 ms refractory period. Upper and lower insets in panel D show two different time spans. Optical artifacts, when present, occur only at the onset and offset of optical stimulation (117) and do not exhibit typical action potential waveform shapes. The sustained increase in firing rate during continuous laser stimulation (E) and the distinct waveform shape (D top inset, E left insets) are consistent with light-induced action potentials. We found normally shaped distributions of the ISIs instead of artefact sharp peaks corresponding to the end points of each laser pulse. During pulsed stimulation (D, bottom inset) the responses are distributed around the duration of each laser cycle period, without an intermediate peak at 10 ms corresponding to offset (width) of each individual laser pulse. Similarly during continuous stimulation (E, bottom right inset) there is no second peak that would correspond with the laser offset.

(F) Distribution of optically-induced activity across electrode contacts for one example session. Inter-contact spacing is 100  $\mu\text{m}$  (most superficial channel is labeled '1'). Inset shows the zoomed effect of the first two laser pulses (scale bar represents 50 ms).

(G) Spatial spread of laser activation. Normalized firing rates were aligned with the channel showing the largest change in laser-induced activity, interpolating for distances between channels, and averaged across sessions. Negative inter-contact distances represent channels above (closer to the surface of the brain) the reference contact. Dashed lines and arrows show the spatial spread of laser activity at full width at half maximum. Error envelope represents s.e.m.

Figure 1



**Figure S1**

### **Figure S1 | Propagation of optically-induced neuronal activity across the network.**

Two example sessions showing the progression of optically-induced neural activity in time across electrode contacts following the offset of each laser pulse. We hypothesize that this delayed activity is a result of local neurons receiving input from the laser-responsive neurons either directly or indirectly. Laser pulse durations for the left and right plots were 10 ms and 7 ms, respectively. Differences in mean firing rates between laser and control trials were normalized relative to the total activity during these trials for each channel separately. Responses were binned every 2 ms, and smoothed with a 5 ms Gaussian kernel to improve visualization. In cases where more than one neuron was found on a channel, the response of the most responsive neuron was included.

pinwheel center, we henceforth refer to this relationship as functional distance. In each session, we presented one or more stimulus orientations at various contrast levels such that stimulus orientation matched the neurons' preferred orientation or at an approximately orthogonal orientation. Animals were trained to report the presence or absence of a stimulus regardless of its orientation (Fig. 2B). Stimuli, covering the receptive fields of the recorded population, consisted of four different luminance-varying contrast gratings, presented for 1300 ms on a dark screen, and were randomly interleaved with 'catch' trials in which no stimulus was present (50% of trials). In order to

maximize the potential impact of the light-evoked spikes, we purposefully chose stimulus contrast parameters that would minimally drive neurons, while at the same time providing clear psychometric curves in each animal. Our design was motivated by previous reports that electrically evoked signals can summate in the cortex at distances of up to 1 mm (78)). Optogenetic stimulation (“laser”) was present on 50% of trials, and laser and control (no-laser) trials were randomly interleaved (Fig. 2A). The mean optical stimulation duration was  $315 \text{ ms} \pm 18 \text{ s.e.m.}$  with laser pulses delivered at 35 Hz in 85% of sessions (range was 15-50 Hz; data was combined since we did not find significant differences in neuronal and behavioral responses within this range of stimulation parameters, Fig. S2). The laser pulses were synchronized to the onset of the visual stimulus in order to approximately coincide with the robust transient response of V1 neurons. This was chosen because there was a clear decay in the ability of the optical stimulation to drive V1 responses with each subsequent laser pulse (Fig. 1C-E). We used a pulsed rather than continuous light protocol in order to precisely drive neuronal firing and avoid potential cell damage (117). We divided sessions into two broad categories – near and far - based on the difference in the preferred orientation (PO) of the recorded population compared to the orientation of the visual stimulus. The PO of the population was the average of the POs of the cells recorded in each session. This was done because our linear array was advanced perpendicularly with respect to the cortical surface and cells within a cortical column of V1 share similar orientation preferences. Fig. 2C shows a typical tuning curve for one example cell illustrating that ‘near’ stimuli were presented close to the peak of the tuning curve whereas the ‘far’ stimuli were presented at an orthogonal orientation. The cutoff criteria between groups was set to 45 degrees. Across sessions, the mean near

group orientation difference was 26.6 degrees  $\pm$  2.9 s.e.m. (29 sessions), while the mean far group orientation difference was 65.6 degrees  $\pm$  2.7 s.e.m. (27 sessions), shown in Fig. 2C-D ( $P < 0.001$  Wilcoxon rank sum test). As expected, behavioral performance was independent of stimulus orientation on control trials without optical stimulation, i.e., across sessions contrast detectability did not differ between the near and far stimulus orientations (Fig. 2E,  $P > 0.05$ , Kruskal-Wallis test). Optical stimulation, when introduced, had differential effects on detection performance in the near and far conditions. There was a significant improvement in the detectability of the two lowest contrast stimuli in the near condition, but no change in contrast detectability in the far condition. In the near condition (Fig. 2F), detection performance was improved by  $9.9\% \pm 2.9$  s.e.m. for the 0.25 contrast and  $7.6\% \pm 1.9$  s.e.m. for the 0.36 contrast (Kruskal-Wallis test  $P < 0.001$ , post hoc Wilcoxon signed rank test). Results were consistent for individual monkeys as well (M1:  $7.3\% \pm 0.3$  s.e.m.,  $P < 0.001$ , Kruskal-Wallis test, post hoc Tukey-Kramer test; M2,  $9.2\% \pm 0.5$  s.e.m.,  $P < 0.001$  for low contrast conditions together). No significant difference was seen in the far condition (Fig. 2G,  $P > 0.05$ , Kruskal-Wallis test). The improvement at low contrasts is expected, as the detection of such stimuli can only be based on very sparse spiking, so the addition of light-driven spikes will push the population response above the detection threshold more often. To more finely test the relationship between the perceptual improvement on functional distance, we analyzed the laser-induced changes in contrast detectability as a function of the orientation difference between the two populations. Behavioral results from smaller groups of sessions were averaged according to the difference in orientation between the session PO and that of the visual stimulus, into 10 degree bins. For each bin we calculated the corresponding laser-

induced change in detection performance. As shown in Fig. 2H, there was a parametric decrease in the observed change in detectability as the functional distance between the laser-driven and visually-driven populations increased; this trend was best described by an inverse exponential function (Fig. 2H, gray line). Note that the orientation information itself is irrelevant for the detection task, but provides a useful proxy for the lateral distance separating the visually-driven and optogenetically-driven neural populations. These results reveal that information can be combined from neural populations spaced, likely less than half of a millimeter apart. Any further, the populations appear to be functionally independent. To derive this estimate, we postulated that since a hypercolumn, containing all stimulus orientations spans about 1 mm (131), then every 10 degrees is represented within about 100 microns, thus, since we observed a stark difference for near (<45 degrees delta orientation) compared to far (>45 degrees), we estimate, admittedly very coarsely, this corresponds to about 500 microns of physical distance. This calculation has two important assumptions. First, it describes a portion of V1 in an iso-orientation domain where orientation changes vary linearly across the surface. There are, however, portions of V1 where orientation preferences change non-linearly, especially closer to pinwheel centers where orientation preferences spiral out and increase in size with distance from a single pin point. Second, it assumes orientation preference changes are isotropic, which is not always the case. However, qualitative inspection of orientation maps (129) reveals large portions of cortex where our assumptions *are* met and the likelihood of encountering a pinwheel center or fracture in the orientation map has surprisingly never been measured.

**Figure 2 | Detection performance is enhanced with optical stimulation according to functional distance.**

(A) To test the orientation specificity of information integration in a local cortical circuit, we activated two neural populations – one with a visual stimulus, the other with optogenetic activation. The functional distance between the two populations could be altered by changing the orientation of the visual stimulus to be near (upper) or far (lower) from the preferred orientation of the light-driven population.

(B) Detection task design. Following a fixation period, oriented gratings of 4 contrasts were presented. Half of trials contained no visual stimulus. Stimulus orientation varied across sessions and/or trials. Half of the trials were paired with optical stimulation. All contrasts and orientations were randomly interleaved. Monkeys were cued to report the presence or absence of a stimulus by a change in fixation point color.

(C) Example orientation tuning curve of one neuron. Arrows represent the orientation of the near (blue) and far (red) stimuli presented in that session.

(D) Mean difference between the population preferred orientation and that of the 2 stimuli across all sessions. \*\*  $P < 0.001$ , Wilcoxon rank sum test.

(E) In the control (no laser) condition, detection performance for near and far stimulus orientations was similar for all contrast levels.

(F-G) Percent target reports across sessions. Optical stimulation-induced change in behavioral performance when the neural population is exposed to the near (F) and far stimulus (G). Optical stimulation improved the detection of the two lowest luminance contrast stimuli in the near condition (\*  $P < 0.05$ , paired t-test), but had no significant effect in the far condition (G). Error bars show s.e.m. across sessions. See text for details.

(H) Light-induced activity increases detection performance exponentially decay as the functional distance between the two subpopulations grows. Black dots represent the mean change in target reports associated with the laser stimulation for groups of trials binned across sessions according to the orientation difference between the visual stimulus and the preferred orientation of the light-activated population. Bins were distributed in approximated 10 degree intervals. Vertical dashed line shows the division between near and far categories as defined in panels C-G. (From left to right,  $n=6,6,4,7,6,5,5,6$  sessions.) Error bars show s.e.m. Fit is exponential.

**Figure 2**

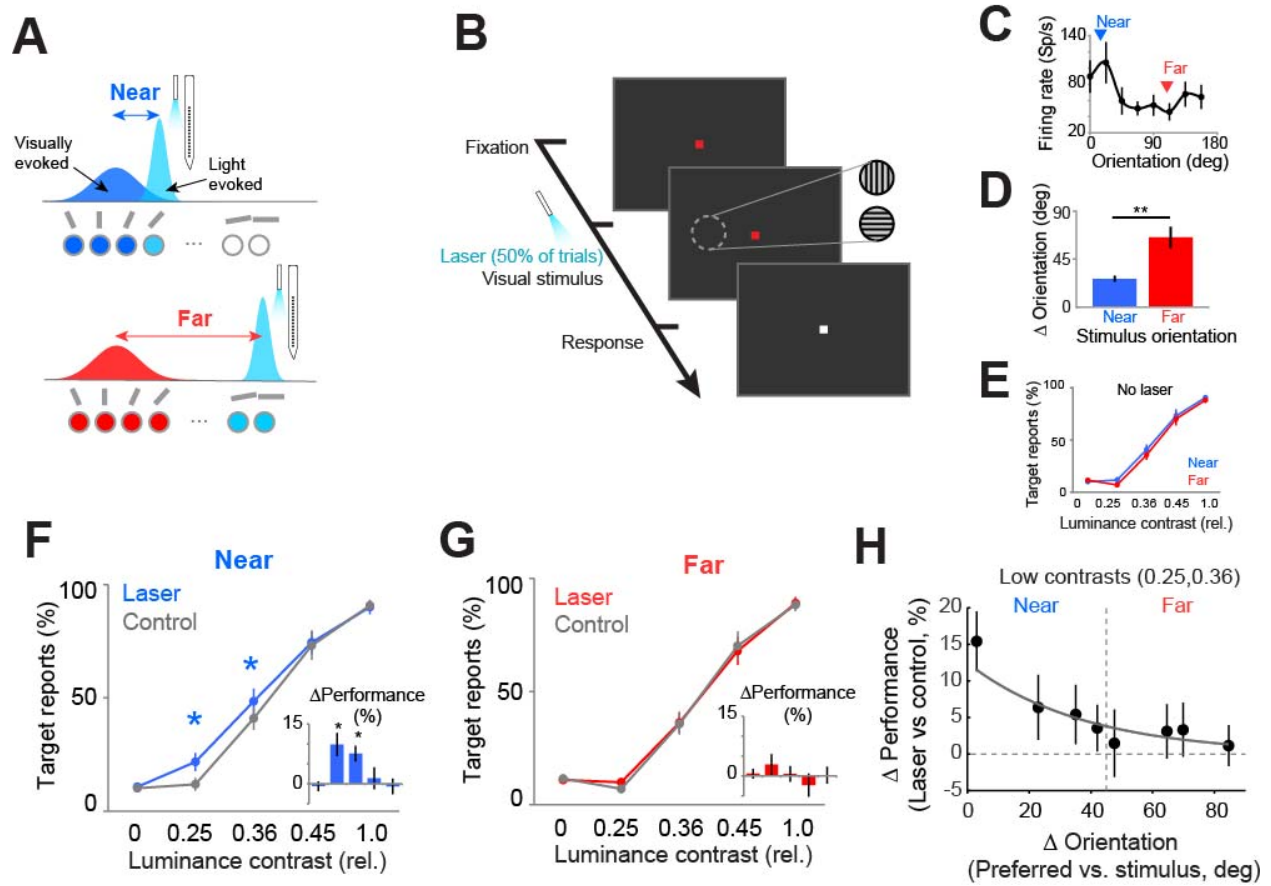
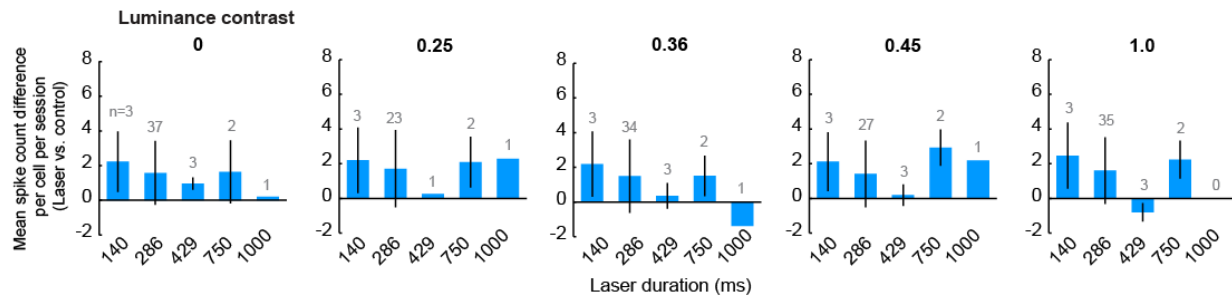




**Figure S2**

**A**



**B**

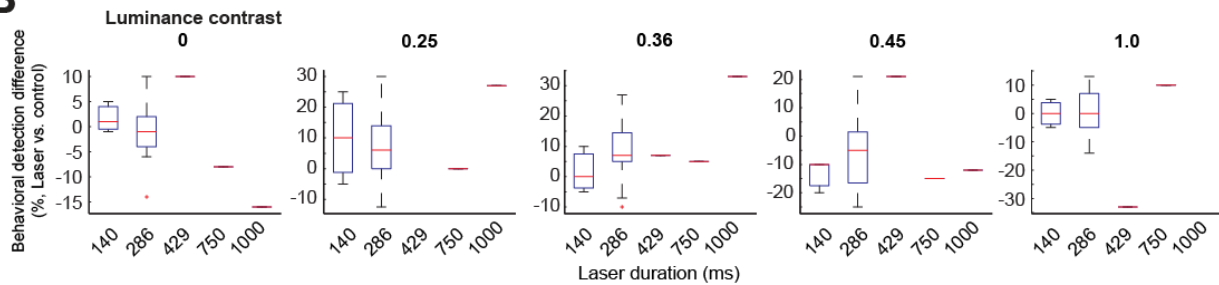


**Figure S2 | Differences in optogenetic stimulation parameters did not cause systematic differences in firing rates and perceptual detection performance.**

(A) The mean difference in spike counts for each laser-responsive neuron in the laser vs. control conditions, averaged for each session. The duration of laser stimulation produced no significant difference in the mean spike count change observed across conditions. This is not surprising given that the majority of firing rate change occurs during the first few laser pulses (Fig. 1), and is due to the inactivation kinetics of this variant of ChR2.

(B) Perceptual contrast detection performance (laser vs. control) for each luminance contrast level was not systematically altered when the duration of optogenetic stimulation was varied.

### **3.3 Behavioral changes are unlikely to be caused by phosphene induction**

Electrical stimulation has long been known to induce artificial percepts known as phosphenes (e.g., Brindley and Lewin, 1968). Optogenetic stimulation has also been

hypothesized to be capable of inducing phosphenes (11). To test whether our behavior effects could be accounted for by phosphene induction, we examined four measures that would be reflective of phosphene induction in our experiments: 1) false alarm rates; aborted trials due to 2) fixation breaks or 3) premature response bar releases, and 4) microsaccade counts. First, we examined the differences in false alarm rates (type 1 errors) between control and laser trials, when monkeys produce the behavioral response associated with the visual stimulus when, in fact, no visual stimulus is present. We found no significant difference in false alarm rates in any session type in which laser responses were recorded (Fig. 3A,  $P > 0.05$  Wilcoxon signed rank test after Kruskal-Wallis test). Second, we reasoned that the sudden appearance of a phosphene may be distracting to the animal and lead to reflexive shifts in attention that may result in erroneous eye movements or behavioral responses. Such breaks in fixation or premature behavioral responses would result in aborted trials. Again, we found no significant difference between laser and control trials in the number of aborted trials in each session due to fixation breaks (Fig. 3B,  $P > 0.05$  Wilcoxon signed rank test for all comparisons in this figure) and premature bar releases (Fig. 3C,  $P > 0.05$ ). Lastly, we counted the number of microsaccades that occurred during optogenetic stimulation and control trials in each session (Fig. 3D), but the differences were not statistically significant across the two animals ( $P = 0.57$ ). We thus conclude that the improvement in behavioral performance is unlikely to have been caused by optogenetically-induced phosphenes or by differences in eye movements.

**Figure 3**

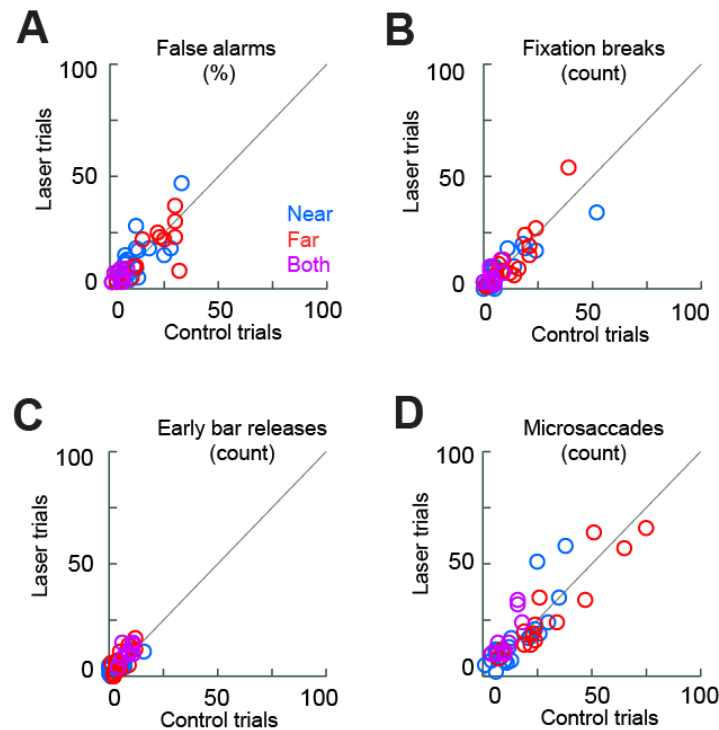


**Figure 3 | Optogenetic stimulation is unlikely to induce phosphenes.**

(A) False alarm rate - percent detections reported during no-stimulus (luminance contrast 0) trials. Circles represent individual sessions in which stimuli were presented at the near orientation (blue circle), far orientation (red circle), or both (magenta circles). ANOVA comparing across session types revealed no difference between groups ( $P=0.41$ ), and no difference between laser and control trials ( $P=0.45$ , Wilcoxon signed rank test).

(B) Fixation breaks - number of trials aborted in each session due to eye movements outside the fixation window. ANOVA comparing across session types revealed no difference between groups ( $P=0.60$ ), and no difference between laser and control trials ( $P=0.75$ , Wilcoxon signed rank test).

(C) Early bar releases - number of trials aborted in each session due to monkey releasing the response bar before the cued time. ANOVA comparing across session types revealed no difference between groups ( $P=0.11$ ), and no difference between laser and control trials ( $P=0.12$ , Wilcoxon signed rank test).

(D) Microsaccades - total number of microsaccades in each session during a 350ms window aligned with the start of the laser, or the mean time of the laser for control trials.

Further, to ensure that the behavioral effects reported here were solely due to optogenetic stimulation (rather than laser-induced local heating, or some other unexpected variable), additional control experiments were performed (5 sessions) in which the optical fiber and recording electrodes were positioned distal (1-3 mm) from the nearest injection site. As expected, optogenetic stimulation had no effect on neural activity (Fig. S3A-B,  $P > 0.05$ , Wilcoxon rank sum test), and although the cells were tuned to the stimulus orientation, there was no significant change in behavioral performance between the laser and control trials (Fig. S3C,  $P > 0.05$  Kruskal-Wallis test). In addition, even when we recorded at the injection site (4 sessions), when optogenetic stimulation was ineffective (no laser-induced spikes) there was no change in task performance (Fig. S3D).

### ***3.4 Optogenetic stimulation increases V1 responses uniformly across conditions***

To investigate the neural source of the behavioral improvement following optogenetic stimulation, we first examined the laser-driven changes in firing rates for the population of light-responsive neurons used in our detection task ( $n=597$  total units, see Methods for selection criteria, with each session contributing an average of  $14.2 \pm 1.5$  s.e.m. light-responsive units). Fig. 4 shows population firing rates evoked by **optogenetic** stimulation across stimulus conditions for the near (Fig.4A, blue traces) and far (Fig.4B, red traces) conditions. Note, that for the subset of units that were strongly driven by the low contrast stimuli used in this experiment, we saw evidence of contrast gain modulation following laser application, and exhibited decreased laser modulation as stimulus contrast was increased, Fig.S4. However, for the majority of units, we found that the laser drove neural

**Figure S3**

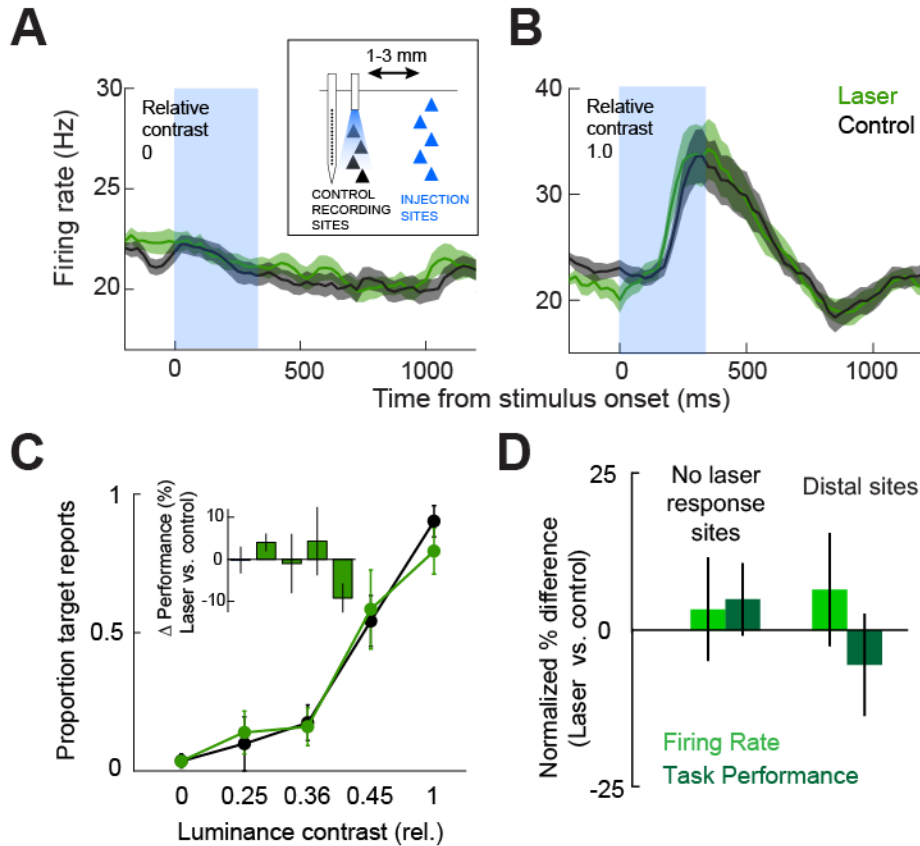


**Figure S3 | Optical stimulation of untransfected cortex.**

(A-B) Mean firing rate of neurons recorded away from the injection sites ( $n=56$  cells, 5 sessions) during the (A) no-stimulus, luminance contrast 0 condition and (B) strongest stimulus, relative luminance contrast 1.0, condition during control (black) and laser (green) trials. Optical stimulation parameters were identical to those described previously.

(C) Behavioral performance. Proportion of trials in which monkeys reported the presence of a stimulus (proportion of stimulus detections;  $P>0.05$  for all contrasts, Wilcoxon signed rank test). Inset shows mean percent change (laser vs. control).

(D) Summary of changes in neural responses and task performance across two types of control experiment. Bars represent the change in mean firing rate (light green, for all neurons in the two types of control sessions), and behavioral performance (dark green, relative luminance contrast 0.36) in the laser vs. no-laser conditions, respectively ( $P>0.05$ , Wilcoxon signed rank test).

activity, strongly and fairly uniformly across stimulus contrasts in both near and far conditions. We quantified the laser-evoked changes in firing rates for individual units (0-335 ms from laser onset) across stimulus conditions (Fig.4C,E,G). For simplicity, since the behavioral and firing rate changes were similar for these stimulus conditions, we grouped results from low contrasts (0.25 and 0.36) and high contrasts (0.45 and 1). Firing rates for individual units were z-scored across stimulus conditions. The distributions of the changes in the normalized firing rates across the entire population are shown for the no stimulus (Fig.4C), low contrasts (Fig.4E) and high contrasts (Fig.4G), for both near (n=329 cells) and far (n=268 cells) conditions. For all but one stimulus condition, the mean z-scored change in firing rate with the laser was 0.6. For the low contrast, far condition, this change was 0.5, which was significantly different from the other means ( $P < 0.01$ , Kruskal-Wallis test across all conditions, posthoc Tukey-Kramer test different from Fig.4E, left different from others). To examine whether this very small difference in firing rate change between the near and far conditions for the low contrast stimuli was systematic and could account for the differences in behavior, we examined the changes in firing rate as a function of the change in orientation (Fig.4D,F,H). As in Fig.2H, data from sessions were organized by the difference in orientation between the neural preferred versus the stimulus orientation, with the near condition spanning 0-44.9 degrees and the far representing greater than 45 degrees difference (Fig.4D,F,G, horizontal bars show the mean across near, shown in blue, and far, shown in red, conditions). The changes in firing rate were not significantly different across orientation difference or stimulus contrast ( $P = 0.35$ , Kruskal-Wallis test, across both near and far conditions and across stimulus contrasts). Unlike behavior, we observed no systematic change in firing

rate as a function of stimulus orientation for any stimulus contrast, and conclude that any small changes in firing rate across conditions was not sufficient to explain the improved detection performance on low contrast stimuli.

### ***3.5 Optogenetic stimulation influences population coding***

We next examined whether optogenetic stimulation influences the capacity of the network of cells to encode information. Since the information encoded in population activity is limited by correlated firing (72, 73, 82, 123), we calculated noise correlations (trial-by-trial covariation in spike counts) between the pairs of simultaneously recorded laser-responsive neurons during the stimulation period. Noise correlations are often said to arise from common input to the cell pair that causes their firing rates to modulate in a similar direction across trials (133–135). The effects of optogenetic stimulation on noise correlations are currently unknown. In principle, optogenetic stimulation increases firing rates by adding a common drive to nearby neurons which could increase correlated variability. Alternatively, if the underlying source of common drive to the cell pair is unaffected, the optogenetic stimulation may have no effect on noise correlations. We first focused on the low contrast condition, as this was the stimulus condition in which we saw an improvement in detection performance. Like for firing rates, we combined the data from the two lowest contrasts and the two highest contrasts to compute noise correlations, which increased the number of trials used in the calculation of noise correlations and hence the estimation accuracy. We found that the laser stimulation was associated with a significant reduction in correlations when the stimulus was optimally oriented (near condition, 28% reduction, Fig. 5A-B,  $P < 0.001$ , Wilcoxon signed rank test), but had no

#### **Figure 4 | Light-induced changes in neuronal responses.**

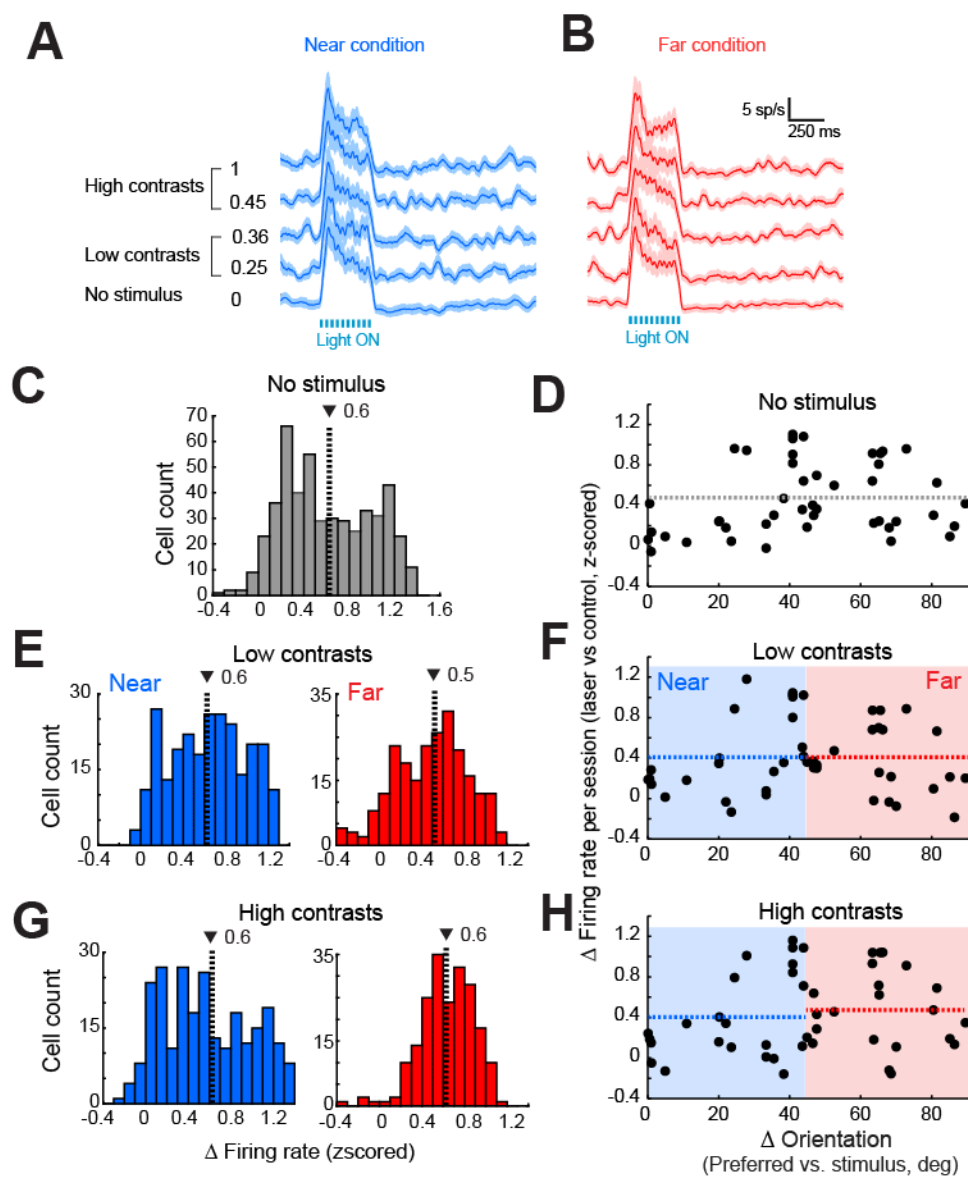
(A-B) Peristimulus time histograms (PSTH) for light evoked activity in the population of neurons significantly responsive to the light across stimulus contrast conditions for an example near session (A, blue) and far session (B, red).

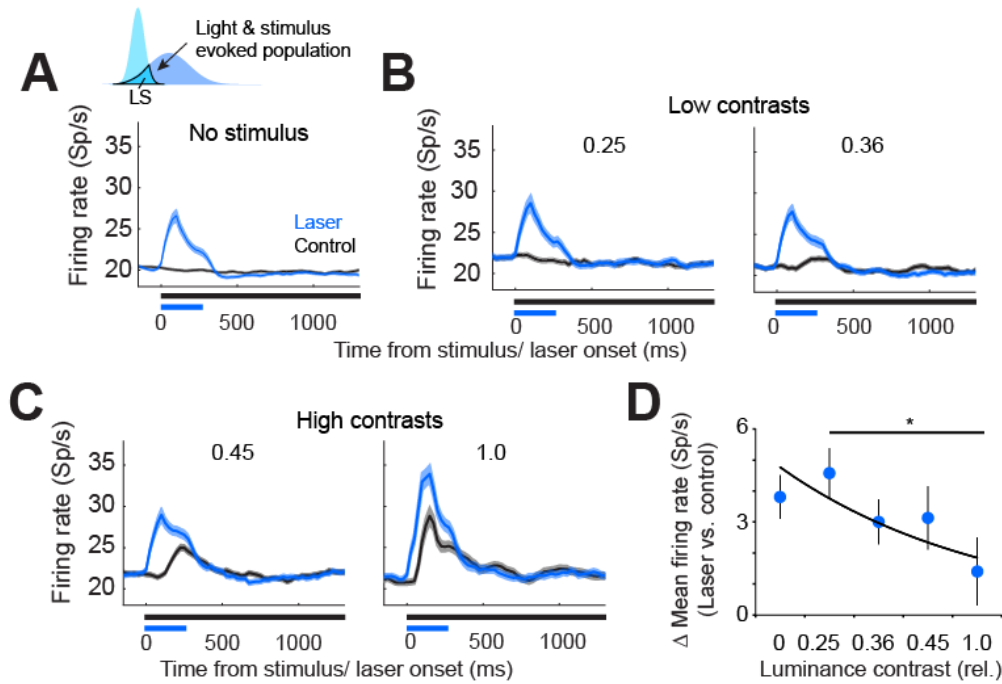
(C,E,G) Distribution of individual cell changes in firing rate in the no stimulus (C), low contrast stimuli (E) and high contrast stimuli (G) conditions for near (left, blue) and far (right, red) designated sessions. Vertical dashed line shows the mean of each distribution.

(D,F,H) Mean firing rate change with light across sessions with no visual stimulus (D), low contrast stimuli (F) and high contrast stimuli. (H) Black circles show average firing rate changes across cells in individual sessions. Dashed horizontal lines show the mean changes in the near (blue) or far (red) categories. The differences in laser-evoked firing rates was not statistically significant across stimulus contrast conditions ( $P=0.35$ , Kruskal-Wallis test).



Figure 4



**Figure S4****Figure S4 | Non-linear laser-induced changes in neuronal responses.**

(A-C) Mean responses of the population of neurons that showed the strongest responses to the visual stimuli and were also responsive to the optogenetic stimulation (n=89 cells) during the (A) no stimulus condition, and during presentation of (B) low contrast stimuli, and (C) high contrast stimuli. The ability of the laser to drive firing above the control condition can be seen to decrease as the stimulus contrast increases. The laser condition is shown in blue, and the control in black. Error envelopes show the s.e.m.

(D) Mean difference in firing rate in laser vs. control conditions for each stimulus luminance contrast. (\*  $P < 0.0001$ , Kruskal-Wallis test, posthoc Tukey-Kramer test). Black line shows the best exponential fit to the data.

impact on correlations when the stimulus was non-optimally oriented (far condition; contrast 0.36:  $P > 0.05$ , Wilcoxon signed rank test). We next examined noise correlation changes across all stimuli in the When the laser and visually driven populations were nearby, the combination of a low contrast visual stimulus and the optogenetic stimulation

resulted in a mean decrease in noise correlations between light-driven cells (Fig.5C, light blue distribution, laser minus control correlation difference mean  $-0.035 \pm 0.053$  standard deviation). This was significantly different from the effect of optogenetic stimulation in combination with a high contrast visual stimulus (mean change  $0.024 \pm 0.056$  s.d.) or no visual stimulus (mean change  $-0.009 \pm 0.17$  standard deviation) (all distributions different from one another,  $P < 0.001$ , Kruskal-Wallis test, post hoc Tukey test). In contrast, when the visually-driven population distal to the optogenetically driven population, the optogenetic stimulation had no effect on local noise correlations (Fig.5D,  $P > 0.05$  Kruskal-Wallis test). These result suggests that the strength of a visual stimulus differentially primes a local network for either correlation (high contrast) or decorrelation (low contrasts) in a functionally, and possibly spatially, defined manner. This underlying network correlation structure was revealed by probing the circuit with the optogenetic stimulation, which provided an additional drive to the neuron pairs and pushed the circuit in its primed direction. The lack of changes in correlation in the far and no stimulus conditions show that during this period the optogenetic stimulation alone has little to no effect on correlations.

Correlations have been hypothesized to limit the benefits of pooling across populations of neurons by imposing an upper asymptotic limit on the signal-to-noise ratio (123). To estimate how these changes may impact the local network encoding the stimulus, we quantified the light-induced changes in noise correlations on the signal-to-noise ratio (SNR) as a function of increasing population size (123). We examined the impact of the combined laser- induced increase in firing rates and decrease in noise correlations on the

SNR for near (Fig. 5E) and far conditions (Fig. 5F). In the near condition, the laser-induced changes in firing rates combined with the reduction in noise correlations led to a 20.1% improvement in the asymptotic SNR, compared to the no-laser condition (Fig. 5E). To assess the potential contribution to SNR of the firing rate changes alone, we recalculated SNR by ignoring the changes in correlated variability (assuming that optogenetic stimulation left the control correlations unchanged from the no laser control condition). Firing rate changes alone, in the near sessions, were associated with only a 10.6% increase in the population SNR (Fig. 5E, dashed purple line), which was comparable to changes observed in the far condition (Fig. 5F, solid red and dashed purple lines). Similarly, in the control (no-stimulus) condition, the firing rate increase in the absence of changes in noise correlations led to a small increase in population SNR of 9.8% compared to the no laser condition. These results are consistent with previous adaptation studies (136) showing that the modulation of network accuracy by changes in correlations is more than twofold stronger than the modulation due to changes in mean firing rates.

### ***3.6 Spatially-limited signal pooling captures changes in behavioral performance***

One key measure of stimulus detectability is the neurons' signal-to-noise ratio (SNR, Fig. 6A), which has long been proposed as a measure of the fidelity of signal transmission and detection by neurons and synapses(123). Simply, this model pools signals from a population of cells, and if the sum of their activity surpasses a set threshold, it leads to a sensory perception (as measured by a behavioral report). The previous analysis of SNR

**Figure 5 | Effect of optogenetic stimulation on noise correlations and network performance.**

(A) Changes in noise correlations for one example session. Each point represents correlation coefficients in control and laser trials for one pair of cells.

(B) Population mean noise correlations for laser responsive neurons during control (gray bars) and laser trials (colored bars) for near (left panel, blue) and far (right panel, red) conditions. \*\*  $P < 0.001$ , Wilcoxon signed rank test. Error bars represent s.e.m.

(C -D) Changes in noise correlation distributions following optogenetic stimulation for near (C) and far (D) stimulated subpopulations for the three visual stimulus conditions. Distributions were created by bootstrapping (with replacement) across all near (C) or far (D) sessions in each stimulus condition. The distribution for the no stimulus conditions was created using data from both near and far sessions, as this condition was identical to both groups. Arrowheads represent the mean of each distribution.

(E-F) The reduction in noise correlations in the near condition can increase the population SNR by 20 percent. Plots show the SNR with increasing population size for near (E) and far (F) subpopulations, during presentation of low contrast stimuli. Solid lines show the SNR values during the control (black), and laser conditions for near (blue, E) and far (red, F) activated populations. Dotted magenta lines shows the change in SNR that is attributable to the increased firing rate induced by the laser alone, if noise correlations had remained unchanged (calculated using the firing rates from the laser trials and noise correlations from control trials). Dashed black line represents the SNR in the absence of correlated noise in the control condition (black).

Figure 5

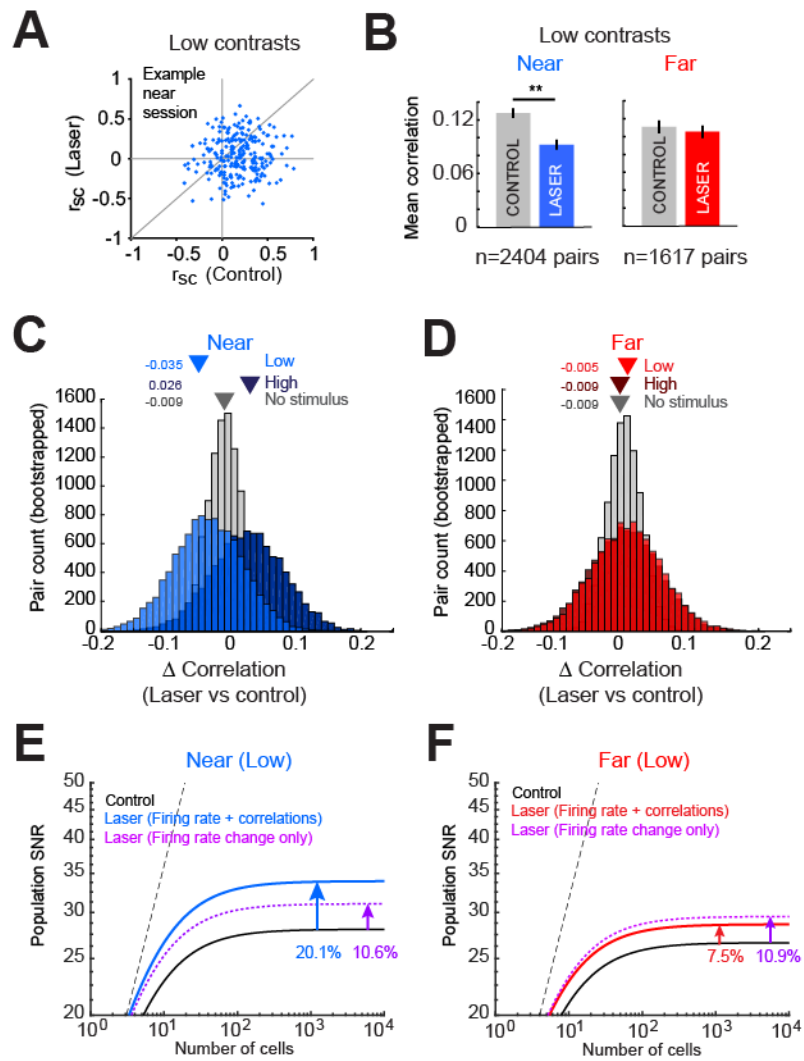


(Fig.5E,F) considers both firing rates and noise correlations, and has been used as a measure of stimulus detectability in neural populations in area MT (123) and V4 (137) under a pooling model that assumes that a decoder sums spikes from all cells in the pool without reference to their origin (138). In other words, it pools uniformly across all available neurons and assumes correlations are uniform across this population. Our results comparing optogenetic stimulation of near and far populations show that while firing rate changes with optogenetic stimulation are fairly uniform, noise correlations and behavioral changes are not. We next sought to expand this SNR model of how information might be pooled across multiple neuronal populations while taking in to account different correlation structures. Two possible pooling schemes were considered (Fig. 6B). 1) Pooling that samples uniformly across all active neural populations, regardless of functional distance ('uniform pooling', see also 'scaled uniform pooling', Fig. S5B-C), and 2) pooling that samples in a spatially-limited fashion according to the distance between neuronal populations ('spatially-weighted pooling'). Both of these models assume that the total SNR is calculated based on the SNR of specific orientation-tuned subpopulations (Fig. 5E-F). Data was organized according to the difference in orientation between the cell's PO and the stimulus orientation ( $\Delta$  Orientation), from which firing rates and noise correlations were used to compute SNR. We estimated the SNR of the visually driven population from the data on control, no laser, trials for the near sessions (Fig.6B, solid gray distribution). This was integrated with the SNR of the laser driven population as a function of orientation difference (Fig. 6B, colored outline distributions), according to the various pooling rules.

## Figure 6 | Spatially-weighted signal pooling models observed behavioral changes.

(A) Basic model of sensory detection relies on pooling signals across a neural population. If the pooled signal crosses a critical signal to noise threshold, this results in the perception of the stimulus, otherwise the stimulus is not observed.

(B) Two possible models of signal pooling over closely spaced neural populations. *Upper* A uniform pooling rule in which the total SNR of the area is a simple summation of the visually driven population (gray) and any one of the possible laser-driven (colors). *Lower* A spatially-weighted pooling rule, in which the contribution of the laser-driven population is weighted by its function distance from the visually driven population.

(C) Uniform pooling model results. Laser-driven activity in both the near (blue) and far (red) increased the total SNR substantially above the control (gray), purely visually-driven, condition. Results are for the low contrast stimuli. Dashed horizontal line estimates the global SNR threshold based on the control condition. In Fig.S4 we explore a scaled uniform pooling rule, to account for the size differences in the 2 populations. Findings were similar for both uniform models. High contrast results are shown in Fig.S4.

(D) Spatially-weighted pooling model results. Laser-driven activity only in the near (blue) sessions increased the total SNR substantially above the control condition, matching well with behavioral observations (E). The weight is described in the main text. High contrast results are shown in Fig.S4.

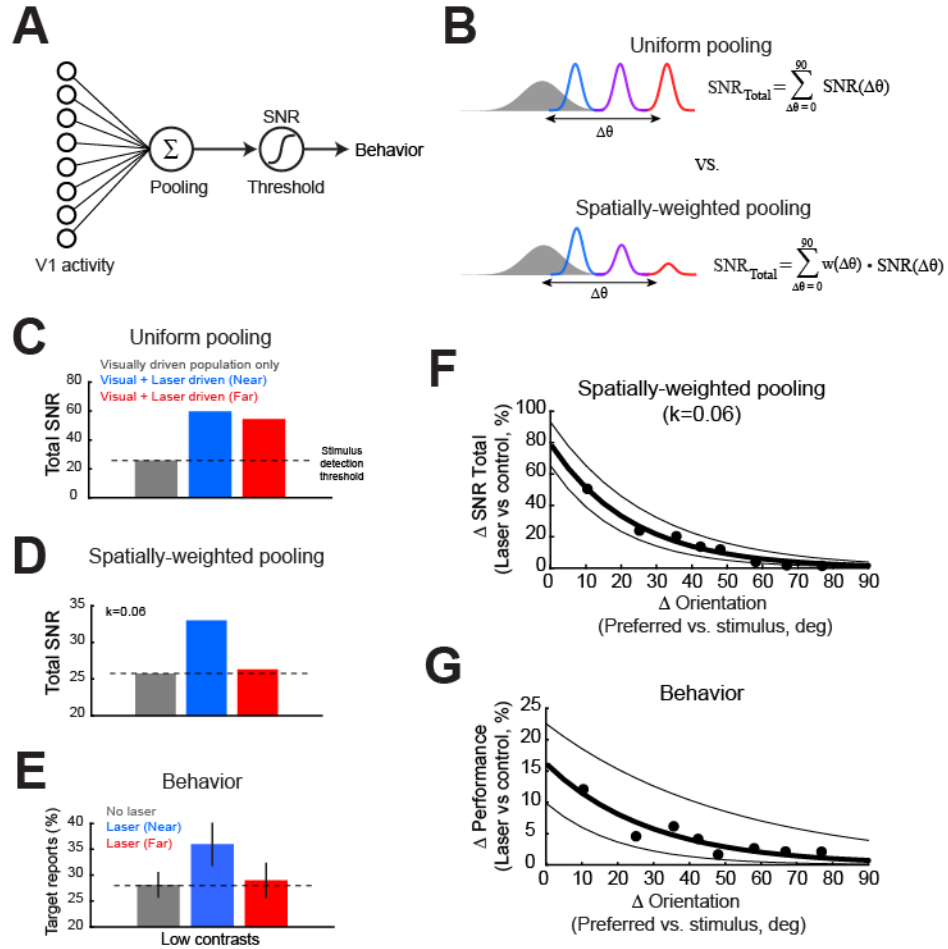
(E) Behavioral detection performance for low contrasts in the absence of laser stimulation (gray), with near stimulation (blue) or far stimulation (red). Error bars represent s.e.m. across sessions.

(F) Spatially-weighted pooling results as a function of orientation difference, showing the percentage change in the total SNR with the laser stimulation from the visually-driven SNR alone. The total SNR was calculated as in (D), independently for various functional distances. To estimate the SNR across functional distances, sessions were first ordered from smallest to largest orientation preference difference from the visual stimulus. Next, to overcome the noisiness of estimates from individual sessions, the variables required for the SNR (firing rate, standard deviation, and noise correlations), were estimated from bootstrapping across data from 10 sessions at a time, with a 5 session slide. The bootstrapped-estimated variables were used to calculate the SNR of the laser driven population. This laser-driven SNR was then added to the visually-driven SNR according to the equation in (B, lower). The difference in orientation (abscissa) is the average across the 10 sessions sampled for each point. Thick black bar shows an exponential fit to the data points. Flanking thin black lines show the 95% confidence intervals for the fit.

(G) Behavioral change in detection performance with laser stimulation, averaged across the same groups of sessions used in (F). Thick black bar shows an exponential fit to the data points. Flanking thin black lines show the 95% confidence intervals for the fit.



Figure 6



We computed the total SNR for the control condition alone, and the combination with optogenetic stimulation of near or far subpopulations. Uniform pooling across a small cortical area can be described as a linear summation of the relevant neural signals (78), regardless of functional distance. Thus, combining the SNRs associated with the laser-driven and visually-driven subpopulations (Fig. 6C) yields a robust increase in the total SNR in both near and far conditions (with respect to control) that is, however, inconsistent with the laser-induced changes in behavioral performance (Fig. 6E). To account for the idea that the visually-driven population was most likely larger in size than the laser-driven one (owing to visual stimuli of 2-3 degrees, which exceed the size of most V1 receptive fields, and optogenetic stimulation was fairly localized, see Fig 1G), we also considered a version of this pooling rule that uniformly reduced the weight of the laser-driven pool (called ‘Scaled uniform pooling’, Fig.S5B-C). The weight was adjusted such that total SNR in the near condition was a value similar to that produced by the spatially-weighted pooling rule (discussed below). Even with this scaling, the uniform pooling model still failed to capture the differences in behavior, continuing to predict an increase in detection performance in the far condition. Our behavioral results were best captured by the pooling model (Fig. 6B *lower*, D), in which the contribution of the laser-driven population to the visual percept drops off exponentially as the functional orientation difference between the light and visually-driven populations. For simplicity, “spatially-weighted” in this context refers to the functional distance between the populations, estimated by the orientation difference.

### Figure S5 | Estimating the total SNR to predict behavioral performance.

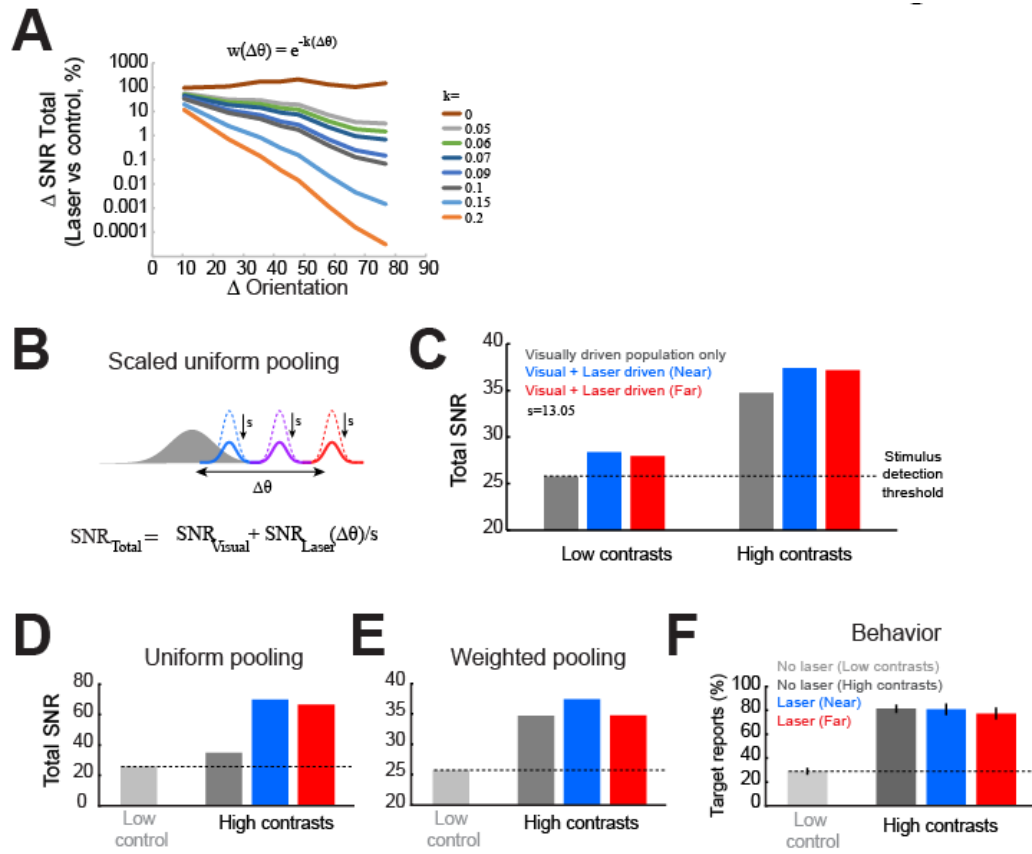
(A) Spatially-weighted pooling model weighs the contribution of the laser-driven population as inversely proportional to the function distance to the visually-driven population. The weight is given by the equation in the center. The figure show the effect of varying the value of the constant,  $k$ , on the total SNR computed for the low contrast stimulus condition. Estimates shown in Figures 6D and 6F used  $k=0.06$ , chosen as the best fit to the behavioral data.

(B, left) Scaled uniform pooling results. It is quite likely that the visually-driven population is much larger in terms of the number of neurons, than the laser-driven population. We asked whether the addition of a scaling factor to the uniform pooling model would result in a total SNR similar to the observed behavioral changes. The scaling constant,  $s$ , was chosen so that the total SNR resulting from the nearby stimulation (blue) would match that obtained by the spatially-weighted model in the same condition. The results show that even with the scaled uniform pooling model, the total SNR resulting from stimulation of the far population above the control condition, and very similar to the nearby condition.

(B,right –D,E) Total SNR for the high contrast condition for the scaled uniform pooling model (B,right), the uniform pooling model (D) and the spatially-weighted pooling model (E), in the visually-driven (no laser) condition (dark gray bar), or with the laser-driven population nearby (blue) or far away (red). The light gray bars in D and E, show the total SNR in the low contrast condition which we use as an estimate of the stimulus detection threshold (shown by the black dotted line). For a detection task, it is expected that once the threshold is surpassed, detection will be reliable, and further increases in the SNR will not affect detection performance (ceiling effect).

(F) Behavioral detection performance for low contrasts in the absence of laser stimulation (light gray), and for high contrasts without laser (dark gray), or with nearby laser stimulation (blue) or far away stimulation (red). Error bars represent s.e.m. across sessions.

Figure S5



The weight ( $w$ ) is given by

$$w(\Delta\theta) = e^{-k(\Delta\theta)}$$

where  $k$  is a constant, and  $\Delta\theta$  is the orientation difference between the visually-driven and laser-driven subpopulations. With this pooling model, only the laser-driven population in the near condition elicited a large change in the total SNR, well above the stimulus detection threshold, and captured the observed improvement in behavioral detection performance (Fig. 6E). The detection threshold here is given by the detection rate of the stimulus in the absence of optogenetic stimulation (Fig.6.C-E black dashed line).

To test the spatially-weighted pooling model further, we checked whether the neural changes in total SNR would match the behavioral results if the orientation difference (and hence, spatial distance) between the two subpopulations was varied more gradually. To do this, we again ordered our data according to the orientation difference between the neurons' PO and the orientation of the stimulus. To compensate for the inherent noisiness present in data from individual sessions, we calculated the laser-driven SNR firing rates and noise correlations by sampling from groups of 10 sessions at a time (ordering according to functional distance,  $\Delta\theta$ ), sliding every 5 sessions. This was then added to the visually-driven SNR according to the same spatially-weighted pooling rule as described above, using the same constant  $k$  as in Figure 6D (see also Fig.S5A). Figure 6F shows the percent change in the total SNR when the laser was applied as a function of distance, and Figure 6G illustrates the percent change in behavioral detection performance (the behavior was averaged across the same sessions sampled for the total SNR in Fig.6F).

We found that the spatially-weighted pooling rule provides remarkably good agreement between laser-induced changes in total SNR and the animal's detection performance ( $r=0.95$ , Pearson correlation between data points). For both the total SNR and the behavioral data, we note that the percent change in either measure falls to less than 50% of the maximum when the functional distance between the two populations exceeds 20 degrees. We also calculated the total SNR for the high contrast stimuli. However, in this case, since the SNR in the control condition already exceeds the hypothesized detection threshold (dashed horizontal lines in Fig.6C-E), the additional laser-driven activity was not expected to modulate behavior, due to ceiling effects. This is reflected in all SNR pooling models considered and is consistent with the observed behavior (Fig.S5B-F)].

### **3.7 Discussion**

Here we have shown for the first time that selective optogenetic activation of excitatory cells in V1, using ChR2, is able to improve the detection of low contrast visual stimuli. By varying the orientation of the visual stimulus we were able to vary the distance between the light-driven and the stimulus-driven populations. With this manipulation we demonstrated that the improvement in detection performance is inversely proportional to the functional distance between the two populations. For perceptual read out, signal integration across the two populations is achieved only when the distance between the two populations is less than 45 degrees, dropping to 50% of the maximum at orientation differences of 20 degrees (corresponding to about 0.4 mm across the cortex(139)). Secondly, due to our ability to simultaneously record from neural populations while stimulating, we were able to identify population-level changes associated with successful

signal integration, which has never before been possible. Namely, we found that the laser-driven firing rate increases were associated with a reduction in pairwise noise correlations and an increase in the population SNR when the two populations were proximal, but not distal. No changes were found when the network was driven solely by light. These findings suggests that the presence of a visual stimulus itself evokes changes in the local network and alters the local underlying correlation structure, which is unmasked by the optogenetic stimulation.

Which neurons are actually used to guide perceptual decisions? In principle, a simple strategy to guide perceptual detection would be for downstream areas to decode the activity of all V1 neurons with receptive fields at the visuospatial location of the stimulus. Then, if a fraction of the neurons increases its firing rate as a consequence of optogenetic or visual stimulation, the downstream neurons could use this information to signal the presence of the stimulus. If this were the case, optogenetic stimulation would be expected to enhance perceptual detectability irrespective of stimulus orientation, and perhaps induce a percept even in the absence of the stimulus. However, this is not what we found – although the firing rates of neurons were strongly increased by light regardless of the stimulus properties, the laser-induced behavioral changes were only observed when the visual stimulus was presented near the preferred orientation of the activated cell population. This suggests that only information from spatially proximal neural populations is integrated and subsequently decoded by downstream areas. While not explicitly tested, this finding is consistent with many other results. Indeed, in sessions ( $n=10$ ) in which the optogenetic stimulation was paired with two orthogonal stimuli, (one of which was near

the preferred orientation of the stimulated/recorded cells), and randomly interleaved across trials, detection was only improved in the near condition, remaining unaltered in the far condition. The idea that the functional architecture of V1 could be used for sensory coding and perceptual judgments has been previously suggested. Nienborg and Cumming (2014) have reported choice-like behavior in V1 neuronal populations during a discrimination task for stimulus features that have a functional organization (such as orientation), but not for stimulus features that are not functionally organized in the cortex (such as disparity). Several other studies that have combined electrical microstimulation with visual stimuli in extrastriate areas, have shown that visual neurons may contribute to perception based on their tuning to a feature that may seem to be task irrelevant but that is spatially organized (18, 141, 142). For example, middle temporal neurons (MT) in macaques are organized topographically according to direction of motion and/or binocular disparity. On a pure motion discrimination task, microstimulation of neurons tuned to both features had little to no effect on behavioral performance, unless the test stimulus is also presented at the cells preferred plane (142). Similarly, in our study orientation was a task irrelevant feature that is topographically represented. Few studies have addressed spatial integration directly, with one notable exception. Using paired electrical microstimulation of V1, Ghose and Maunsell showed that when the stimulation sites were spaced at distances less than 1 mm, the monkeys' detection ability was best described as a linear summation of single site current levels, but as a winner-takes-all competition at larger separations (78). Further work is required to determine whether the size of functional integration area is stable across stimulus conditions (i.e. receptive fields of V1 neurons are known to change size depending on stimulus strength), as well as across cortical



areas, in which local populations encode increasingly diverse stimulus features(1), as we ascend through the sensory processing cortical hierarchy.

One important finding in our study is that optogenetic stimulation reveals differences in the capacity of the V1 network involved in stimulus processing to encode information. Previous electrical and optogenetic stimulation studies have either focused on the effect of external stimulation on individual cell responses and behavioral performance while ignoring its impact on neural network performance. Our study found that changes in pairwise correlations were different across conditions. Optogenetic stimulation was able to augment percepts in the near condition, but not in the far condition. As we did not see changes in correlations during optogenetic stimulation alone, these changes likely reflect differences in the underlying local network state induced by the visual stimulus and revealed by optogenetic stimulation. Various manipulations have shown that networks are able to switch from a correlated to an uncorrelated state (82, 143, 144). One possible mechanism for the observed results is that when visual stimuli are presented in conjunction with optogenetic stimulation, the extra drive to excitatory cells (due to the targeted ChR2 expression) is passed along to local inhibitory neurons, which will more effectively track excitation to reduce correlations between excitatory cell pairs (82, 143). A similar mechanism has been recently proposed to explain the reduction in noise correlations during spatial attention (84, 145, 146) and the columnar architecture has been suggested to play a crucial role in generating the required noise correlation structure (140). Our results are also consistent with a recent study in mouse visual cortex (147), showing that detection performance is better decoded from the of heterogeneity of neural

responses (akin to changes in pairwise correlations), rather than from global activity changes.

The most compelling alternative explanation for our results that we extensively considered, but ultimately rejected, was that the optogenetic stimulation was evoking phosphenes in some cases but not others, in a manner unrelated to spatial integration of cortical signals. There is a long history of brain stimulation producing artificial sensory percepts. Previous attempts to establish causal links between neuronal activity in sensory cortex and perceptual decisions have involved studies in which neurons were stimulated either electrically (3, 5, 93, 148) or optogenetically (11–13, 94, 112). The underlying assumption is that if a neural population is directly involved in a perceptual decision, the external activation of that population should bias the animal's decision towards the stimulus feature encoded by the population, with the artificial stimulation acting as a surrogate for natural afferent input. For example, in the somatosensory system, Romo *et al.* (93) demonstrated that electrical activation of quickly adapting neurons in primary somatosensory cortex, S1, is sufficient to drive the cognitive processes involved in a somatosensory discrimination task. In primary visual cortex, Jazayeri *et al.* (11) optogenetically stimulated large pools of both excitatory and inhibitory V1 neurons, and observed a tendency for monkeys to saccade in the direction corresponding to the receptive field locations of the stimulated cells. These studies have cited the production of sensory phosphenes by the stimulation procedure as the underlying mechanism for the behavior changes. That is, the stimulation *caused* a subjective experience of the sensory modality being stimulated, that the animals would base their decisions on.

While our stimulation protocol was able to bias perceptual decisions, we did not see an increase in the false alarm rate (target reports in the absence of the visual stimulus), and found no other evidence of phosphenes (though we cannot ever be absolutely certain of the monkeys' subjective experiences). This might seem somewhat surprising given that electrical stimulation of V1 has been routinely shown to induce phosphenes in both humans and monkeys (89, 132, 149, 150) and to increase the false alarm rate (4, 91, 92). Following optogenetic stimulation of V1, Jazayeri et al., (2012) concluded their behavioral results were due to phosphene production(11). This latter study differs from ours primarily in the choice of the viral vector and promoter sequence. Jazayeri et al., (2012) used adeno-associated virus (AAV) and the pan-neuronal Synapsin promoter(11). This combination likely transfected a larger number of neurons (116) and was not cell-type specific, much like electrical microstimulation. It is possible that the simultaneous activation of excitatory and inhibitory neurons is more likely to be propagated than the activation of excitatory neurons alone. Our study, which targeted only excitatory neurons, may not have produced phosphenes due the targeting of a smaller number of cells, compared with Jazayeri et al (11). Together these studies point to the importance of viral construct choices in non-human primate optogenetics studies. Overall, the paucity of studies showing clear behavioral modifications utilizing optogenetic stimulation in non-human primates suggest that optogenetic stimulation provides a much weaker drive to the network than electrical microstimulation. Indeed, the more localized, subthreshold nature of optogenetic stimulation has been demonstrated by direct side-by-side comparisons with electrical microstimulation (94, 113), by spatial measurements of optogenetic activation by fMRI (13, 113), and intrinsic imaging (47). For instance,

experiments combining ChR2 stimulation and electrical microstimulation with fMRI revealed no discernable BOLD activity at the electrode tip with optogenetic stimulation, but strong activity after electrical stimulation (113). The optogenetic stimulation had an effect similar to low current electrical stimulation. While it is possible for animals to learn to detect low current electrical stimulation in V1, reliable performance requires many weeks of extensive training, unlike higher current stimulation (151). Further, Murasugi et al. (152) found that the false alarm rates are only weakly modulated when electrical currents used for stimulation have low amplitude and low frequency. In our study, we propose that the percepts were primarily driven by the visually stimulated population whose activity was transmitted to other cortical areas. When the stimulus contrast was quite low, optogenetic stimulation of nearby populations was able to join and augment this transmitted signal and thus make stimulus detection more probable. Low contrast stimuli have been shown to increase the size of V1 receptive fields (27), and also increase correlations between pairs of cells compared to stimuli with ineffective orientations (153). All of these phenomena are consistent with a reduction in local inhibitory drive, which might allow signals from more distal neural pools to be integrated and transmitted. We hypothesize that in our experiment the optogenetic stimulation acted a sort of booster for the endogenous signal, but alone was insufficiently strong to propagate and generate a visual percept. Until technological advances allow light to be delivered to a larger swath of cortex, there will be a trade-off between cell-type specificity and targeting a behaviorally relevant population. This may be mitigated by experimental designs that are sensitive to relatively small changes in overall neural activity produced by cell-type specific constructs.

## ***CHAPTER IV: PINGING THE NETWORK REVEALS TENDENCY TO DECORRELATE***

### ***4.0 Introduction***

In the previous section we saw that simultaneous activation of a population of excitatory cells can have differential effects on the correlated variability between pairs of cells depending on whether those cells were partaking in the formation of a percept or not. In this section we will explore whether and how optogenetic stimulation alters network correlations more generally. Can optogenetics be used as a tool to causally manipulate network correlation structures?

Correlated variability (also known as noise correlations) is a ubiquitous feature of cortical networks, but its source and causal impact on behaviors is unknown. Presently, noise correlations between pairs of simultaneously recorded neurons have been extensively measured, as it is a simple but rich descriptive statistic by which population activity can be quantified. Changes in noise correlations have been linked to an assortment of behavioral conditions, including attention (84), arousal (154) as well as experience and learning (136, 155). When the firing rate of individual neurons are well correlated to an animal's behavioral choice on a trial by trial basis (termed a high "choice probability"), this property is thought to be conferred by the fact that neurons are correlated with a the larger group of cells that jointly contribute to decisions (134). Correlation analyses have also been able to provide crucial information about the functional architecture of a network, providing a signature of

network functioning that is not discernable from the single neuron firing rates, as we showed in the previous chapter. One important finding is that noise correlations decrease when an animal attends to the location of the receptive fields of recorded cells, and increase when the animal attends away (84, 137). In the previous chapter, we found that correlations were decreased in instances when the optogenetic stimulation was able to positively influence behavioral detection. Combined, these results suggest that a decorrelated network is favorable for information encoding. Theoretical work on the topic of correlated variability has suggested that correlations may either be beneficial or detrimental for stimulus encoding depending on the task and the tuning properties of cells in which correlations are measured (88, 156, 157). Currently, there exists no method to causally manipulate correlations between neurons independent of other task parameters. Thus, if correlations themselves are crucial for stimulus encoding, or merely an epiphenomenon remains to be determined. Using optogenetic stimulation of a group of excitatory cells in V1, we demonstrated that the neural network responds hundreds of milliseconds later by reducing noise correlations between pairs of stimulated neurons while preserving the firing rates of the individual neurons. We further show that this effect is likely due to an intrinsic property of the network, rather than the effect of plasticity. This finding provides a novel method by which we can causally test the impact of correlated variability in a network.

#### ***4.1 Delayed decrease of noise correlations following optogenetic stimulation***

To investigate how optogenetic stimulation of glutamatergic neurons affects the structure of correlations, we re-examined the data recorded in section 3.1. As previously mentioned, our analysis was based on laminar recordings, perpendicular to the cortical surface, with optogenetic stimulation delivered via a tightly couple fiber optic connected to a blue laser. Excitatory neurons were targeted for optogenetic stimulation by transfecting them with the channelrhodopsin-2 gene, packaged in a lentiviral vector, under the control of an  $\alpha$ -CaMKII promoter. Since not all recorded neurons were responsive to the light stimulation, we separated cells and cell pairs into those that were light responsive and those that were not (Fig.7A). We chose all sessions that had identical laser stimulation parameters (35 Hz, 10 cycles) and focused on trials when animals maintained fixation but no visual stimulus was present. Since the animal was performing a detection task (Fig.7B), we only analyzed trials in which the correct response was given (correctly reported the absence of a stimulus), in order to eliminate the possibility that lapses in attention could be responsible for any potential effects. Attention has been repeatedly shown to alter noise correlations in visual cortical areas(84). Our question was whether optogenetic stimulation had any effect on noise correlations. Figure 7C shows an example session, with multiple laser-responsive neurons recorded across multiple channels of the laminar electrode. It is clear that while some neurons fire synchronously, others become active tens of milliseconds after the onset of the laser pulse, indicating that the optogenetic stimulation is propagating through the local network and is not merely confined to neurons expressing ChR2. We identified neurons based on their response to the

optogenetic stimulation (Fig.7D; “laser-responsive” or “non-laser pairs”). Cells that did respond to the laser were identified by either their waveform shape (clearly isolated single units, see Methods) or functionally based on statistically significant responses to a visual stimulus. By definition, laser responsive cells showed a robust increase in firing rate when the light was on, while the non-laser cells showed no change (Fig.7D).

We next examined the correlated variability between pairs of cells in each group. Previously, we calculated noise correlations during the 335 ms window corresponding to the time the light was on. In the absence of a visual stimulus, we found no change in this condition. We reasoned that changes in correlation structures, thought to be mediated by changes in local inhibition (143), might develop in time as subsequent components of the network become active. To examine the temporal dynamics of noise correlations, we calculated correlations between spikes counts across trials for pairs of neurons using a 200 ms sliding window, shifting in increments of 50 ms across the duration of each trial. We performed this calculation for pairs of laser responsive (n=1396) and non-laser pairs (n=117) separately. Surprisingly, we found that on trials with optogenetic stimulation, noise correlations between laser responsive cells began to drop dramatically, and very significantly ( $P < 0.0017$  Wilcoxon rank sum test, Bonferroni corrected) below control levels *after* the light was extinguished (Fig.7E). The maximum reduction in noise correlations was observed approximately 300 ms after the laser was turned off. No differences in noise correlations were found between cells that were not responsive to light (Fig.7F).



**Figure 7 | Abrupt reduction in noise correlations after optogenetic stimulation of glutamatergic neurons.**

(A) Glutamatergic neurons in V1 were targeted by expressing ChR2 packaged in a lentivirus vector under the control of an  $\alpha$ -CaMKII promoter. Recordings used a 16 channel laminar electrode. Optogenetic stimulation consisted of a laser-couple fiber optic adjacent to the electrode. We recorded responses from neurons which were responsive or not to the laser light.

(B) Monkeys performed a detection task, but only pure fixation trials in which no visual stimulus was present on the screen are included in this analysis. 50% of trials had optogenetic stimulation (35Hz, 10 cycles).

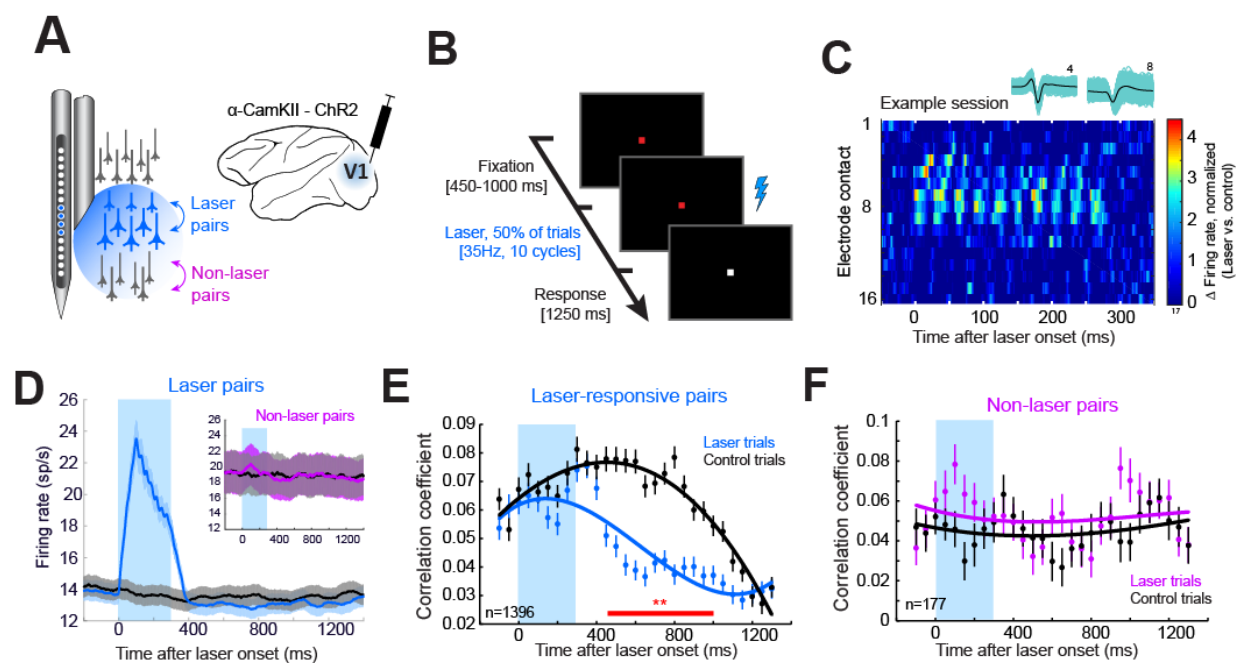
(C) Example recording from a laminar electrode showing light induced activity across multiple channels. Channel 1 is closest to the surface of the cortex. Example waveforms of laser-responsive units are shown in the top right corner.

(D) Optogenetic stimulation substantially increased the firing rates of laser-responsive neurons ( $n=282$ ), but not other neurons (inset).

(E) Noise correlations between laser-responsive cells decrease significantly below control levels in the time period following light offset. Noise correlations were computed using z-scored firing rates from a 200 ms window, sliding every 50 ms. (\*\*  $P<0.0017$ , Wilcoxon rank sum test, Bonferroni corrected). Only trials in which the animals' corrected reported the absence of a visual stimulus were used.

(F) Noise correlations between non-laser cell pairs were unaffected by the optogenetic stimulation. All error representations show s.e.m. Fits in panels E&F are polynomial.

**Figure 7**



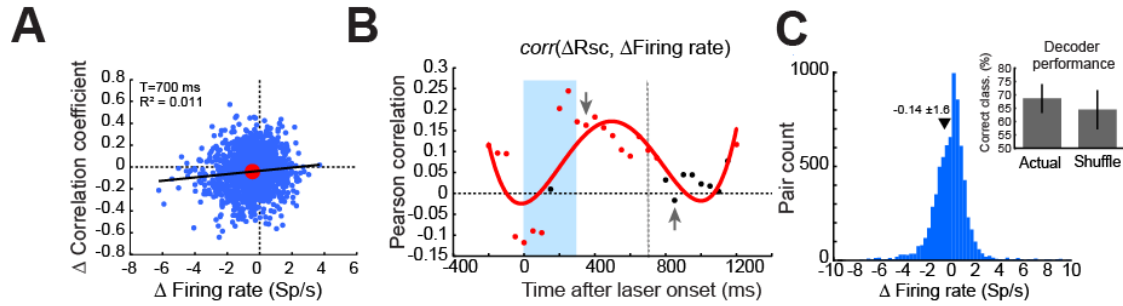
## ***4.2 Correlated variability changes are not due to firing rate changes***

Noise correlation estimates can be significantly affected by firing rate changes (87, 153). Differences in firing rates between the individual cells comprising each pair are normalized by z-scoring the firing rates prior to computing correlations. Could the reduction in correlations be due to the differences in firing rates that occur after the light offset? For instance, was there rebound inhibition following the laser stimulation that might explain the reduced correlations. To address this, across all pairs we calculated whether the change in firing rate between laser and control trials was correlated (Pearson correlation) with the difference in noise correlations between laser and control trials (Fig.8A). Again, this was done for all timebins for which noise correlations were calculated (Fig.8B). Interestingly, we found that during the times in which the light was on, the correlation between the changes in firing rates and noise correlations reverses polarity between the beginning and end of the light period. During the early period (approximately the first 200 ms) of light, the changes in firing rates and noise correlations are negative. That is, as firing rates increase positively with the light, noise correlations decrease with the light, and correlation between these changes is thus negative. In subsequent timebins, we found a reversal of this trend, with correlations being significantly positive and then slowly dropping down to non-significant levels. This unstable decrease in correlation between firing rates and noise correlations during the timebins in which the noise correlations are significantly reduced (Fig.8B, timebins between gray arrows), imply that the changes in firing rate alone cannot account for the changes in noise correlations. To further test this, we looked at whether a classifier could be trained to predict the direction of change of

noise correlations with the laser, based on the direction of change in firing rate of the cell pair. To do this, we grouped data across all timebins with significant noise correlation changes after the laser (Fig.8C shows the distribution of observed firing rate changes used as input to the classifier). A support vector machine (SVM) classifier (“SVMclassify” function in MATLAB) was trained on 80 percent of the data and tested on the remaining 20%. This was done repeatedly (1000 times), each time sampling a different 80% of data pairs. The decoder performance was compared to results obtained by randomly shuffling the link between the firing rate and noise correlation changes. We found that the decoder was not able to classify above chance level the direction of noise correlation change following laser stimulation based on the difference in firing rate (Fig.8C, inset). This further confirms that the observed changes in noise correlations are not likely to be caused by a change in firing rate following laser stimulation.

#### ***4.3 Delayed correlation change is an intrinsic network feature, not plasticity***

Having ruled out differences in firing rates, we then explored possible network mechanisms that might account for this surprising finding. Since the laser stimulation took place over hundreds of trials, spaced across multiple hours, it is reasonable that repeatedly driving the same network of neurons could induce plastic changes in some if not all synapses. Alterations in synaptic weights between pairs of light-driven cells could very well alter the correlated firing patterns between the individual cells. To test for this possibility, we reasoned that plastic changes would develop over time,

**Figure 8**

### Figure 8 | Noise correlation changes are not due to changes in firing rates

(A) Example timebin, 700 ms after laser onset, shows the difference in firing rate and noise correlation between laser and control conditions for each pair of cells. Fit is linear. Red dot shows the mean.

(B) Across time, the Pearson correlation between the difference in firing rate and noise correlation between laser and control conditions for all pairs. Red points indicate statistically significant different from zero ( $P < 0.05$ , Rank sum test). Shaded blue area is the time the optogenetic stimulation is on. Vertical dashed line shows the timebin in panel A. The arrows indicate the time points between which noise correlations are significantly different between laser and control trials (Fig.7E). Fit is polynomial.

(C) Histogram of firing rate changes associated with laser stimulation during time bins when correlated variability was significantly different from the control trials (time points between arrows in panel B). Inset. A support vector machine classifier used to test whether changes in firing rate could be reliably used to predict the changes in noise correlations produced by the laser stimulation. The decoder was trained on 80% of trials, then tested on the remaining 20%, using data from the same time points. The decoder's performance was not significantly above chance levels (shuffled trials,  $P > 0.05$ , Wilcoxon rank sum test).

becoming progressively stronger throughout the course of the session, as the number of laser stimulation iterations increases. We recalculated noise correlations between pairs of cells as a function of time. Trials were organized from first to last, and noise correlations were calculated separately for all pairs using blocks of 20 trials at a time. It is not possible to calculate noise correlations for 1 trial at a time, and even this

small number of trials introduces considerable noise into the measurements. However, since we do not have direct access to the synaptic weights, this measure provided an available proxy. Again noise correlations were calculated using a sliding window across timebins within the course of a trial. Figure 9A illustrates the change in noise correlations between laser and control trials as a function of trial block (again, each block consisted of 20 trials). We were surprised by two distinct observations. First, during the time when the laser is on (0-335 ms) noise correlations were increased above control conditions in the early blocks of trials and then dropped below the control levels in late trials (Fig.9C, compare magenta and green traces during the light period, shaded blue area). Notably, firing rate changes during this time were remarkably similar across all trial blocks (Fig.9B). This suggests that plastic changes induced over the course of multiple trials specifically shifts correlations between pairs of cells, without altering their firing rates. Over time, the network appears to adapt to the optogenetic stimulation (Fig.9D, left panel). This effect is lost when noise correlations are calculated across all available trials and as we had previously done in Figure 8E. Secondly, in the time period following the light, we found that the decrease in correlations was present across all trial blocks, from early to late (Fig.9C-D right panel). This stable change in late occurring correlations suggests the presence of a stable network feature that comes online at a later time point during the trial and alters the correlation structure between cell pairs. What sort of network feature might be able to induce this shift in correlations? One possible candidate is a type of inhibitory interneuron that is immunopositive for somatostatin (SOM). In mice,

**Figure 9**

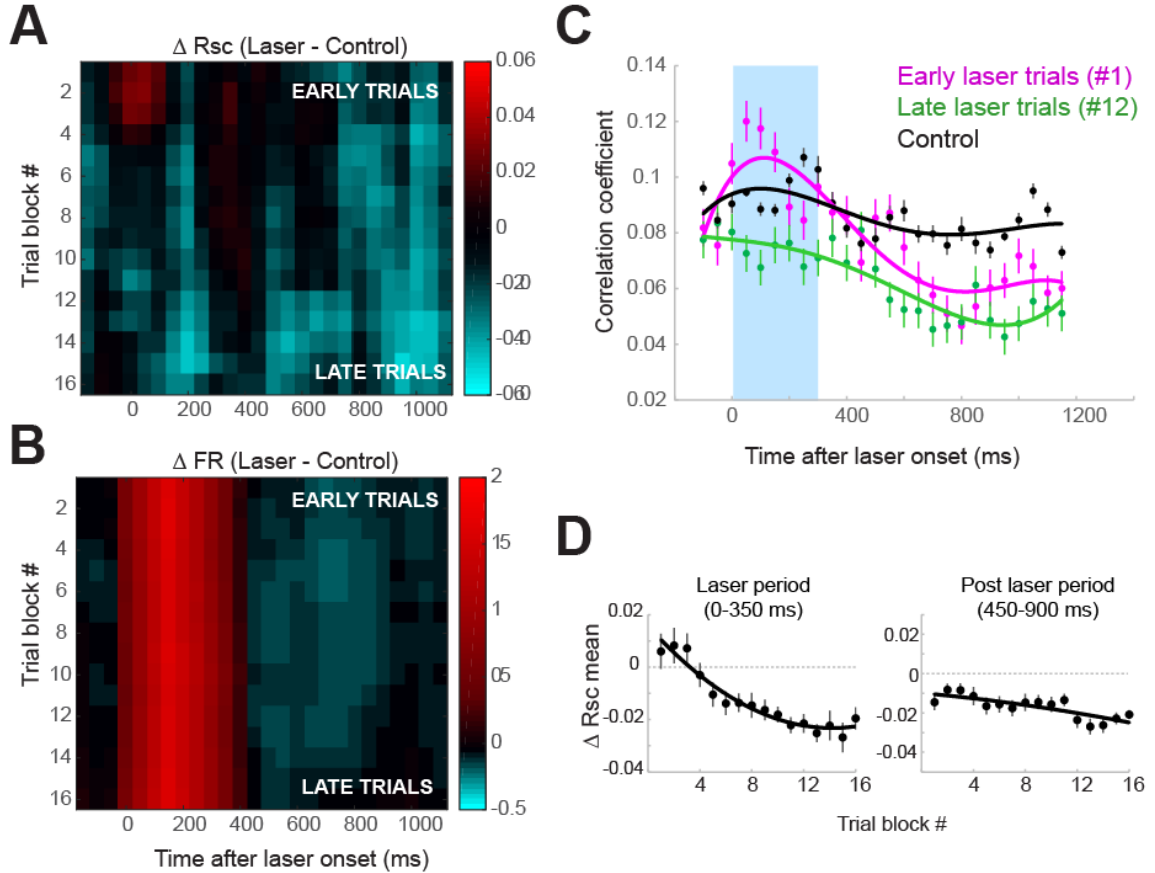


**Figure 9 | Late reduction in correlations due to network property, not plasticity.**

(A) Changes in noise correlations following laser stimulation across trials. Trials were ordered from first to last, and correlations were calculated using blocks of 20 trials, in increments of 2 trials at a time. Figure shows the difference in noise correlations between laser and control trials for equivalent blocks of trials.

(B) Firing rate differences between laser and control trials across the same trials block as in panel A, ordered from early (top) to late (bottom).

(C) Mean noise correlations across the population of cell pairs during early trials (purple, trial block #1) and late (green, trial block #12) compared to control (black, averaged across

(D) Drop in mean noise correlations gradually drop across trials for the time period during laser stimulation (left panel, exponential fit), suggestive of a plastic change, while are present from the first block of trials in the post-laser period (right panel, linear fit), suggestive of an intrinsic network mechanism for this change. All error bars are SEM.

the SOM+ cells have been shown to respond maximally to weak visual stimuli hundreds of milliseconds after the stimulus onset, and hundreds of milliseconds later compared to other types of neurons (158). This timing is consistent with the delayed drop in noise correlations observed in our experiment. Additional experiments are required to specifically address whether the activity of SOM+ neurons in monkeys and mice are more responsible for changes in correlations than other cell types. An unlikely alternative that we cannot rule out is that plastic changes may have quickly occurred within the time period of the first 20 trials. When working optimally, monkeys can perform this task at a rate of 10 trials per minute. If we include the other types of trials present in this task, the quickest the first 20 trials could have occurred is in 8 minutes, which is a short time compared to other studies of induced plasticity (159).

#### ***4.4 Discussion***

In this section we have shown that optogenetic stimulation can be used as an effective tool to causally decrease noise correlations between pairs of cells without otherwise affecting their firing rates. Further, we have shown that this dramatic decrease in correlations hundreds of milliseconds after light offset is not likely due to plastic changes in the local circuit, but rather, activation of a local feature of network capable of decorrelating pairs of neurons.

To date, most interest in correlations has been focused on a neural population's ability to encode and decode information regarding a highly specific stimulus feature (such as



orientation), with little attention paid to the mechanistic origin of the correlations. A few recent studies have begun to address this point. For example, Rosenbaum et al (2017) (160) using a combination of in vivo electrophysiology and computational modeling showed that lateral connectivity patterns between spatially distinct populations across layers 2/3 can account for the observed patterns of correlations in macaque primary visual cortex. Notably, they observed that neurons recorded from closely-spaced electrodes (between 0 to 2 mm) are positively correlated, while neurons recorded from distally-spaced electrodes (tested up to 6 mm) are not correlated, and neuron pairs spaced at an intermediate distance are negatively correlated. This type of concentric opposition in neural activity is reminiscent of the surround suppression feature of V1 discussed earlier, whereby a stimulus of a size that exceeds beyond the boundaries of a neuron's classic receptive field will reduce the firing rate response to the stimulus. Somatostatin-positive (SOM+) neurons in mouse V1 make a large contribution to surround suppression. In the presence of small stimuli, these neurons stay largely silent, but as stimulus size increases, these neurons ramp up their activity in a manner proportional to the extent of surround suppression. Networks of inhibitory neurons also have been proposed to be the mechanism by which noise correlations in early parts of the visual processing hierarchy might be readily decorrelated by high level features such as attention or task type (143, 161). Our results suggest that it might be these SOM+ interneurons that are responsible for decorrelating pairs of neurons following optogenetic stimulation. We infer this based on the slow stimulus response dynamics exhibited by SOM+ neurons in response to weak visual stimuli (162) that matches the dynamics of decorrelation we observed. Other types of interneurons that have been characterized in mice do not exhibit this slow dynamic, but

rather rapidly track the activity of local excitatory neurons (158, 162, 163). Future experimental work is required to determine whether these SOM+ interneurons are mechanistically responsible for both surround suppressions and distance dependent correlation patterns. The results of this study provide a powerful, novel tool by which to study the functional impact of changes in correlation structures on perceptual decision-making and stimulus encoding, both of which have been postulated to depend strongly on noise correlations. A fruitful future line of experiments could include presenting visual stimuli ~500ms *after* optogenetic stimulation, during the time of minimal noise correlations to test whether the reduced correlations make the stimulus more or less perceptible.

# **CHAPTER V: SUPPRESSING VISUAL CORTICAL NETWORKS**

## **5.0 Introduction**

In the previous sections, we have examined the effects of activating excitatory neurons in V1 and revealed its impact on encoding visual information. Recently, John Spudich and his group made a stunning discovery of a class of exquisitely light-sensitive channelrhodopsins that conduct anions (mainly chloride) across the cell membrane (99), and the opportunity to test out these novel inhibitory opsins in non-human primates suddenly presented itself. We had the channel packaged in the same viral vector as we had done with the original excitatory channelrhodopsins (lentivirus, with expression driven by an  $\alpha$ -CaMKII promoter) and proceeded to reproduce the original experiments. It was the perfect yin to our original yang, and where we had previously augmented perceptual performance we expected to impair with this opsin. Biology, however, had multiple surprises in store for us.

Prior to the implementation of optogenetic techniques, suppressing neural activity relied upon either application of pharmacological agents(164), or the installation of cooling coils that could reduce the temperature of the cortex (165), thereby reducing activity levels. These methods lacked the timescale resolution required to accurately track the dynamic activity of awake, functional cortical networks, and often lacked cell type specificity. Recently, these issues were overcome by several optogenetic means by which to suppress activity in primate cortex that have been implemented, the most

common of which are Archeorhodopsin (12, 51), a proton pump, and Halorhodopsin (113), a chloride pump. The discovery of this novel anion-conducting channelrhodopsin, *GtACRs* (99) greatly improves upon the current state of the art as these channels are able to match conductance changes of Arch but with 1/1000 the amount of light. This increased sensitivity to light is crucially important for any optogenetically-gated channel for use in primates, where delivering a sufficient amount of light to a neural population of sufficient size to modulate perception is limited by the light absorption properties of cortical tissue (117). Hence, a channel that can produce a strong photocurrent with less light would be able to drive a larger population of cells further from the light source compared to a less light-sensitive channel.

### ***5.1 Gt-ACR2 suppresses neural activity in monkey cortex***

We examined whether GtACR2 could be successfully implemented in non-human primate cortex. The gene encoding this channel was packaged in a lentivirus vector, with expression controlled by an  $\alpha$ -CaMKII promoter (see Methods for details). The virus was injected into V1 of two monkeys. Injections were spaced vertically and laterally, delivering a total of 20  $\mu$ l to an area of cortex approximately 6.4 mm<sup>2</sup>, and throughout the depth of the cortex (Fig.10A). Electrophysiological recordings began 6 weeks following the injections, using 16-24 channel laminar electrodes. Optogenetic stimulation was achieved via a fiber optic encased in a stainless steel cannula, positioned adjacent to the recording electrode (Fig.10A), coupled to a 473nm, 100 mW, blue laser.

We first confirmed electrophysiological results from cultured neurons (99) and from cortical slices (120) and showed that neurons in visual cortex of awake macaques could be effectively suppressed using GtACR2. While monkeys maintained fixation on a computer screen, light was applied for 300ms continuously. Figure 10C shows the firing rates of two example neurons that exhibit marked reduction in activity following laser onset. Moreover, this suppressed activity could be seen across multiple channels on the laminar electrode (Fig.10D), with the area of maximum suppression corresponding to the position of the light source relative to the recording contacts. During the light presentation, firing rates decreased by  $29.0\% \pm 3.4$  sem on average ( $n=17$  cells). As has been previously described, the kinetics of GtACR2 are somewhat slower than those of other channelrhodopsins. Following light offset, the channel remains open, and firing rates do not return to baseline until  $258 \pm 27.6$  ms after the light has been turned off. Maximum suppression of activity was found  $221.8 \pm 16.3$  ms after light onset. At the synaptic terminal the extracellular chloride concentration is markedly reduced compared to that in elsewhere around the cell. Thus, opening of GtACR2 at the terminal has been previously shown to depolarize neurons, and induce spiking at light onset (120, 166). This paradoxical excitation can be mitigated and confined to a single spike at the onset of light by using continuous rather than pulsed light protocols(120). We found evidence of this paradoxical excitation at the light onset in 2/17 light responsive cells. Following this brief excitation, firing rates were suppressed similarly to cells that did not show the initial augmentation. Unlike other inhibitory opsins (12, 167), we did not observe any rebound activation at light offset, likely due to the slow closing time of this particular

channel. In 2 sessions, however, we did observe some slight activation following light offset on channels that were not suppressed by the light (Fig.10D, channels 10-15). In subsequent experiments, light was applied continuously. To characterize expressions patterns of GtACR2 in non-human primate cortex, we developed a novel needle aspiration technique to acquire a small sample of transfected tissue, without significant harm to our well-trained monkey collaborator. The cortex sample was fixed in paraformaldehyde solution and labeled with multiple cell type specific markers, as well with a newly generated anti-ACR2 antibody. Immunostaining was done against the excitatory neuron-specific marker  $\alpha$ -CaMKII, and the pan-neuronal marker NeuN (Fig.10B). Thus we were able to definitively confirm that lenti-virus expressing GtACR2 under the  $\alpha$ -CaMKII promoter is able to produce expression patterns capable of functionally suppressing neural activity in monkey primary visual cortex.

## ***5.2 Novel circuit dynamics revealed by optogenetic inhibition***

Next, we used this novel suppression tool to investigate the question of how the local network contributes to cortical responses to visual stimuli. Cortical columns are the most striking architectural feature of the cortex. The columns are defined by the prevalence of connections between neurons distributed in the vertical axis, but comparatively sparse connections laterally between cells across columns (41, 43, 46, 168). The horizontal connections that do exist have been found to monosynaptically connect similarly tuned pyramidal cells at distances of 6-9 mm (diameter), running parallel to the cortical surface in layer 2/3 (46, 62), but also present in layers 4B (upper) and 4C $\alpha$ , and 5 and 6 of primates and carnivores (169). About 20% of

projections from these long range connections activate short range inhibition, mediated by smooth stellate cells, via disynaptic inhibitory interactions (43, 170). Horizontal connections have been implicated in a range of physiological properties of V1 neurons, including surround suppression of nearby cells (58, 171, 172) , contrast gain control(60, 173), and in laminar differences in correlation structures(82). Here we sought to examine the contribution of the local surrounding network to ongoing and stimulus-driven responses in V1. To do this, we separated the recording electrode from the light source by approximately 300  $\mu\text{m}$  (Fig.11A). This allowed us to record from one population of cells while optogenetically silencing a neighboring population. Animals performed a simple detection task in which orientated gratings of varying contrasts (range was 3.5 to 100% sinusoidal gratings presented on a gray screen) were presented for 300 ms over the receptive fields of the recorded cells (stimuli ranged in size between 2-3 degree in diameter, sufficient in size to activate cells in the extraclassical receptive field). (Fig.11B). Half of trials had no visual stimulus (0%) and half had optogenetic activation of Gt-ACR2 (synchronized with the visual stimulus when present). Since the recording electrode and the fiber optic were separated by a small distance, they were both present in the virus injection zone. In the absence of strong excitatory drive, activity across laterally connected neurons is weak(47, 170). We used this feature to first confirm that there was sufficient separation between the two devices such that the light was not directly modulating neural responses in the population of cells being recorded. We identified sessions (n=20, 10 from each monkey) that showed no light-induced firing rate changes in spontaneous activity when the animals were purely fixating (0% contrast, Fig.11C-E,

left most column), but that did show light-modulated activity in the presence of a visual stimulus. Given the lack of response in the spontaneous condition, we infer this to confirm that the light was not directly responsible for the observed firing rate changes, but rather that the light modulated the local network that indirectly altered the firing rates of the recorded population. So, what does inhibition of neighboring cortical columns reveal about the functional role the near surround plays in modulating stimulus responsive activity? In each monkey, we found two distinct types of responses to the optogenetic neighborhood suppression. First, we observed a class of cells that showed suppressed activity when the light was paired with a high contrast visual stimulus, but was facilitated when the light was paired with a low contrast stimulus (Fig.11C-E shows three example cells). Overall amongst this population, we saw a median increase in firing rates of  $14.8 \pm 1.2 \%$ , at 5% contrast, and a median decrease of  $18.4 \pm 2.1 \%$  at 100% contrast ( $P < 0.02$  two-tailed, paired T-test, Fig.11F-G). Neurons exhibiting this pattern comprised 22% of the total light modulated neurons we recorded. Perhaps not coincidentally, inhibitory neurons comprise about 20% of post synaptic targets of horizontal collaterals (170), and is remarkably consistent with the proportion of cells exhibiting this firing pattern. Such a connection pattern is depicted in Figure 12, showing how the activity of a pyramidal neuron can be modulated by a local neighboring network via an inhibitory interneuron link. Changes in the contrast of a visual stimulus, alters the amount of inhibition present in the network. Variations in inhibitory drive as a function of stimulus contrast have been indirectly demonstrated using optogenetic stimulation. For example, shining light on ChR2-expressing pyramidal cells in the presence of a low



**Figure 10 | Suppression of monkey visual cortex with novel anion channelrhodopsin.**

(A) Hyperpolarizing GtACR-2 was delivered to neurons in primary visual cortex of two monkeys, packaged in a lentivirus vector, driven by the  $\alpha$ -CamKII promoter. Injection sites were spaced in 3 dimensions. Recordings were done using laminar electrodes, closely coupled with an fiber optic delivering blue light from a 473 nm laser.

(B) Cortical biopsy results showing immunofluorescence of anti-ACR2 antibody (green, bottom left) along with NeuN (blue, top left),  $\alpha$ -CaMKII (red, top right) and the merge (bottom right). Arrows indicate GtACR2- $\alpha$ -CaMKII positive neurons.

(C) Examples of mean firing rates of two light-responsive neurons during laser stimulation (blue traces, 300 ms continuous light), and without stimulation (black traces). Monkeys maintained fixation throughout the trial. Horizontal black line denotes the time when laser is on.

(D) Example of 24 simultaneously recorded channels across a laminar electrode, showing the difference between laser and control trials. Widespread suppression (dark blue patch) is clear on channels 1-9. White horizontal line denotes time when laser is on.

(E) Average firing rate changes (n=17 cells). Blue horizontal line denotes time when laser is on. Shaded envelopes denote standard error of the mean.

Figure 10

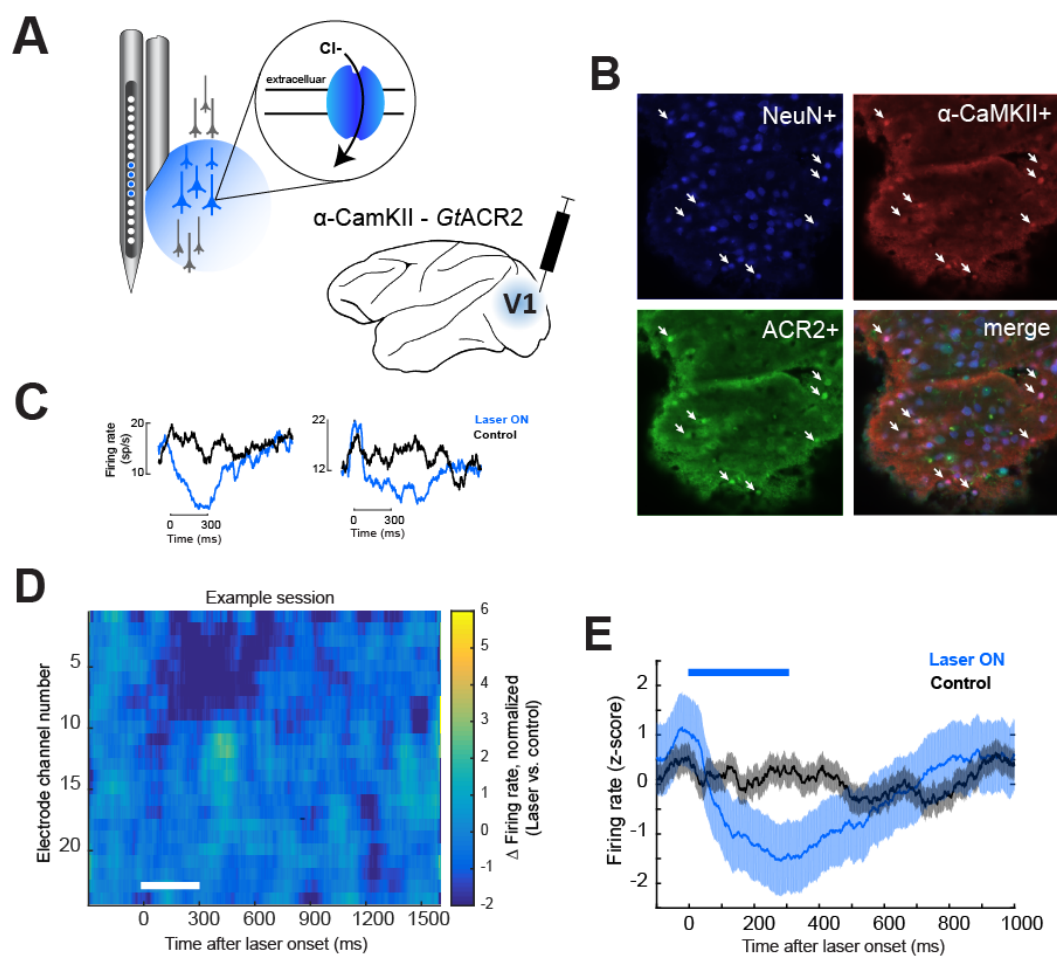


**Figure 11**

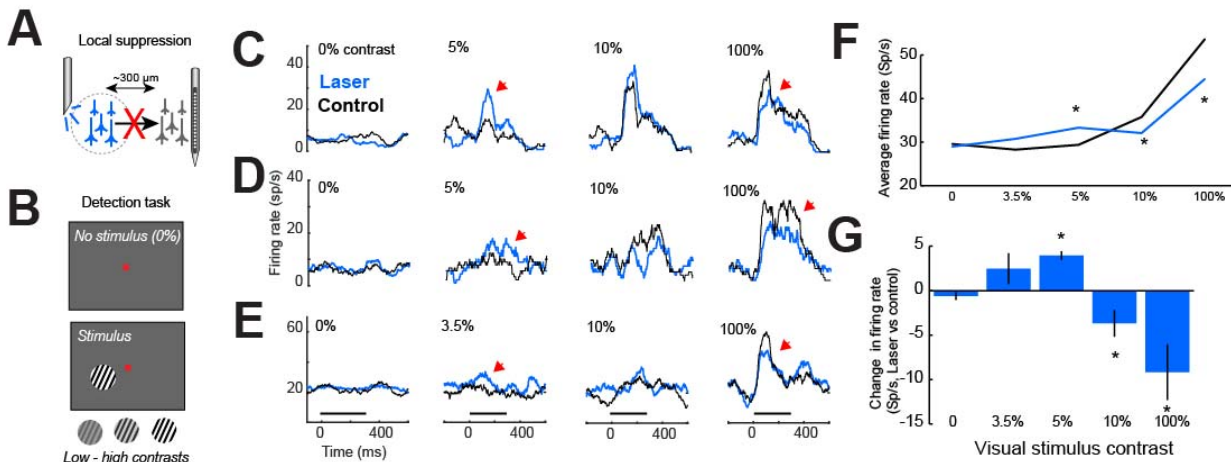


**Figure 11 | Neighborhood suppression non-linearly affects firing rates**

(A) Experimental setup. The optical fiber was distanced from the recording electrode by a small distance ( $\sim 300 \mu\text{m}$ ) in order to suppress the surrounding population of cells to those being recorded.

(B) Detection task design. Animals maintained fixation on a central point for a variable amount of time (see Methods chapter). On 50% of trials an oriented sinusoidal grating of one of four contrast levels was presented for 300 ms. The remaining trials had no visual stimulus present and animals had to maintain fixation, and report the absence of a stimulus. 50% of all trials had laser stimulation (300 ms, continuous light), synchronized with the visual stimulus, when present. All trials were randomly interleaved.

(C,D,E) Example responses of 3 cells during neighborhood network suppression under 4 different contrast conditions, ranging from 0-100%, with (blue lines) and without (black lines) laser stimulation. Horizontal black line denotes the time when laser is on. Red arrow heads show facilitation at low contrasts and suppression at high contrasts.

(F) Mean firing rate (200 ms window centered on maximum response during stimulus presentation time) following neighborhood suppression across all cells exhibiting facilitation at low contrasts and suppression at high contrasts ( $n=27$ ). \*  $P<0.02$ , paired, two-tailed T-test.

(G) Mean change in firing rate, light minus control condition for the same cells presented in E) across visual stimulus contrasts. Error bars show sem. \* same as panel F.

**Figure 12**

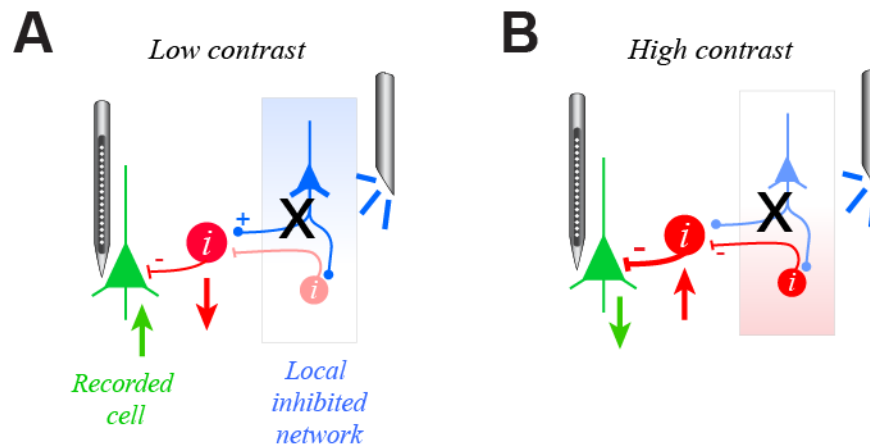


**Figure 12 | Local network modulates inhibition to neighboring cell responses as a function of visual stimulus strength**

(A) Schematic of possible local circuit to explain results from Fig.11, with two excitatory neural populations (represented by triangular cells) connected via an inhibitory interneuron (red circles). In the presence of a low contrast stimulus, the inhibitory drive coming from the local network is in a low state and excitation is able to flow more freely. When light is used to suppress the local network, this reduces the drive to the interneuron (red arrow) connecting the local network with the recorded cell, thereby reducing inhibition and leading to the increased firing rate observed (green arrow).

(B) In the presence of a high contrast stimulus, the opposite is true, with inhibition in the local network being strongly activated by the visual stimulus. Inhibition with light now results in an increase in inhibitory drive to the connecting interneurons, which then acts to decrease the firing of the neighboring neuron being recorded.

contrast grating causes increases in firing rate as expected, but paired with a high contrast stimulus, opening the same ChR2 channels leads to an overall reduction in firing rate, because the additional excitatory drive is quickly quenched by the local network of strongly driven inhibitory cells (50). This is interpreted as evidence of divisive normalization, or gain control mechanisms that have been activated in the

local circuit. Hence, with a low contrast stimulus, the local network is in a relatively low state of inhibition, while with a high contrast stimulus, the local network is in a high state of inhibition. In our experiment, by suppressing the network in these different states enabled us to unmask the role the network plays in modulating responses of neurons they are connected to.

The second type of response pattern we saw, neurons (n=78) showed no modulation with the light during spontaneous activity, but were suppressed during simultaneous presentation of low contrast stimuli. Unlike the previous class of cells, this firing pattern is best described by an excitatory connection between the light suppressed and the recorded neural population (Fig.13A). Figure 13B-D show the mean responses of 3 example cells exhibiting this type of light modulation. We found significant reductions in firing rates for low contrasts of 5% ( $10.6 \% \pm 5.3$ ,  $P=0.00096$ , paired, two-tailed T-test) and 10% ( $5.9\% \pm 4.8$ ,  $P=0.0058$ ). At high contrasts, overall we saw no significant change in firing rates in the group of cells (Fig.13E-F). However, individual cells showed a broad range of responses to the light (see Fig.13B-D right column).

### **5.3 Discussion**

To summarize, we have shown that 1) a novel opsin, Gt-ACR2, is capable of suppressing neural activity in monkey cortex and 2) using this novel method, we examined how inactivating a portion of the nearby surrounding network impacts

**Figure 13**

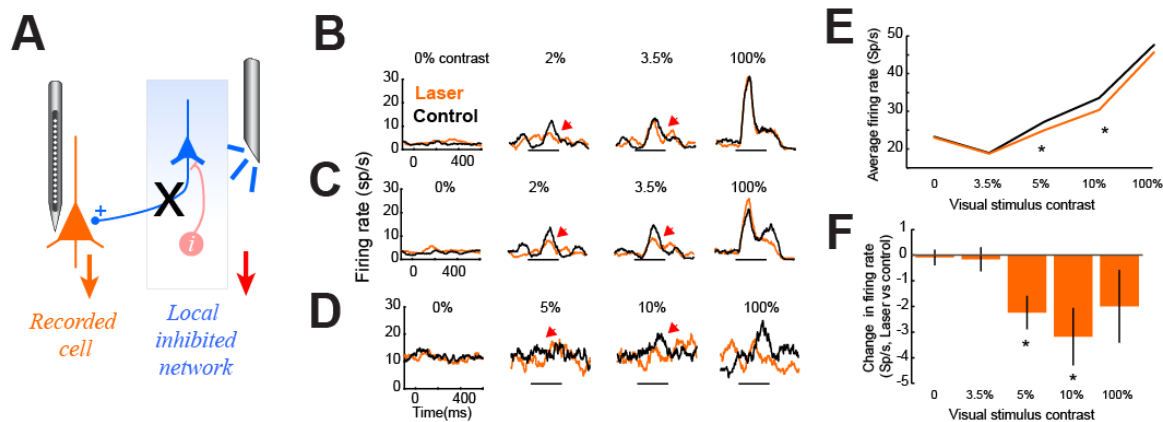


**Figure 13 | Most neurons are suppressed at lower contrasts following suppression of neighboring activity.**

(A) Illustration of a possible circuit connecting the recorded population to the inhibited population, exhibiting overall suppression. Cells are connected via excitatory connections, thereby suppressing the neighboring population (red arrow), suppresses the recorded population (orange arrow).

(B,C,D) Example responses of 3 cells during neighborhood network suppression under 4 different contrast conditions, ranging from 0-100%, with (orange lines) and without (black lines) laser stimulation. Horizontal black line denotes the time when laser is on (300 ms). Red arrow heads show suppression at lower contrasts.

(E) Mean firing rate across stimulus contrasts with (orange line) and without (black line) light activation of GtACR2. \* P<0.006, paired, two-tailed T-test.

(F) Mean change in firing rate across all cells (n=78), laser minus control condition. \* same as panel E.

stimulus processing in primary visual cortex. These two aspects are discussed in detail below.

Direct stimulation with light resulted in a drop in firing rate by about 29%, and lasting over 250 ms after the light has been extinguished. The particular kinetics of this channel make it an interesting choice for optogenetic experiments in non-human primates. It has previously been reported that if Gt-ACR2 is activated at the synaptic terminal, it will induce a transient spike (120, 166) In our study, we observed light onset activation infrequently (2/17 directly responsive cells, 0/105 indirectly responsive cells). When the spike burst was present, it was quickly quenched by long lasting suppression. This brief onset excitation has been argued to limit the usefulness of this channel in further optogenetic studies (166), however, it should be noted that other inhibitory opsins have been shown to have very large rebound excitations after light offset (167), which, for studies measuring behavior, is very likely to intrude upon the time during which a decision is formed and thus produce possible experimental confounds. Further, the long lasting effects of inhibition *after* light offset is quite stable – our cells very comparable to those of Malyshev et al(120). The prolonged time course of inhibition after light offset is advantageous when long periods of inhibition are required but when light-induced local heating and possible tissue damage (117, 174) are of concern.

Next, we used this novel channel to ask to what extent the local network contributes to stimulus responses in V1. Cortical columns are defined by the prevalence of vertical connectivity between cells, and very sparse lateral connections across layers. To better understand how the local network shapes stimulus responses, we inactivated a portion of the nearby columns and while recording cell activity in

response to visual gratings of varying contrasts. We found that cells might be either inhibited or excited by suppression of their neighbors in conjunction with a low contrast stimulus, or be inhibited in conjunction with a high contrast stimulus. These findings are consistent with anatomical tracing studies, and intracellular recordings in cortical slices showing that long range horizontal connections may connect distal populations via monosynaptic excitatory connections or via disynaptic inhibitory connections(46, 48, 62). Previous studies of the spatial extent over which V1 neurons pool visual signals have relied upon varying the size and contrast of a visual stimulus but could not otherwise modulate selective components of the neural circuit. They observed that V1 responses are dramatically modulated by the activity of the surrounding network, and that spatial extent of signal pooling was dependent on the contrast of the visual stimulus, with a low contrast summation field spanning up to three times the size of a high contrast summation field (59, 61, 62). These studies postulated that these dynamics could be due to lateral connections between cortical columns, but did not test this explicitly. Here, by suppressing a nearby cell population we have uncovered a potential circuit mechanism that may underlie these dynamic functional properties. We have discovered that even with a low contrast stimulus, when the summation field is large and inhibition is presumably low, about 25% of neurons driven by the stimulus are actually inhibited by the local network. This opens up additional questions about the different functional roles and possible impacts on local computations that are executed by these different subpopulations of neurons. Additional analysis is required to determine whether the optogenetic silencing had an



impact on the animal's detection performance or on noise correlations between these distinct classes of cells.

## ***CHAPTER VI: CONCLUSIONS AND FUTURE DIRECTIONS***

As the tools for non-human primate optogenetics continue to expand (114), dissecting the neural circuitry for sensory perception and decision making with cell-type resolution is increasing probable. In this collection of three studies, we have shown that 1) optogenetic activation of excitatory neurons can be used to modulate neural activity and behavior in awake, behaving monkeys and that perceptually-relevant information is grouped functionally and spatially across cortical populations, 2) we have discovered a novel application of optogenetics whereby noise correlations within a network can be causally manipulated in the absence of firing rate changes, and 3) we have validated a novel optogenetic tool for use in non-human primates that allows for silencing of targeted neural populations, which can be used to reveal, previously invisible underlying network dynamics. To put these results into a broader context, only nine other studies starting in 2012 have been able to show clear changes in behavior following optogenetic stimulation of non-human primates (11–13, 94, 112, 114, 167, 175, 176). This is in stark contrast to the veritable explosion of studies in mice that have been able to modulate behaviors easily by comparison. A quick PUBMED search shows 272 entries related to behavioral modulation by optogenetics in mice. This observation simultaneously highlights the importance of developing novel tools for non-human primates and begs the question why is optogenetic modulation different across species? These sparse behavioral results in non-human primates is also rather surprising compared to studies using electrical microstimulation. Using fairly low currents, ranging from 3-25  $\mu$ A(149), changes in behavior have been readily observed stimulating across various cortical sites (6, 90, 91,

96, 132, 150, 177–179). The radial spread of current used in electrical microstimulation studies has been mathematically defined(180), with 169  $\mu$ A required to directly activate 1 mm of V1 tissue. This observation suggests that electrical stimulation is able to modulate behavior by directly activating a patch of cortex starting at ~130 microns across. Most studies I examined used a range of currents with clear behavioral reports starting with stimulation using about 20  $\mu$ A, covering a cortical patch of about 340  $\mu$ m in diameter. To our best estimate, based on the vertical distance optogenetic modulation of firing rates were observed, the optogenetic stimulation spreads to an area of at least 190  $\mu$ m in diameter. Acker et al (2016)(167) designed an optical fiber capable of large scale illumination (>1mm of cortex), but still observed changes in behavior not strikingly different from ours. So why is optogenetic stimulation less capable of modulating behavior compared to electrical microstimulation? To tackle this perplexing issue, several studies(13, 113, 130) have directly compared optogenetic and electrical stimulation. Compared to electrical stimulation, optogenetic activation of a patch of cortex leads to a more constricted pattern of local network activity, that is, electrical activity spreads further and is more likely to activate other parts of the network. Optogenetic stimulation utilizes the neurons' own spike generating machinery to drive connected neurons. Due to this, optogenetic stimulation is more susceptible to modulation by other neurons present in the local circuit, such as inhibitory circuits required to curb runaway excitation. Using a combination of voltage sensitive dye imaging on the cortical surface and electrical or optogenetic stimulation of thalamic nuclei monosynaptically connected, Millard et al (130) demonstrated that electrical stimulation spreads laterally to affect a portion of cortex many times greater than the area affected by the optogenetic stimulation. Interestingly, Gerits

et al (13), using fMRI to image the effects of optogenetic stimulation found that using channels packed in an adeno-associated virus vector (AAV) produced sufficient activity to be visible in an fMRI voxel, but that channels packaged in lentiviral vectors (LVV) did not produce noticeable neural changes. Thus, the difficulties in modulating behavior in non-human primates using optogenetics is likely due to a combination of 1) the ability to deliver light to a sufficiently large population of neurons; 2) the likelihood that the induced activity change will be propagated through to downstream areas in the network and 3) the ability of promoter sequences and viral vectors to specifically target the desired neural population. This brings us to the important topic of construct choices for use in non-human primates.

One major difference between our study and the others, mentioned above, is that our study was the only one to use a construct (105) capable of targeting a specific cell type (glutamatergic cells in our case). Six out of these nine studies specifically chose promoter sequences that would express their opsin in *all* transfected neurons. One imagines the only reason for doing this is to transfect the largest group of neurons possible, however, this is of limited scientific value if the goal is to dissect any sort of real circuit. There are two major advantages of using an AAV versus an LVV. First, AAVs do not integrate into the genome of the host cell, thus making them of greater potential value human therapeutic interventions. Second, viral titers can be much higher with AAVs compared to LVVs, resulting in more viral particles capable of transfecting unsuspecting neurons. One additional factor that is worth considering regards the immune system's reaction to the introduction of viruses into the brain. Following injections of AAV, strong humoral

immune responses have been measured in monkeys that were serotype specific to the injected virus(181). It has been suggested (181) that using differing serotypes if multiple injections are required, as the immune response may quench transfection levels. Two of the remaining studies of optogenetic modulation of monkey behavior (94, 112) used an  $\alpha$ -CaMKII promoter, but in conjunction with an AAV. While the  $\alpha$ -CaMKII promoter should target just glutamergic neurons, in combination with AAV spurious expression in non-targeted neurons has been demonstrated, thus compromising targeted specificity (116).

There is a clear tradeoff between targeting a specific population of neurons, versus being able to modulate the activity of sufficient neurons to bias behavior. Why then were we able to increase the activity of glutamatergic neurons using ChR2 and still observe an improvement in detection performance, while other groups had to use more ubiquitously expressing constructs? One major difference is that we did not rely solely on the optogenetic stimulation to drive the perception of a visual stimulus. In other words, we were not actively trying to evoke a phosphene. We used the optogenetic stimulation to augment the activity of a subset of neurons that contribute to the perception of a stimulus. Moreover, we modified our visual detection task to maximize the impact the optogenetically-evoked spikes would produce, by choosing a dark background screen color, and the lowest contrast visual stimuli that the animals could reliably detect. This type of visual stimulus resulted a small number of spikes evoked in individual neurons, but that the animals could detect some percentage of the time. Under these conditions, we were able to increase the perceptual importance of the small number of extra spikes evoked by the optogenetic stimulation, and did not have to rely on the optogenetic

stimulation to be entirely responsible for the percept. In Chapter IV, I discussed a novel tool used for silencing neurons in V1. In those experiments, monkeys again performed a detection task, however this time we switched to the standard gray background screen color. In these experiments, we did not observe any systematic changes in behavior (though for some sessions, performance was clearly impaired with the optogenetic silencing). It is possible that further analysis, including systematic assessment of population tuning preference may shed light on the matter, it might also be possible that behavioral changes were less observable due to our choice of more potent visual stimuli which reduced the overall impact of reducing the firing rate of some neurons.

Two of the more recent studies in non-human primates have begun to devise ways to target a broader range of cell types. Stauffer et al (114) created a novel two virus system to specifically target dopaminergic neurons in the monkey midbrain. To isolate dopaminergic neurons from neighboring glutamatergic or GABAergic neurons, they injected a combination of 2 viruses, the first targeted dopaminergic neurons by using a 5' tyrosine hydroxylase (TH) promoter that expressed Cre recombinase, and a second virus that carried a more standard Cre-recombination-dependent ChR2 construct packaging in an AAV. Only cells that took up both viruses would be able to express ChR2.

Future studies should take into consideration 4 factors when designing experiments for non-human primates: 1) viral vector type, 2) promoter sequence, 3) opsin properties and 4) light source. These factors will affect the quantity and type of neurons experimenters will be able to manipulate and should be optimized for the specific aims of the experiment.

The results to date, including ours, suggest that evoking large changes in behavior similar to those found using electrical stimulation will likely require techniques that can deliver

more light to transfected cells, or experimental designs sensitive to the activity of small cell populations. Our study, further demonstrates that optogenetics can also be used to probe the state of neural network that would otherwise remain invisible, and provides key insights about population coding during the stimulation previously unavailable. This general strategy could be extended to the study of neural populations at a variety of scales, and under numerous stimulus conditions.

## REFERENCES

1. Tong, F. 2003. Primary visual cortex and visual awareness. *Nat. Rev. Neurosci.* 4: 219–29.
2. Miyashita, T., and D. E. Feldman. 2013. Behavioral detection of passive whisker stimuli requires somatosensory cortex. *Cereb. Cortex* 23: 1655–62.
3. de Lafuente, V., and R. Romo. 2005. Neuronal correlates of subjective sensory experience. *Nat. Neurosci.* 8: 1698–703.
4. Britten, K. H., W. T. Newsome, M. N. Shadlen, S. Celebrini, and J. A. Movshon. 1996. A relationship between behavioral choice and the visual responses of neurons in macaque MT. *Vis. Neurosci.* 13: 87–100.
5. Salzman, C. D., C. M. Murasugi, K. H. Britten, and W. T. Newsome. 1992. Microstimulation in visual area MT: effects on direction discrimination performance. *J. Neurosci.* 12: 2331–55.
6. Bisley, J. W., D. Zaksas, and T. Pasternak. 2001. Microstimulation of cortical area MT affects performance on a visual working memory task. *J. Neurophysiol.* 85: 187–96.
7. Leopold, D. A., and N. K. Logothetis. 1996. Activity changes in early visual cortex reflect monkeys' percepts during binocular rivalry. *Nature* 379: 549–53.
8. Born, R. T. T., J. M. M. Groh, R. Zhao, and S. J. J. Lukasewycz. 2000. Segregation of object and background motion in visual area MT: effects of microstimulation on eye movements. *Neuron* 26: 725–34.
9. Fries, P., P. R. Roelfsema, A. K. Engel, P. König, W. Singer, and P. König. 1997.



Synchronization of oscillatory responses in visual cortex correlates with perception in interocular rivalry. *Proc. Natl. Acad. Sci.* 94: 12699–12704.

10. Purushothaman, G., and D. C. Bradley. 2005. Neural population code for fine perceptual decisions in area MT. *Nat. Neurosci.* 8: 99–106.

11. Jazayeri, M., Z. Lindbloom-Brown, and G. D. Horwitz. 2012. Saccadic eye movements evoked by optogenetic activation of primate V1. *Nat. Neurosci.* 15: 1368–70.

12. Cavanaugh, J., I. E. E. Monosov, K. McAlonan, R. Berman, M. K. K. Smith, V. Cao, K. H. H. Wang, E. S. S. Boyden, and R. H. H. Wurtz. 2012. Optogenetic inactivation modifies monkey visuomotor behavior. *Neuron* 76: 901–7.

13. Gerits, A., R. Farivar, B. R. Rosen, L. L. Wald, E. S. Boyden, and W. Vanduffel. 2012. Optogenetically induced behavioral and functional network changes in primates. *Curr. Biol.* 22: 1722–6.

14. Znamenskiy, P., and A. M. Zador. 2013. Corticostriatal neurons in auditory cortex drive decisions during auditory discrimination. *Nature* 497: 482–5.

15. Huber, D., L. Petreanu, N. Ghitani, S. Ranade, T. Hromádka, Z. Mainen, and K. Svoboda. 2008. Sparse optical microstimulation in barrel cortex drives learned behaviour in freely moving mice. *Nature* 451: 61–4.

16. Houweling, A. R., and M. Brecht. 2008. Behavioural report of single neuron stimulation in somatosensory cortex. *Nature* 451: 65–8.

17. Nienborg, H., and B. G. Cumming. 2006. Macaque V2 neurons, but not V1 neurons,

show choice-related activity. *J. Neurosci.* 26: 9567–78.

18. Uka, T., and G. C. DeAngelis. 2004. Contribution of area MT to stereoscopic depth perception: choice-related response modulations reflect task strategy. *Neuron* 42: 297–310.

19. Hubel, D. H., and T. N. Wiesel. 1968. Receptive fields and functional architecture of monkey striate cortex. *J. Physiol.* 195: 215–43.

20. Rockland, K. S., and G. W. Van Hoesen. 1994. Direct temporal-occipital feedback connections to striate cortex (V1) in the macaque monkey. *Cereb. Cortex* 4: 300–313.

21. Petro, L. S., L. Vizioli, and L. Muckli. 2014. Contributions of cortical feedback to sensory processing in primary visual cortex. *Front. Psychol.* 5: 1223.

22. Muckli, L., and L. S. Petro. 2013. Network interactions: non-geniculate input to V1. *Curr. Opin. Neurobiol.* 23: 195–201.

23. Budd, J. M. L. 1998. Extrastriate feedback to primary visual cortex in primates: a quantitative analysis of connectivity. *Proc. R. Soc. B Biol. Sci.* 265: 1037–1044.

24. Felleman, D. J., and D. C. Van Essen. 1991. Distributed hierarchical processing in the primate cerebral cortex. *Cereb. Cortex* 1: 1–47.

25. Yukie, M., and E. Iwai. 1985. Laminar origin of direct projection from cortex area V1 to V4 in the rhesus monkey. *Brain Res.* 346: 383–6.

26. Riesenhuber, M., and T. Poggio. 1999. Hierarchical models of object recognition in cortex. *Nat. Neurosci.* 2: 1019–25.

27. Nurminen, L., and A. Angelucci. 2014. Multiple components of surround modulation

in primary visual cortex: multiple neural circuits with multiple functions? *Vision Res.* 104: 47–56.

28. Daniel, P. M., and D. Whitteridge. 1961. The representation of the visual field on the cerebral cortex in monkeys. *J. Physiol.* 159: 203–221.

29. Vnek, N., B. M. Ramsden, C. P. Hung, P. S. Goldman-Rakic, and A. W. Roe. 1999. Optical imaging of functional domains in the cortex of the awake and behaving monkey. *Proc. Natl. Acad. Sci. U. S. A.* 96: 4057–60.

30. Lu, H. D., and A. W. Roe. 2008. Functional Organization of Color Domains in V1 and V2 of Macaque Monkey Revealed by Optical Imaging. *Cereb. Cortex* 18: 516–533.

31. Hubel, D. H., and D. C. Freeman. 1977. Projection into the visual field of ocular dominance columns in macaque monkey. *Brain Res.* 122: 336–43.

32. Bartfeld, E., and A. Grinvald. 1992. Relationships between orientation-preference pinwheels, cytochrome oxidase blobs, and ocular-dominance columns in primate striate cortex. *Proc. Natl. Acad. Sci. U. S. A.* 89: 11905–9.

33. Landisman, C. E., and D. Y. Ts'o. 2002. Color processing in macaque striate cortex: relationships to ocular dominance, cytochrome oxidase, and orientation. *J. Neurophysiol.* 87: 3126–37.

34. Economides, J. R., L. C. Sincich, D. L. Adams, and J. C. Horton. 2011. Orientation tuning of cytochrome oxidase patches in macaque primary visual cortex. *Nat. Neurosci.* 14: 1574–1580.

35. Bonhoeffer, T., and A. Grinvald. 1991. Iso-orientation domains in cat visual cortex

are arranged in pinwheel-like patterns. *Nature* 353: 429–431.

36. Liu, Y.-J., M. Hashemi-Nezhad, and D. C. Lyon. 2017. Differences in orientation tuning between pinwheel and domain neurons in primary visual cortex depend on contrast and size. *Neurophotonics* 4: 31209.

37. Federer, F., J. M. Ichida, J. Jeffs, I. Schiessl, N. McLoughlin, and A. Angelucci. 2009. Four Projection Streams from Primate V1 to the Cytochrome Oxidase Stripes of V2. *J. Neurosci.* 29: 15455–15471.

38. Nauhaus, I., K. J. Nielsen, A. A. Disney, and E. M. Callaway. 2012. Orthogonal micro-organization of orientation and spatial frequency in primate primary visual cortex. *Nat. Neurosci.* 15: 1683–1690.

39. Mountcastle, V. 1957. Modality and topographic properties of single neurons of cat's somatic sensory cortex. *J. Neurophysiol.* 20: 408–34.

40. Hubel, D. H., and T. N. Wiesel. 1974. Uniformity of monkey striate cortex: A parallel relationship between field size, scatter, and magnification factor. *J. Comp. Neurol.* 158: 295–305.

41. Ts'o, D. Y., M. Zarella, and G. Burkitt. 2009. Whither the hypercolumn? *J. Physiol.* 587: 2791–805.

42. Hubel, D. H., and T. N. Wiesel. 1977. Ferrier lecture. Functional architecture of macaque monkey visual cortex. *Proc. R. Soc. London. Ser. B, Biol. Sci.* 198: 1–59.

43. Hirsch, J. A., and L. M. Martinez. 2006. Laminar processing in the visual cortical column. *Curr. Opin. Neurobiol.* 16: 377–84.

44. Chisum, H. J., and D. Fitzpatrick. 2004. The contribution of vertical and horizontal connections to the receptive field center and surround in V1. *Neural Netw.* 17: 681–93.
45. Douglas, R. J., and K. A. C. C. Martin. 2004. Neuronal circuits of the neocortex. *Annu. Rev. Neurosci.* 27: 419–51.
46. Gilbert, C., and T. Wiesel. 1989. Columnar specificity of intrinsic horizontal and corticocortical connections in cat visual cortex. *J. Neurosci.* 9: 2432–2442.
47. Huang, X., Y. M. Elyada, W. H. Bosking, T. Walker, and D. Fitzpatrick. 2014. Optogenetic assessment of horizontal interactions in primary visual cortex. *J. Neurosci.* 34: 4976–90.
48. McGuire, B. A., C. D. Gilbert, P. K. Rivlin, and T. N. Wiesel. 1991. Targets of horizontal connections in macaque primary visual cortex. *J. Comp. Neurol.* 305: 370–392.
49. Angelucci, A., M. Bijanzadeh, L. Nurminen, F. Federer, S. Merlin, and P. C. Bressloff. 2017. Circuits and Mechanisms for Surround Modulation in Visual Cortex. *Annu. Rev. Neurosci.* 40: annurev-neuro-072116-031418.
50. Sato, T. K., M. Häusser, and M. Carandini. 2013. Distal connectivity causes summation and division across mouse visual cortex. *Nat. Neurosci.* 17: 30–32.
51. Nassi, J. J., M. C. Avery, A. H. Cetin, A. W. Roe, and J. H. Reynolds. 2015. Optogenetic Activation of Normalization in Alert Macaque Visual Cortex. *Neuron* 86: 1504–1517.
52. Carandini, M., and D. J. Heeger. 2011. Normalization as a canonical neural

computation. *Nat. Rev. Neurosci.* 13: 51–62.

53. Carandini, M., D. J. Heeger, and J. A. Movshon. 1997. Linearity and normalization in simple cells of the macaque primary visual cortex. *J. Neurosci.* 17: 8621–44.

54. Ruff, D. A., J. J. Alberts, and M. R. Cohen. 2016. Relating normalization to neuronal populations across cortical areas. *J. Neurophysiol.* 116: 1375–1386.

55. Wilson, N. R., C. A. Runyan, F. L. Wang, and M. Sur. 2012. Division and subtraction by distinct cortical inhibitory networks in vivo. *Nature* 488: 343–8.

56. Koch, E., J. Jin, J. M. Alonso, and Q. Zaidi. 2016. Functional implications of orientation maps in primary visual cortex. *Nat. Commun.* 7: 13529.

57. Ichida, J. M., L. Schwabe, P. C. Bressloff, and A. Angelucci. 2007. Response Facilitation From the ‘Suppressive’ Receptive Field Surround of Macaque V1 Neurons. *J. Neurophysiol.* 98: 2168–2181.

58. Angelucci, A., and P. C. Bressloff. 2006. Contribution of feedforward, lateral and feedback connections to the classical receptive field center and extra-classical receptive field surround of primate V1 neurons. *Prog. Brain Res.* 154: 93–120.

59. Levitt, J. B., and J. S. Lund. 2002. The spatial extent over which neurons in macaque striate cortex pool visual signals. *Vis. Neurosci.* 19: 439–452.

60. Cavanaugh, J. R., W. Bair, and J. A. Movshon. 2002. Nature and interaction of signals from the receptive field center and surround in macaque V1 neurons. *J. Neurophysiol.* 88: 2530–46.

61. Shushruth, S., J. M. Ichida, J. B. Levitt, and A. Angelucci. 2009. Comparison of

- spatial summation properties of neurons in macaque V1 and V2. *J. Neurophysiol.* 102: 2069–83.
62. Angelucci, A., J. B. Levitt, E. J. S. Walton, J.-M. Hupe, J. Bullier, and J. S. Lund. 2002. Circuits for local and global signal integration in primary visual cortex. *J. Neurosci.* 22: 8633–46.
63. Webb, B. S., C. J. Tinsley, N. E. Barraclough, A. Parker, and A. M. Derrington. 2003. Gain control from beyond the classical receptive field in primate primary visual cortex. *Vis. Neurosci.* 20: 221–230.
64. Angelucci, A., and K. Sainsbury. 2006. Contribution of feedforward thalamic afferents and corticogeniculate feedback to the spatial summation area of macaque V1 and LGN. *J. Comp. Neurol.* 498: 330–51.
65. Freeman, J., G. J. Brouwer, D. J. Heeger, and E. P. Merriam. 2011. Orientation decoding depends on maps, not columns. *J. Neurosci.* 31: 4792–804.
66. Georgopoulos, A. P., A. B. Schwartz, and R. E. Kettner. 1986. Neuronal population coding of movement direction. *Science* 233: 1416–9.
67. Lee, C., W. H. Rohrer, and D. L. Sparks. 1988. Population coding of saccadic eye movements by neurons in the superior colliculus. *Nature* 332: 357–60.
68. Sparks, D. L. 1986. Translation of sensory signals into commands for control of saccadic eye movements: role of primate superior colliculus. *Physiol. Rev.* 66: 118–71.
69. Paradiso, M. A. 1988. A theory for the use of visual orientation information which exploits the columnar structure of striate cortex. *Biol. Cybern.* 58: 35–49.

70. Sanger, T. D. 2003. Neural population codes. *Curr. Opin. Neurobiol.* 13: 238–249.
71. Shadlen, M. N., K. H. Britten, W. T. Newsome, and J. A. Movshon. 1996. A computational analysis of the relationship between neuronal and behavioral responses to visual motion. *J. Neurosci.* 16: 1486–510.
72. Abbott, L. F., and P. Dayan. 1999. The effect of correlated variability on the accuracy of a population code. *Neural Comput.* 11: 91–101.
73. Sompolinsky, H., H. Yoon, K. Kang, and M. Shamir. 2001. Population coding in neuronal systems with correlated noise. *Phys. Rev. E. Stat. Nonlin. Soft Matter Phys.* 64: 51904.
74. Graham, N. V. S. 1989. *Visual Pattern Analyzers*,. Oxford University Press.
75. Robson, J. G., and N. Graham. 1981. Probability summation and regional variation in contrast sensitivity across the visual field. *Vision Res.* 21: 409–418.
76. Meese, T. S., and C. B. Williams. 2000. Probability summation for multiple patches of luminance modulation. *Vision Res.* 40: 2101–2113.
77. Busse, L., A. R. Wade, and M. Carandini. 2009. Representation of concurrent stimuli by population activity in visual cortex. *Neuron* 64: 931–42.
78. Ghose, K., and J. H. R. Maunsell. 2012. A strong constraint to the joint processing of pairs of cortical signals. *J. Neurosci.* 32: 15922–33.
79. Doiron, B., A. Litwin-Kumar, R. Rosenbaum, G. K. Ocker, and K. Josić. 2016. The mechanics of state-dependent neural correlations. *Nat. Neurosci.* 19: 383–93.
80. Kanitscheider, I., R. Coen-Cagli, and A. Pouget. 2015. Origin of information-limiting



- noise correlations. *Proc. Natl. Acad. Sci. U. S. A.* 112: E6973-82.
81. Ecker, A. S., P. Berens, R. J. Cotton, M. Subramaniyan, G. H. Denfield, C. R. Cadwell, S. M. Smirnakis, M. Bethge, and A. S. Tolias. 2014. State Dependence of Noise Correlations in Macaque Primary Visual Cortex. *Neuron* 82: 235–248.
82. Hansen, B. J., M. I. Chelaru, and V. Dragoi. 2012. Correlated Variability in Laminar Cortical Circuits. *Neuron* 76: 590–602.
83. Smith, M. A., X. Jia, A. Zandvakili, and A. Kohn. 2013. Laminar dependence of neuronal correlations in visual cortex. *J. Neurophysiol.* 109: 940–7.
84. Cohen, M. R., and J. H. R. Maunsell. 2009. Attention improves performance primarily by reducing interneuronal correlations. *Nat. Neurosci.* 12: 1594–600.
85. Ramalingam, N., J. N. J. McManus, W. Li, and C. D. Gilbert. 2013. Top-down modulation of lateral interactions in visual cortex. *J. Neurosci.* 33: 1773–89.
86. Nienborg, H., M. R. Cohen, and B. G. Cumming. 2012. Decision-related activity in sensory neurons: correlations among neurons and with behavior. *Annu. Rev. Neurosci.* 35: 463–83.
87. Smith, M. a, and A. Kohn. 2008. Spatial and temporal scales of neuronal correlation in primary visual cortex. *J. Neurosci.* 28: 12591–603.
88. Kohn, A., R. Coen-Cagli, I. Kanitscheider, and A. Pouget. 2016. Correlations and Neuronal Population Information. *Annu. Rev. Neurosci.* 39: 237–256.
89. Penfield, W., and T. Rasmussen. 1950. *The cerebral cortex of man: A clinical study of localisation of function*,. Macmillan, New York.

90. Afraz, S.-R., R. Kiani, and H. Esteky. 2006. Microstimulation of inferotemporal cortex influences face categorization. *Nature* 442: 692–5.
91. Ditterich, J., M. E. Mazurek, and M. N. Shadlen. 2003. Microstimulation of visual cortex affects the speed of perceptual decisions. *Nat. Neurosci.* 6: 891–8.
92. Daniel, C., H. Britten, and T. Newsome. 1992. Microstimulation in Visual Area MT : Effects Discrimination Performance on Direction. 72.
93. Romo, R., A. Hernández, A. Zainos, C. D. Brody, and L. Lemus. 2000. Sensing without Touching. *Neuron* 26: 273–278.
94. Dai, J., D. I. Brooks, and D. L. Sheinberg. 2014. Optogenetic and electrical microstimulation systematically bias visuospatial choice in primates. *Curr. Biol.* 24: 63–9.
95. Lin, D., M. P. Boyle, P. Dollar, H. Lee, E. S. Lein, P. Perona, and D. J. Anderson. 2011. Functional identification of an aggression locus in the mouse hypothalamus. *Nature* 470: 221–6.
96. Tehovnik, E. J., W. M. Slocum, and P. H. Schiller. 2002. Differential effects of laminar stimulation of V1 cortex on target selection by macaque monkeys. *Eur. J. Neurosci.* 16: 751–60.
97. DeYoe, E. A., J. D. Lewine, and R. W. Doty. 2005. Laminar variation in threshold for detection of electrical excitation of striate cortex by macaques. *J. Neurophysiol.* 94: 3443–50.
98. Bartlett, J. R., E. A. DeYoe, R. W. Doty, B. B. Lee, J. D. Lewine, N. Negrão, and W.

- H. Overman. 2005. Psychophysics of electrical stimulation of striate cortex in macaques. *J. Neurophysiol.* 94: 3430–42.
99. Govorunova, E. G., O. A. Sineshchekov, R. Janz, X. Liu, and J. L. Spudich. 2015. Natural light-gated anion channels: A family of microbial rhodopsins for advanced optogenetics. *Science (80-. )*. 349: 647–650.
100. Gradinaru, V., F. Zhang, C. Ramakrishnan, J. Mattis, R. Prakash, I. Diester, I. Goshen, K. R. Thompson, and K. Deisseroth. 2010. Molecular and cellular approaches for diversifying and extending optogenetics. *Cell* 141: 154–65.
101. Diester, I., M. T. Kaufman, M. Mogri, R. Pashaie, W. Goo, O. Yizhar, C. Ramakrishnan, K. Deisseroth, and K. V. Shenoy. 2011. An optogenetic toolbox designed for primates. *Nat. Neurosci.* 14: 387–97.
102. Boyden, E. S., F. Zhang, E. Bamberg, G. Nagel, and K. Deisseroth. 2005. Millisecond-timescale, genetically targeted optical control of neural activity. *Nat. Neurosci.* 8: 1263–8.
103. Nagel, G., T. Szellas, W. Huhn, S. Kateriya, N. Adeishvili, P. Berthold, D. Ollig, P. Hegemann, and E. Bamberg. 2003. Channelrhodopsin-2, a directly light-gated cation-selective membrane channel. *Proc. Natl. Acad. Sci.* 100: 13940–13945.
104. Masse, N. Y., and E. P. Cook. 2010. Behavioral time course of microstimulation in cortical area MT. *J. Neurophysiol.* 103: 334–45.
105. Han, X., X. Qian, J. G. Bernstein, H.-H. Zhou, G. Talei, P. Stern, R. T. Bronson, A. M. Graybiel, R. Desimone, E. S. Boyden, and G. T. Franzesi. 2009. Millisecond-

timescale optical control of neural dynamics in the nonhuman primate brain. *Neuron* 62: 191–8.

106. Arandia-Romero, I., S. Tanabe, J. Drugowitsch, A. Kohn, and R. Moreno-Bote.

2016. Multiplicative and Additive Modulation of Neuronal Tuning with Population Activity Affects Encoded Information. *Neuron* 89.

107. Lee, S.-H., A. C. Kwan, and Y. Dan. 2014. Interneuron subtypes and orientation tuning. *Nature* 508: E1–E2.

108. Sato, T. K., B. Haider, M. Häusser, and M. Carandini. 2016. An excitatory basis for divisive normalization in visual cortex. *Nat. Neurosci.* 19: 568–70.

109. Olsen, S. R., D. S. Bortone, H. Adesnik, and M. Scanziani. 2012. Gain control by layer six in cortical circuits of vision. *Nature* 483: 47–52.

110. Namboodiri, V. M. K., and G. D. Stuber. 2016. Cell-Type-Specific Optogenetics in Monkeys. *Cell* 166: 1366–1368.

111. Ruiz, O., B. R. Lustig, J. J. Nassi, A. H. Cetin, J. H. Reynolds, T. D. Albright, E. M. Callaway, G. R. Stoner, and A. W. Roe. 2013. Optogenetics through windows on the brain in the nonhuman primate. *J. Neurophysiol.* 37240.

112. May, T., I. Ozden, B. Brush, D. Borton, F. Wagner, N. Agha, D. L. Sheinberg, and A. V Nurmikko. 2014. Detection of optogenetic stimulation in somatosensory cortex by non-human primates--towards artificial tactile sensation. *PLoS One* 9: e114529.

113. Ohayon, S., P. Grimaldi, N. Schweers, and D. Y. Tsao. 2013. Saccade modulation by optical and electrical stimulation in the macaque frontal eye field. *J. Neurosci.* 33:

16684–97.

114. Stauffer, W. R., A. Lak, A. Yang, M. Borel, O. Paulsen, E. S. Boyden, and W. Schultz. 2016. Dopamine Neuron-Specific Optogenetic Stimulation in Rhesus Macaques. *Cell* 166: 1564–1571.e6.

115. May, T., I. Ozden, B. Brush, D. Borton, F. Wagner, N. Agha, D. L. Sheinberg, and A. V. Nurmikko. 2014. Detection of Optogenetic Stimulation in Somatosensory Cortex by Non-Human Primates - Towards Artificial Tactile Sensation. *PLoS One* 9: e114529.

116. Nathanson, J. L., Y. Yanagawa, K. Obata, and E. M. Callaway. 2009. Preferential labeling of inhibitory and excitatory cortical neurons by endogenous tropism of adeno-associated virus and lentivirus vectors. *Neuroscience* 161: 441–50.

117. Yizhar, O., L. E. Fenno, T. J. Davidson, M. Mogri, and K. Deisseroth. 2011. Optogenetics in neural systems. *Neuron* 71: 9–34.

118. Denève, S., and C. K. Machens. 2016. Efficient codes and balanced networks. *Nat. Neurosci.* 19: 375–382.

119. Brainard, D. H. 1997. The Psychophysics Toolbox. *Spat. Vis.* 10: 433–6.

120. Malyshev, A. Y., M. V Roshchin, G. R. Smirnova, D. A. Dolgikh, P. M. Balaban, M. A. Ostrovsky, M. M. Shemyakin, and Y. A. Ovchinnikov. 2017. Chloride conducting light activated channel GtACR2 can produce both cessation of firing and generation of action potentials in cortical neurons in response to light. *Neurosci. Lett.* 640: 76–80.

121. Dragoi, V., C. Rivadulla, and M. Sur. 2001. Foci of orientation plasticity in visual cortex. *Nature* 411: 80–6.

122. Dragoi, V., J. Sharma, E. K. Miller, and M. Sur. 2002. Dynamics of neuronal sensitivity in visual cortex and local feature discrimination. *Nat. Neurosci.* 5: 883–91.
123. Zohary, E., M. N. Shadlen, and W. T. Newsome. 1994. Correlated neuronal discharge rate and its implications for psychophysical performance. *Nature* 370: 140–3.
124. Palmer, C., S.-Y. Cheng, and E. Seidemann. 2007. Linking neuronal and behavioral performance in a reaction-time visual detection task. *J. Neurosci.* 27: 8122–37.
125. Parker, A. J., and W. T. Newsome. 1998. Sense and the single neuron: probing the physiology of perception. *Annu. Rev. Neurosci.* 21: 227–77.
126. Campbell, F. W., and J. G. Robson. 1968. Application of Fourier analysis to the visibility of gratings. *J. Physiol.* 197: 551–66.
127. Barlow, H. B. 1972. Single units and sensation: A neuron doctrine for perceptual psychology? *Perception* .
128. Michel, M. M., Y. Chen, W. S. Geisler, and E. Seidemann. 2013. An illusion predicted by V1 population activity implicates cortical topography in shape perception. *Nat. Neurosci.* 16: 1477–1483.
129. Ikezoe, K., Y. Mori, K. Kitamura, H. Tamura, and I. Fujita. 2013. Relationship between the Local Structure of Orientation Map and the Strength of Orientation Tuning of Neurons in Monkey V1: A 2-Photon Calcium Imaging Study. *J. Neurosci.* 33: 16818–16827.
130. Millard, D. C., C. J. Whitmire, C. A. Gollnick, C. J. Rozell, and G. B. Stanley. 2015.

Electrical and Optical Activation of Mesoscale Neural Circuits with Implications for Coding. *J. Neurosci.* 35: 15702–15715.

131. Hubel, D. H., and T. N. Wiesel. 1974. Sequence regularity and geometry of orientation columns in the monkey striate cortex. *J. Comp. Neurol.* 158: 267–293.

132. Brindley, G. S., and W. S. Lewin. 1968. The sensations produced by electrical stimulation of the visual cortex. *J. Physiol.* 196: 479–93.

133. de la Rocha, J., B. Doiron, E. Shea-Brown, K. Josić, and A. Reyes. 2007. Correlation between neural spike trains increases with firing rate. *Nature* 448: 802–6.

134. Cohen, M. R., and A. Kohn. 2011. Measuring and interpreting neuronal correlations. *Nat Neurosci* 14: 811–819.

135. Salinas, E., and T. J. Sejnowski. 2001. Correlated neuronal activity and the flow of neural information. *Nat. Rev. Neurosci.* 2: 539–50.

136. Gutnisky, D. A., and V. Dragoi. 2008. Adaptive coding of visual information in neural populations. *Nature* 452: 220–224.

137. Mitchell, J. F., K. A. Sundberg, and J. H. Reynolds. 2009. Spatial Attention Decorrelates Intrinsic Activity Fluctuations in Macaque Area V4. *Neuron* 63: 879–888.

138. Gold, J. I., and M. N. Shadlen. 2007. The neural basis of decision making. *Annu. Rev. Neurosci.* 30: 535–74.

139. Kremkow, J., J. Jin, Y. Wang, and J. M. Alonso. 2016. Principles underlying sensory map topography in primary visual cortex. *Nature* 533: 52–7.

140. Nienborg, H., and B. G. Cumming. 2014. Decision-related activity in sensory

neurons may depend on the columnar architecture of cerebral cortex. *J. Neurosci.* 34: 3579–85.

141. Gu, Y., D. E. Angelaki, and G. C. DeAngelis. 2014. Contribution of correlated noise and selective decoding to choice probability measurements in extrastriate visual cortex. *Elife* 3.

142. DeAngelis, G. C., and W. T. Newsome. 2004. Perceptual “Read-Out” of Conjoined Direction and Disparity Maps in Extrastriate Area MT. *PLoS Biol.* 2: e77.

143. Renart, A., J. de la Rocha, P. Bartho, L. Hollender, N. Parga, A. Reyes, and K. D. Harris. 2010. The asynchronous state in cortical circuits. *Science* 327: 587–90.

144. Ecker, A. S., P. Berens, G. a Keliris, M. Bethge, N. K. Logothetis, and A. S. Tolias. 2010. Decorrelated neuronal firing in cortical microcircuits. *Science* 327: 584–7.

145. Herrero, J. L., M. A. Gieselmann, M. Sanayei, and A. Thiele. 2013. Attention-Induced Variance and Noise Correlation Reduction in Macaque V1 Is Mediated by NMDA Receptors. *Neuron* 78: 729–739.

146. Mitchell, J. F., and J. H. Reynolds. 2014. Spatial attention may regulate noise correlations through increases in local inhibition. In *Neuroscience Meeting Planner*. Washington D.C. 435.03.

147. Montijn, J. S., P. M. Goltstein, and C. M. Pennartz. 2015. Mouse V1 population correlates of visual detection rely on heterogeneity within neuronal response patterns. *Elife* 4: e10163.

148. Murphey, D. K., and J. H. R. Maunsell. 2007. Behavioral detection of electrical



microstimulation in different cortical visual areas. *Curr. Biol.* 17: 862–7.

149. Tehovnik, E. J., and W. M. Slocum. 2007. Phosphene induction by microstimulation of macaque V1. *Brain Res. Rev.* 53: 337–43.

150. Tehovnik, E. J., and W. M. Slocum. 2009. Background luminance affects the detection of microampere currents delivered to macaque striate cortex. *Eur. J. Neurosci.* 30: 263–71.

151. Cicmil, N., and K. Krug. 2015. Playing the electric light orchestra--how electrical stimulation of visual cortex elucidates the neural basis of perception. *Philos. Trans. R. Soc. Lond. B. Biol. Sci.* 370: 20140206.

152. Murasugi, C. M., C. D. Salzman, and W. T. Newsome. 1993. Microstimulation in visual area MT: effects of varying pulse amplitude and frequency. *J. Neurosci.* 13: 1719–29.

153. Kohn, A., and M. a Smith. 2005. Stimulus dependence of neuronal correlation in primary visual cortex of the macaque. *J. Neurosci.* 25: 3661–73.

154. Ecker, A. S., G. H. Denfield, M. Bethge, and A. S. Tolias. 2016. On the Structure of Neuronal Population Activity under Fluctuations in Attentional State. *J. Neurosci.* 36: 1775–89.

155. Ahissar, E., E. Vaadia, M. Ahissar, H. Bergman, A. Arieli, and M. Abeles. 1992. Dependence of cortical plasticity on correlated activity of single neurons and on behavioral context. *Science* 257: 1412–5.

156. Averbach, B. B., P. E. Latham, and A. Pouget. 2006. Neural correlations,

population coding and computation. *Nat. Rev. Neurosci.* 7: 358–66.

157. Averbeck, B. B., and D. Lee. 2004. Coding and transmission of information by neural ensembles. *Trends Neurosci.* 27: 225–30.

158. El-Boustani, S., and M. Sur. 2014. Response-dependent dynamics of cell-specific inhibition in cortical networks in vivo. *Nat. Commun.* 5: 5689.

159. Hager, A. M., and H. C. Dringenberg. 2010. Assessment of different induction protocols to elicit long-term depression (LTD) in the rat visual cortex in vivo. *Brain Res.* 1318: 33–41.

160. Rosenbaum, R., M. A. Smith, A. Kohn, J. E. Rubin, and B. Doiron. 2016. The spatial structure of correlated neuronal variability. *Nat. Neurosci.* 20: 107–114.

161. Litwin-Kumar, A., R. Rosenbaum, B. Doiron, X. A. Litwin-Kumar, R. Rosenbaum, B. Doiron, A. Litwin-Kumar, R. Rosenbaum, and B. Doiron. 2016. Inhibitory stabilization and visual coding in cortical circuits with multiple interneuron subtypes. *J. Neurophysiol.* 115: 1399–409.

162. Adesnik, H., W. Bruns, H. Taniguchi, Z. J. Huang, and M. Scanziani. 2012. A neural circuit for spatial summation in visual cortex. *Nature* 490: 226–31.

163. Atallah, B. V., W. Bruns, M. Carandini, and M. Scanziani. 2012. Parvalbumin-expressing interneurons linearly transform cortical responses to visual stimuli. *Neuron* 73: 159–70.

164. Crystal, J. D., W. T. Alford, W. Zhou, and A. G. Hohmann. 2013. Source Memory in the Rat. *Curr. Biol.* .

165. Nassi, J. J., S. G. Lomber, and R. T. Born. 2013. Corticocortical feedback contributes to surround suppression in V1 of the alert primate. *J. Neurosci.* 33: 8504–17.
166. Mahn, M., M. Prigge, S. Ron, R. Levy, and O. Yizhar. 2016. Biophysical constraints of optogenetic inhibition at presynaptic terminals. *Nat. Neurosci.* 19: 554–556.
167. Acker, L., E. N. Pino, E. S. Boyden, and R. Desimone. 2016. FEF inactivation with improved optogenetic methods. *Proc. Natl. Acad. Sci.* 113: E7297–E7306.
168. Gilbert, C. D., and T. N. Wiesel. 1983. Functional organization of the visual cortex. *Prog. Brain Res.* 58: 209–18.
169. Angelucci, A., and J. Bullier. 2003. Reaching beyond the classical receptive field of V1 neurons: horizontal or feedback axons? *J. Physiol.* 97: 141–154.
170. Hirsch, J. A., and C. D. Gilbert. 1991. Synaptic physiology of horizontal connections in the cat's visual cortex. *J. Neurosci.* 11: 1800–9.
171. Shushruth, S., P. Mangapathy, J. M. Ichida, P. C. Bressloff, L. Schwabe, and A. Angelucci. 2012. Strong recurrent networks compute the orientation tuning of surround modulation in the primate primary visual cortex. *J. Neurosci.* 32: 308–21.
172. Ichida, J. M., L. Schwabe, P. C. Bressloff, and A. Angelucci. 2007. Response facilitation from the “suppressive” receptive field surround of macaque V1 neurons. *J. Neurophysiol.* 98: 2168–81.
173. Henry, C. A., S. Joshi, D. Xing, R. M. Shapley, and M. J. Hawken. 2013. Functional characterization of the extraclassical receptive field in macaque V1: contrast,

orientation, and temporal dynamics. *J. Neurosci.* 33: 6230–42.

174. Han, X. 2012. Optogenetics in the nonhuman primate. *Prog. Brain Res.* 196: 215–33.

175. Inoue, K., M. Takada, and M. Matsumoto. 2015. Neuronal and behavioural modulations by pathway-selective optogenetic stimulation of the primate oculomotor system. *Nat. Commun.* 6: 8378.

176. Afraz, A., E. S. Boyden, and J. J. DiCarlo. 2015. Optogenetic and pharmacological suppression of spatial clusters of face neurons reveal their causal role in face gender discrimination. *Proc. Natl. Acad. Sci.* 112: 6730–6735.

177. Griffin, D. M., H. M. Hudson, A. Belhaj-Saïf, and P. D. Cheney. 2011. Hijacking cortical motor output with repetitive microstimulation. *J. Neurosci.* 31: 13088–96.

178. Moore, T., and K. M. Armstrong. 2003. Selective gating of visual signals by microstimulation of frontal cortex. 421: 370–373.

179. Ni, A. M., and J. H. R. Maunsell. 2010. Microstimulation reveals limits in detecting different signals from a local cortical region. *Curr. Biol.* 20: 824–8.

180. Tehovnik, E. J., A. S. Tolia, F. Sultan, W. M. Slocum, and N. K. Logothetis. 2006. Direct and Indirect Activation of Cortical Neurons by Electrical Microstimulation. *J. Neurophysiol.* 96: 512–521.

181. Mendoza, S. D., Y. El-Shamayleh, and G. D. Horwitz. 2017. AAV-mediated delivery of optogenetic constructs to the macaque brain triggers humoral immune responses. *J. Neurophysiol.* 117: 2004–2013.

## **VITA**

Ariana Ruxandra Andrei was born in Constanta, Romania on March 1, 1980, the daughter of Adriana Andrei and Cezar Vasile Andrei. After completing her work at Unionville High School, Unionville, Canada in 1999, she entered McGill University in Montreal, Canada. She received the degree of Bachelor of Science with an Honors major in physiology from McGill in May, 2003, and a Master of Science from McGill in 2005, followed by a Bachelor of Fine Arts degree in 2009 from York University in Toronto, Canada. For the next two years, she pursued experimental filmmaking and worked as a research technician in the Department of Neurobiology and Anatomy at the McGovern Medical School in Houston Texas. In August of 2011 she entered The University of Texas MD Anderson Cancer Center UTHealth Graduate School of Biomedical Sciences.

Permanent address:

505A W. Alabama St.  
Houston, Texas 77006